Department of Precision and Microsystems Engineering

Shape Optimization of a Flapping Wing for the Atalanta Project FWMAV

Abdelhakim Amer

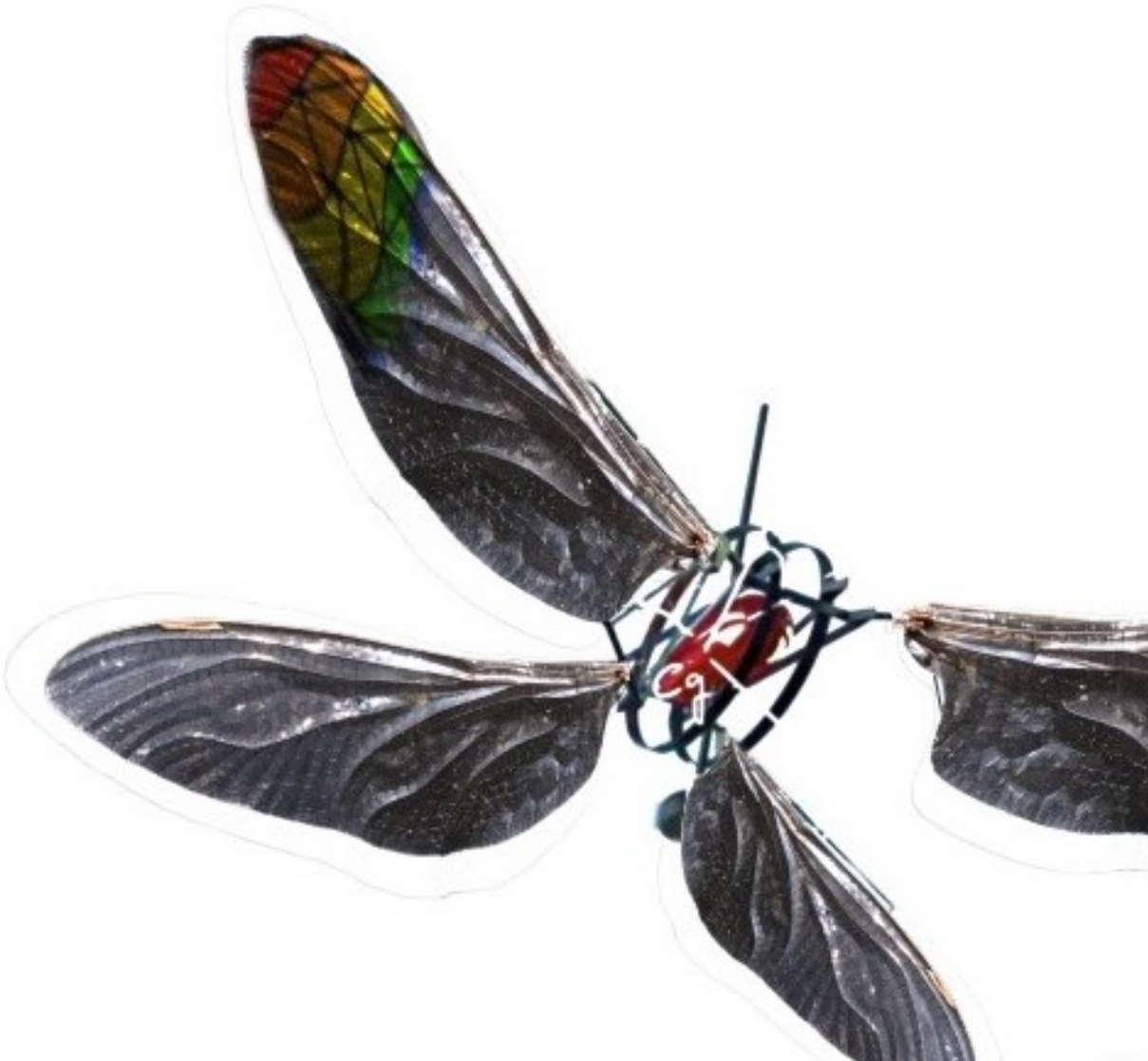
Report no : 2021.015
Coach : Dr.Ir. Hans Goosen
Professor : Dr.Ir. Hans Goosen
Specialisation : Engineering Mechanics
Type of report : Msc. Thesis
Date : 17/2/2021

TU Delft Delft University of Technology

Challenge the future

Shape Optimization of a Flapping Wing for the Atalanta Project FWMAV

Abdelhakim Amer



TU Delft

Shape Optimization of a Flapping Wing for the Atalanta Project FWMAV

by

Abdelhakim Amer

to obtain the degree of Master of Science at the Delft University of Technology,
to be defended publicly on Thursday February 25, 2021 at 12:30 P.M.

Student number: 4557603
Thesis Advisor: Prof. Dr. Ir. H. Goosen, TU Delft, supervisor

An electronic version of this thesis is available at http://repository.tudelft.nl/.

TU Delft Delft University of Technology

Summary

Flapping Wing Micro Air Vehicle (FWMAV) technologies are emerging due to the vast number of applications that they can be utilized in. Researchers and scientists are constantly seeking to push the boundaries to the extreme in terms of miniaturization of this technology, making it smaller, lighter and better performing. In order to achieve this we need to look for new approaches in the design of FWMAVs at the component and at the system level.

This research explores a new approach for the flapping wing design. Inspired by insects, the corrugation pattern on the wing can be optimized in order to achieve the required passive pitching behaviour of the wing. Optimized corrugated wings has the potential to achieve a higher strength to weight ratio than available flapping wing designs, while at the same time exhibiting the required passive pitching behaviour. Moreover, the manufacturing process of the wing is more reproducible compared to conventional wing manufacturing methods. This is important because at such a small scale, a minor deviation in the wing features can drastically affect the wing properties, which has implications on performance and control.

In this study shell shape optimization method was utilized to obtain passively pitching wing designs. The obtained wing designs performance is then evaluated qualitatively and quantitatively, through a time dependant study of the flapping motion of the wing. Finally, a wing prototype is manufactured and the results are experimentally validated.

Acknowledgements

First and foremost, I would like to express my immense gratitude to my supervisor, Hans, for his unmatched support through out this project. His insights and feedback were invaluable in the progress of this research. He gave me the freedom to explore and to make decisions in steering the direction of this project, and at the same time provided very constructive feedback for me to work on. Despite his busy schedule, I appreciate that throughout this project we would have regular weekly meetings that would usually extend for more than hour. He also provided me with all the tools and access to the facilities that i needed to make the most of my research project. I would also like to extend my thanks to Fred for his interesting discussions as well as the courses that he taught me, which has led me to choose to specialize in this focus area. I admire his passion for science and teaching as well as his care about his students. I would also like to thank the technicians at the PME lab: Rob, Patrick, Bradley, Gideon and Spiridon for providing me with all the support i needed for conducting my experimental work as efficiently as possible. Last but not least i would like to thank my family: my parents, my grand parents, my sister and my relatives. Without their emotional and financial support i wouldn't have been able to pursue my dream of doing my master studies abroad at TU Delft.

Contents

Summary i

Acknowledgements ii

1 Introduction 1
- 1.1 Motivation . . . 1
- 1.2 The Atalanta Project . . . 3
- 1.3 Challenges of Flapping Wings Design . . . 3
- 1.4 Aim & Scope . . . 4
- 1.5 Approach adopted in this study . . . 4
- 1.6 Report Structure . . . 4

2 Mechanics of Flapping Wings and Flapping Flight 6
- 2.1 Wing Geometry . . . 6
  - 2.1.1 Geometrical Parameters for Shape Description . . . 6
  - 2.1.2 Optimal Wing Geometrical Parameters . . . 7
- 2.2 Kinematics and Dynamics of Flapping Flight . . . 7
  - 2.2.1 Flapping Wing Kinematics . . . 7
  - 2.2.2 Flapping Cycle Description . . . 8
  - 2.2.3 FWMAV Dynamics . . . 9
- 2.3 Aerodynamics of Flapping Flight . . . 9
  - 2.3.1 Key Scaling Parameters . . . 9
  - 2.3.2 Unsteady lift enhancement mechanisms . . . 10
  - 2.3.3 Aerodynamic Models . . . 11

3 Flapping Wing Designs and Design Approaches 12
- 3.1 Bio Inspiration in Flapping Wing Design . . . 12
- 3.2 FW Design Approaches . . . 14
  - 3.2.1 Morphing Avian Wings . . . 14
  - 3.2.2 Experimental Design approaches with similar FW kinematics . . . 14
  - 3.2.3 Analytical Design approaches with similar FW kinematics . . . 17
- 3.3 Concluding Remarks . . . 18

4 Structural Optimization of Flapping Wings with a Finite Element Model 19
- 4.1 Shell Structures . . . 19
  - 4.1.1 Finite Element Modeling of the Wing . . . 19
- 4.2 Shell structures FE Modeling in COMSOL . . . 20
  - 4.2.1 Strain calculation . . . 21
  - 4.2.2 Fold lines . . . 22
- 4.3 Optimization of structures . . . 22
  - 4.3.1 Problem Formulation . . . 23
  - 4.3.2 Design Parameters . . . 23
  - 4.3.3 Sensitivity Analysis . . . 24
  - 4.3.4 Discrete Sensitivity Analysis . . . 24
- 4.4 Shell Structures Shape Optimization . . . 26
  - 4.4.1 FE based parameterization . . . 26
  - 4.4.2 Examples of shape optimizations of shell structures . . . 27

5 Shell Shape Optimization Method for Passively Pitching Wings 29
- 5.1 Passive Pitching as an Optimization Goal . . . 30
  - 5.1.1 Problem Formulation . . . 32

5.2 Model A . . . 33
5.2.1 Sensitivity Analysis . . . 35
5.3 Model B . . . 37
5.3.1 Model B1 - Non constrained Optimization with angle objective . . . 37
5.3.2 Model B2 - Angle Objective, with constrained leading edge . . . 38
5.4 Optimization to achieve Qi Wang's Wing Optimal Mechanical behaviour . . . 40
5.4.1 Qi Wangs Model . . . 40
5.4.2 Qi Wang Wing Optimal Wing static FE load analysis . . . 40
5.4.3 Least Square Objective Optimization . . . 41

6 Aerodynamic Analysis and Validation of Corrugated Wing Designs 43
6.1 Dynamic Analysis . . . 43
6.2 Aerodynamic Model . . . 47
6.2.1 Kinematics . . . 47
6.2.2 Aerodynamic load model . . . 47
6.2.3 Angle of Attack . . . 49
6.2.4 Adjusting model for deformation . . . 50
6.3 Aerodynamic Model Verification . . . 51
6.4 Aerodynamic Analysis of the wing design . . . 53
6.4.1 Evaluation of the Wing Design . . . 54
6.5 Corrugated Wing Manufacturing . . . 56
6.5.1 Hot compression molding . . . 56
6.5.2 Mold design . . . 56
6.5.3 Vacuum forming . . . 57
6.5.4 Wing root connection manufacturing . . . 58
6.6 Wing Design Experimental Validation . . . 59
6.6.1 setup . . . 59
6.6.2 Measured pitching behaviour . . . 60

7 Retrospection and Discussion 62
7.1 Shell Shape Optimization . . . 63
7.2 Dynamic Analysis . . . 63
7.3 Wing Manufacturing . . . 64
7.4 Testing . . . 65

8 Final Remarks 66
8.1 Conclusion . . . 66
8.2 Future Work . . . 66

A Quasi steady model Matlab code 68
A.1 Main Function . . . 68
A.2 Called Function . . . 71

B Design 1 Deformation Data 75
B.1 Trailing Edge . . . 77
B.2 Leading Edge . . . 78

Bibliography 79

1

Introduction

A Micro Air Vehicle (MAV), also known as an Unmmanned Aerial Vehicle (UAV), is a flying robot that doesn't have a human pilot on board. It can be either remotely controlled or autonomous. MAVs are usually small in size typically smaller than 15cm in length. A palm sized MAV is sometimes referred to as a nano air vehicle. There are three main classes of MAVs, namely *fixed wing*, *rotary wing* and *flapping wing* MAVs. In fixed wing MAVs, which are similar to aeroplanes, the MAV needs to be flying at certain horizontal speed to maintain lift. Examples of fixed wing MAVs are shown in figure 1.1. A rotary wing MAV generates lift by one or several rotating blades, examples include quarotors and helicopters. Finally a flapping wing MAV generates lift by flapping its wing, similar to insects and birds.



Figure 1.1: Examples of Fixed Wing MAVs[39]

1.1. Motivation

As technology advance, we are able to produce smaller and more efficient components. This allows us to make smaller integrated systems which opens a sea of limitless possibilities and applications. Flapping Wing Micro Air Vehicles (FWMAVs) being one of those interesting applications, currently a lot of research is been carried out to develop these small flapping flying machines and the goal is to make them as small and as efficient as possible.

A FWMAV can be used in surveillance, inspection and monitoring as well as many other applications (see figure 1.2). A small sized FWMAV can be used to navigate through tight space where humans or other robots can not reach. Compared to fixed wing UAV's they have the unique and very beneficial ability to hover. At the same time they are more efficient and safer than rotary wing drones, specially as we move towards smaller MAV sizes. Recently commericial use of flapping wing MAVs is being

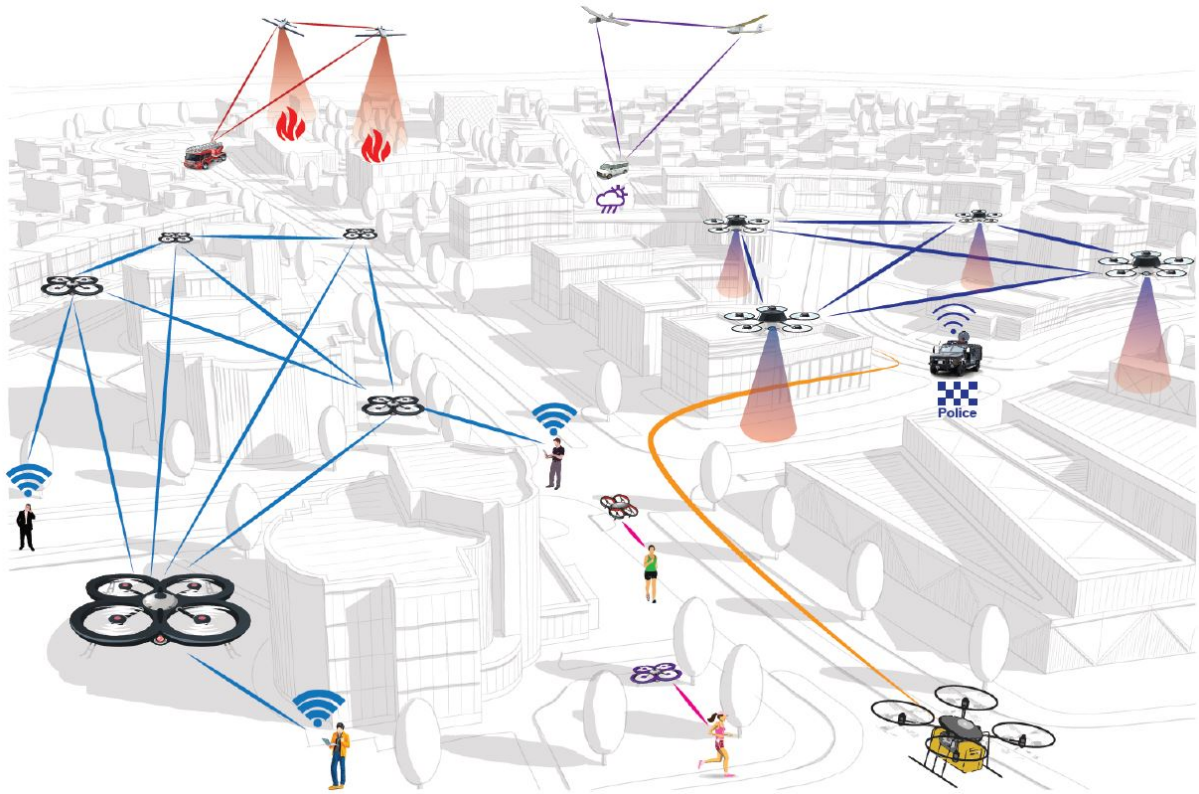


Figure 1.2: Possible Applications of Micro Air Vehicles [28]

implemented. For example, Flapper Drones, a spin-off from TU Delft MAV lab, developed flapping drones with the goal of entrainment.

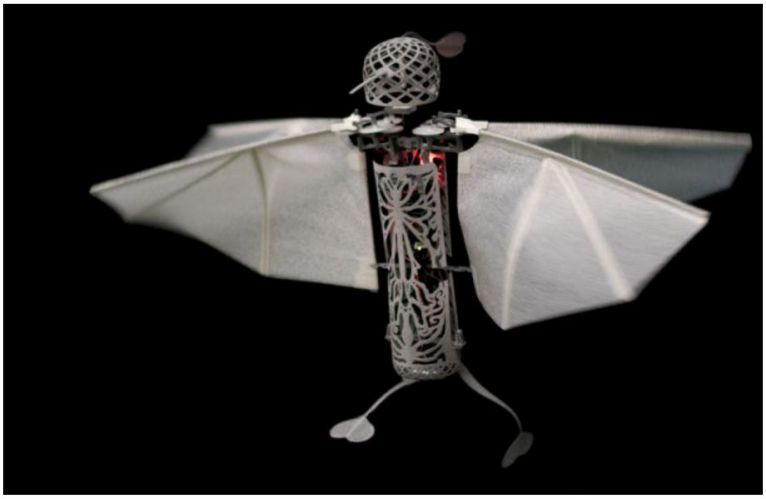


Figure 1.3: Flapper Drone, a drone for entertainment purposes [1]

1.2. The Atalanta Project

The Atalanta Project (figure 1.4) is a research project started at TU Delft Department of Precision and Microsystems in 2005. The aim of the project is to make a Flapping Wing flying device with the following specs [16]:

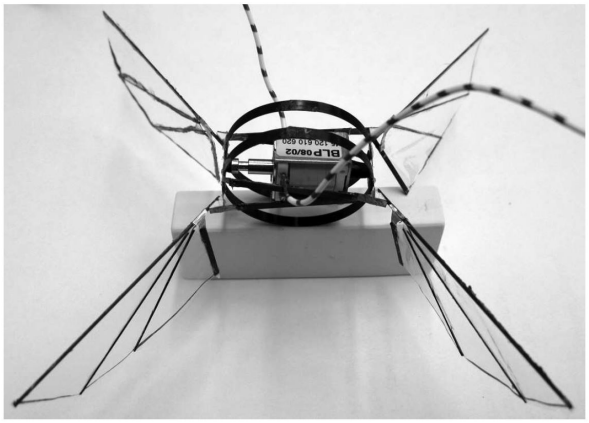


Figure 1.4: Insect Inspired Atalanta Robot [16]

- Fly autonomously
- Hover and fly slowly (main flight state)
- Communicate with others and a base station
- Provide payload capacity
- Be adaptable for many situations

The ambitious design of the FWMAV is small in size and compact, with a maximum total weight of 4 grams and a wing span of 10 cm. Several research papers have been published aiming in solving the major challenges in the design, manufacturing and analysis of different systems that constitute the FWMAV. However, there is still some major challenges to be solved and room for optimization. In this project we are aiming to address the challenges related to the design of the wings, in an effort to reach an efficient wing design.

1.3. Challenges of Flapping Wings Design

The wing is arguably the most critical component in the MAV, as it provides the essential lift for the MAV flight. Normally it is also the most expensive in terms of power consumption which makes it even more important. Power consumption is usually the most critical design requirement in MAVs because it has a direct influence on the operation time. Operation time is crucial because it is one of the limitations of the current MAV technology. This trend can be observed in figure 1.5.

At the scale of the Atalanta project (10cm) most MAVs operation time is so small that they cannot perform any useful task during that time. Therefore there is always the need to optimize all the MAV's subsystems in terms of weight and power consumption, and that includes the wing design.

Designing an efficient wing has many complexities. First of all there are a very large number of parameters that influence the wing performance, so making an optimization that involves all these parameters is usually difficult to perform. Moreover, a major challenge in flapping wing flight is its complex aerodynamics. The aerodynamics of flapping is not yet fully understood and explained, this is due to the unsteady nature of the aerodynamics making it difficult to make accurate predictions for the forces acting on the wing, thus causing an uncertainty in performance evaluation of the design. Moreover, there are structural design problems related to the strength and durability of the wing due to the it being an extremely slender structure. Thus making it susceptible to all kinds of failure mechanisms.

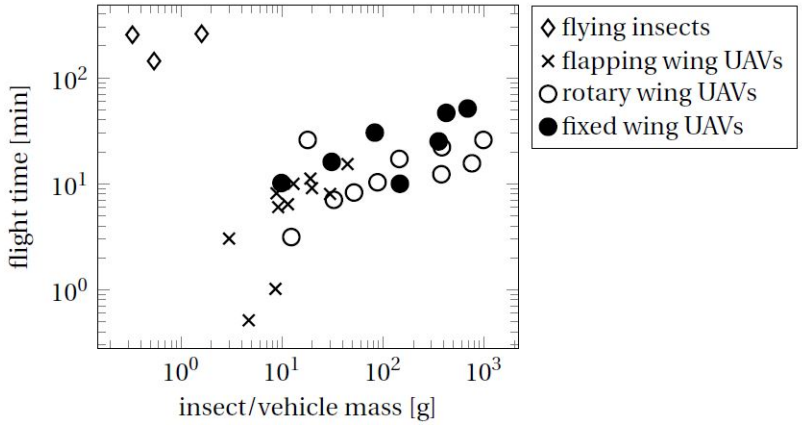


Figure 1.5: Flight time versus mass of insects or unmanned aerial vehicles [72]

1.4. Aim & Scope

The aim of this thesis is to investigate a novel method for FWMAV wing design by optimising the corrugation pattern on the wing. For that purpose, shell shape optimization method will be used. The study is motivated by the drawbacks of current wing designs in terms of reproduciblity and strength to weight ratio.

The scope of this work is includes achieving a wing design based on the Shape optimization method as well as manufacturing a prototype wing. This thesis is a proof of concept, so that in the future this method can be utilized in FW designs. The set of wings are yet to be integrated onto the Atalanta project platform and further testing of the wing performance is needed.

1.5. Approach adopted in this study

In this study Shell Shape Optimization is adopted as a method of wing design. We further evaluate this method by looking at the kinematics from the resulting deformation of the obtained wing designs, as well as calculating the lift and drag forces acting on the wing using a quasi steady aerodynamic model. Finally experimental validation is performed on the physical Wing.

1.6. Report Structure

Chapter 1 Background knowledge of the project and introducing the research topic.

Chapter 2 This chapter discusses the physics of flapping flight and how different aspects of the wing can affect it. The definitions commonly used in the literature for the wing geometry and wing kinematics are presented. Moreover, unsteady aerodynamic mechanisms resulting from flapping flight are introduced, and how aerodynamic models of different fidelity can be used to capture these effects to estimate the loads acting on the wing.

Chapter 3 This chapter introduces different flapping wing design approaches for existing FWMAV. The approaches are divided into two main categories, experimental methods, based on trial and error on an existing platform, and analytical methods based on simplified aerodynamic and mechanical wing models. The advantages and disadvantages of both methods are discussed as well as common features observed in wing designs. Moreover, insect wings are investigated in terms of morphology, shape and structure as a source of inspiration.

Chapter 4 Here the the shell shape optimization method is introduced, which is the method used in the next chapters in obtaining the wing designs. The framework of structural optimization is first introduced as well as the underlying mathematics. The direct adjoint sensitivity analysis is presented. Shell finite elements are also discussed and the use of finite element nodes as design variables for the optimization is shown with some examples from the literature.

Chapter 5 In this chapter the shape shell optimization design problem is formulated according to the insight from insect behaviour and studies on wing pitching and twist. Different Optimization Models are then simulated using COMSOL shell shape optimization feature. Finally a first design is obtained that achieves optimal mechanical behaviour for the wing.

Chapter 6 In this chapter a second design is achieved by using an alternative way of formulating the objective function. After obtaining a second wing design the dynamic behaviour of the wing is investigated, to verify the desired passive pitching behaviour of the wing. The obtained wing kinematics is then used to calculate the Lift and Drag forces acting on the wing using a quasi steady model that is adjusted to take into account wing deformation. Finally the wing is manufactured and the flapping motion of the wing simulated experimentally to validate the simulations performed.

Chapter 7 This chapter is a discussion on the obtained results and a reflection on different aspects that weren't mentioned in earlier parts.

Chapter 8 In this final Chapter, a conclusion of the work done here presented, as well as recommendation for future work.

Appendices Appendix A contains the Matlab for the quasi-steady aerodynamic model. Appendix B contains the deformation of the wing as a function of time at different time instances.

Bibliography Literature that this research is based on

2

Mechanics of Flapping Wings and Flapping Flight

The first step in Wing design is to know the parameters that effect the performance of the wing which is in our case minimizing the power consumption. Such relation can be inferred by analyzing the wing mechanics which is the complex interplay between the properties of the wing, its motion and the generated forces on the wing. This relation can be summarized in the figure 2.1.

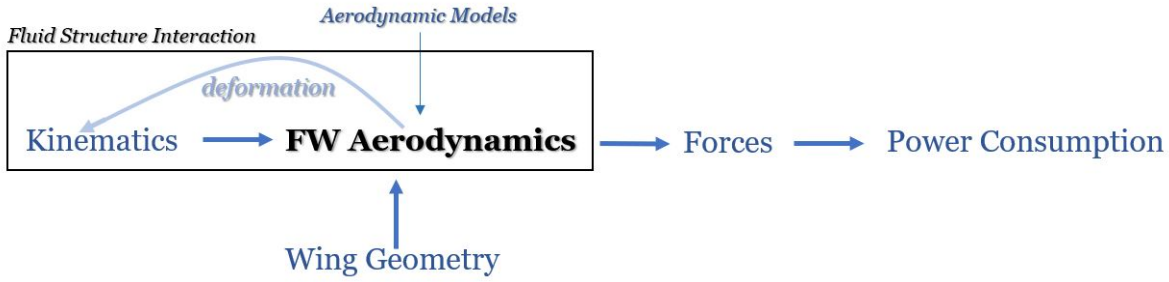


Figure 2.1: Wing Mechanics Map

2.1. Wing Geometry

Wing shape is important in determining the performance of the wing. We can observe in nature that different flyers have different planform shapes which are optimized for different purposes 3.1.

2.1.1. Geometrical Parameters for Shape Description

The area of the wing enclosed by the leading edge and the trailing edge is important to determine the performance of the wing. The area can be defined in terms of the spanwise and chord wise area distributions (SWAD and CWAD). If we use a Beta probability density function (BPDF), the SWAD can be characterized by $\hat{r}_1$, which is related to the the span wise centroid position by $\hat{r}_1$*R. Wings with moderate $\hat{r}_1$ are shown to be most efficient, which is the case in insects [2]. On the other hand CWAD is characterized by the distance between the LE and the pitching axis after normalising by the local strip length and is given the symbol $\hat{d}$. The change of $\hat{d}$ with respect to the span is usually assumed linear with respect to span and is calculated from $\hat{d}_{root}$ and $\hat{d}_{tip}$. Using the convention described here gives us 3 parameters in total that we can manipulate to change the our wing planform. This simplification is useful when optimization of the wing planform is needed such as in [73].

2.1.2. Optimal Wing Geometrical Parameters

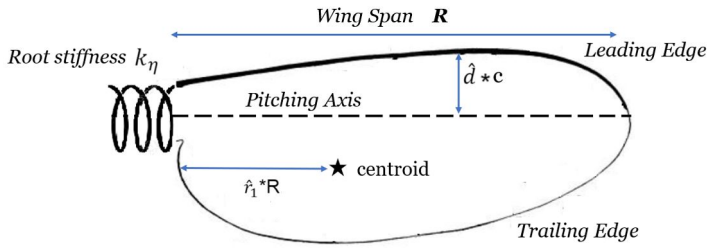


Figure 2.2: Description of shape parameters of the wing model [73]

Although more research have been conducted to investigate the optimal SWAD because of its known influence on wing performance, Wang [76] has shown than CWAD can have a significant effect on power consumption. He optimised the pitching axis of several wings having different SWAD. He showed that having a pitching axis coinciding with the leading edge as most MAV have, is non optimal, and power saving of 33% can be achieved by optimizing the pitching axis. Another aspect to consider is the moment of inertia of the wing which is determined by the span wise and chord wise mass distributions given (SWMD and CWMD). In another research by Wang, he [73] performed an optimization of a rigid wing with root stiffness k_η, with the design parameters being the aspect ration of the wing AR, root stifness k_η, $\hat{d}_{root}$, $\hat{d}_{tip}$ and the flapping frequency. He showed that its optimal in terms of energy saving to have smaller wings aspect ratios and to have a pitching axis located close to the center of pressure and the wing centre line.

2.2. Kinematics and Dynamics of Flapping Flight

2.2.1. Flapping Wing Kinematics

The kinematic design is usually driven by the goal of enhancing control authority, maneuverability and aerodynamic performance [68]. At the same time, it is constrained by the actuating mechanism and the available power. kinematic Configuration in the literature are divided into three main categories. The first type is harmonic motion, which has the advantage of easier analysis. The second type used observed kinematics from insects. The third type is kinematic designed with specific control purpose in mind [68]. The kinematics manipulate the velocity vector seen by the airfoil. This relation can be mathematically expressed in two terms, the first is due to the flapping kinematics relative to the body, and the second is due to the body motion as shown in equation 2.1

$$V_a = V_b + w_{i-b} \times r + w_{b-w} \times r. \tag{2.1}$$

In hovering, we can neglect the first two terms and only consider the velocity component due to flapping. Three euler angles are usually used to describe the wing rotation, namely the sweeping angle Φ, heaving or plunging angle θ and the pitching angle α. These angles alter the velocity vector of the flow relative to the airfoil. The velocity vector and the pitching angle and their time derivatives determine the aerodynamic loads acting on the wing.The wing rotation are defined within two coordinate systems, an inertial axis $x_i y_i z_i$ and a co rotating axes $x_c y_c z_c$ of the body and wing[72]. The body fixed frame can be described with respect to the inertial frame using any sequence of euler angle rotations. However, a common convention used is the yaw pitch roll euler angles sequence. For zero wing kinematic angles, the wing fixed frame can be chosen to coincide with the body-fixed frame. Thus, the euler angles sequence $\phi - \theta - \eta$, can then be used to describe the wing frame relative to the body frame. This sequence of rotation can be represented by the can in series approach shown in figure 2.3.

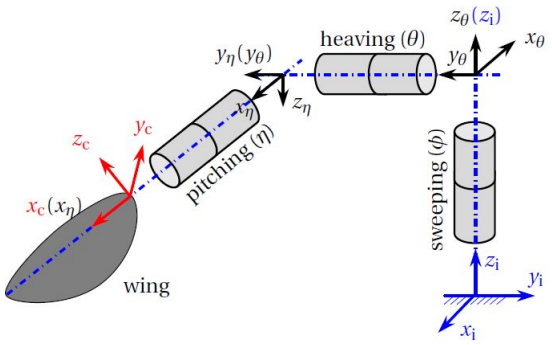


Figure 2.3: Successive wing rotations used to describe the kinematics of a rigid flapping wing, shown using the “cans in series” approach proposed by [61] . Four different frames are involved in these rotations, including an inertial frame $x_i y_i z_i$, two intermediate frames $x_\theta y_\theta z_\theta$ and $x_\eta y_\eta z_\eta$, and a co-rotating frame $x_c y_c z_c$. All these frames share the same origin although they are drawn at various locations [72].

2.2.2. Flapping Cycle Description

The wings main motion is usually acting within a plane called the stroke plane, which can be inclined by a certain angle β. The sweeping motion is the motion within the stroke plane and is usually harmonic because its easier to achieve by many actuation mechanisms [77]. The wing motion consists of two strokes, a down stroke, where the ventral side of the wing leads and an upstroke where the dorsal side is leading.The pitching motion is the rotation about the wing main axis. In order to have a positive angle of attack during the whole motion, pitching needs to performed during the stroke reversal. When this action is performed when switching between down stroke and upstroke it is called pro-nation, and supination if it is the other way round. The wing motion described is shown for β =0 for simplicity in Figure 2.4.

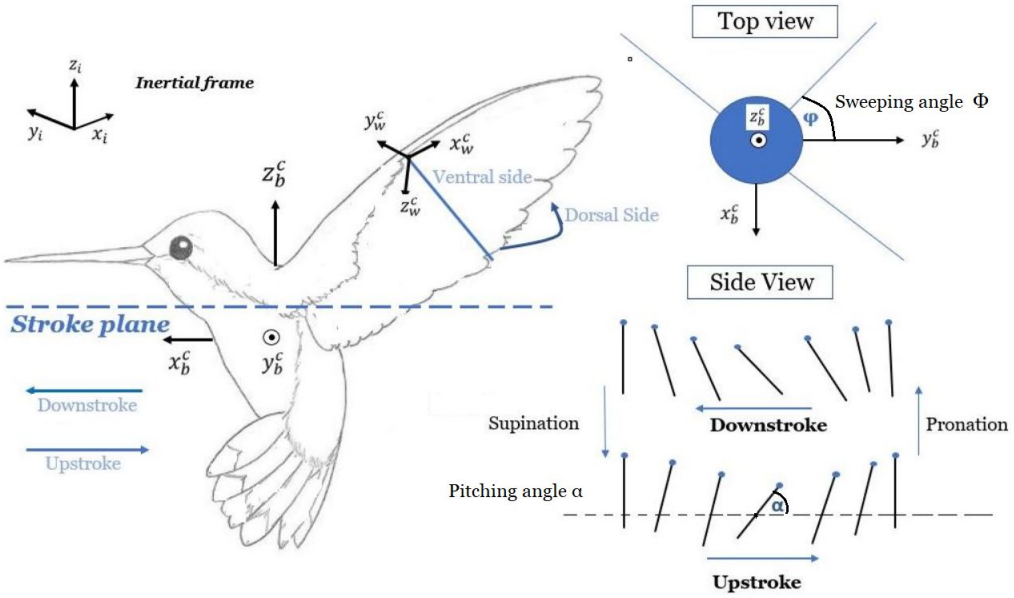


Figure 2.4: Definition of Euler angles for studying flappingwing kinematics. [23]

If this pitching motion is correctly timed it will have a significant aerodynamic advantage. Heaving which is the out of stroke plane motion, also has an important role in aerodynamic force generation as it determines the wing tip trajectory. This effect is used by insects, we can see complex motions that results from the heaving action. For example a hawk moth flaps its wings in a figure eight motion, where the wing crosses the stroke plane twice within one wing cycle [23].

2.2.3. FWMAV Dynamics

Due to high flapping frequency of FWMAV, cycle averaged aerodynamic loads are usually calculated, instead of instantaneous loads. This is called the averaging assumption and is discussed in [68]. This simplifies the dynamics of the system by converting to an autonomous system instead of a non autonomous. The inertia of the wing can also be neglected in the average sense. Thus the equations of motion of an FWMAV can be written in similar fashion to a conventional aircraft as shown in the equations given below.[68].

$$m(\dot{u} + qw - rv) = -mgsin\theta + X \tag{2.2}$$

$$m(\dot{v} + ru - pw) = mgsin\phi cos\theta + Y \tag{2.3}$$

$$m(\dot{w} + pv - qu) = mgcos\phi cos\theta + Z \tag{2.4}$$

$$I_x\dot{p} - I_{xz}\dot{r} + (I_z - I_y)qr - I_{xz}pq = L \tag{2.5}$$

$$I_y\dot{q} - (I_x - I_z)rp + I_{xz}(p^2 - r^2) = M \tag{2.6}$$

$$I_z\dot{r} - I_{xz}\dot{p} + (I_y - I_x)pq + I_{xz}rq = N\dot{\psi} = (qsin\phi + rcos\phi/cos\theta \tag{2.7}$$

$$\dot{\theta} = qcos\Phi - rsin\phi \tag{2.8}$$

$$\dot{\phi} = p + (qsin\phi + rcos\phi)tan\theta. \tag{2.9}$$

The nine equations represent the equations of motion for the body velocities u, v and w are the body velocities, angular velocties p, q and r are the body Euler angles (ψ, θ, ϕ).

2.3. Aerodynamics of Flapping Flight

2.3.1. Key Scaling Parameters

Three-dimensionless parameters are commonly used in the literature flapping wing flight to relate wing kinematics and aerodynamics to the resulting force coefficients. First one is the the Reynolds number *Re* which is the ratio of inertial forces to viscous forces and thus gives information on the relative influence of these forces. The Reynolds number is important in determining the stability and strength of lift enhancing vortices [11], which are discussed in the next section. The reduced frequency *k* is an important similarity parameter which indicates the level of unsteadiness in flapping-wing flight. It is calculated by taking the ratio of the wavelength of of the flow disturbance to the chord length [65]. Finally,the Strouhal number is a non-dimensional parameter that is relevant for the vortex dynamics and provides information of the shedding behavior of the vortices during flapping motion [30].

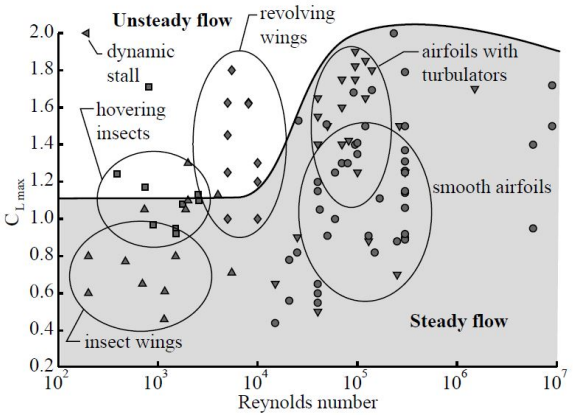


Figure 2.5: Graph showing how lift coefficient changes with Reynolds number. The grey area shows steady flow vs. non grey for unsteady flow [58]

2.3.2. Unsteady lift enhancement mechanisms

Influenced by the Geometry, flapping kinematics and dimensionless parameters of the wing, there are are unsteady lift generating mechanisms which are activated during the flapping motion which makes flight much more efficient as shown in figure 2.5. Unsteady lift enhancement mechanisms include: Leading Edge Vortex (LEV), Wake Capture, Clap and Fling, and Rotational Circulation. The timing of these unsteady phenomena with respect to the flapping cycle is shown in the figure 2.6.

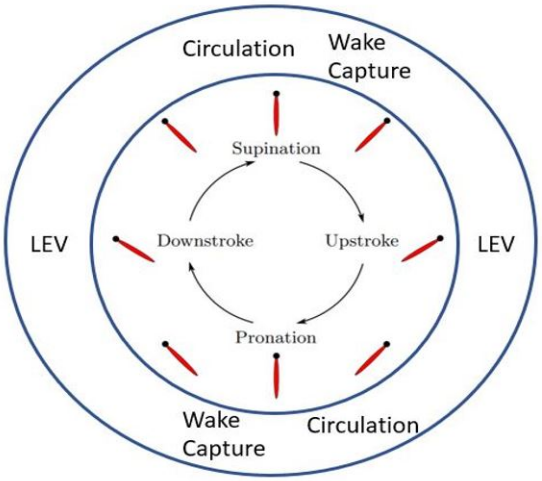


Figure 2.6: Wing Flapping Cycle and different loads acting during the cycle. The figure shows a cross section of the wing undergoing a typical sinusoidal pitching rotation during one cycle. The cycle consists of two strokes an upstroke and a down stroke. During the middle of the two strokes the LEV mechanism is active. During stroke reversal, or the switch in direction of the wing from upstroke to downstroke (pronation) or vice versa (downstroke) the rotational circulation and the wake capture are active. [54]

Leading Edge Vortex : The leading edge vortex is recognized as the most influential mechanism in lift generation for flapping motion. It is also termed delayed stall, as it occurs angles of attack that will cause stall for fixed wings. LEV occurs when the angle of attack associated with stall is reached. When stall occurs the flow separates from the leading edge and reattaches again before reaching the trailing edge, thus maintaining the Kutta condition, and forming the LEV. The presence of the LEV creates a low pressure region on the top surface of the airfoil, causing a resultant lift force [29].
Wake Capture: Another unsteady phenomena that happens is the wing wake interaction. When the wing motion switches from upstroke to down stroke or vice versa, the wing meets the wake that separated from it earlier. This causes an increase in the effective flow velocity, which in turn creates an aerodynamics force peak during this period. Wing kinematics and the airflow structures determine the effectiveness of the wake capture mechanism. [25][65]
Clap and Fling: This is phenomena is caused by the wing interaction. There two phases, during the first phase (Clap) the leading edges approach each other, then the wing rotates about the leading till the wings are approximately parallel. In the second phase (Fling), the opposite happens, the wings form a gap in between by rotating about the trailing edge, then the wings move away from each other.Experiments conducted on insects showed that during the clap-and-fling motion an increase of lift production occurs. The increase in lift can be explained by the following: The interaction of opposing circulation of each wing causes an attenuation of starting vortex formation. Also The air trapped between the wings is forced downwards at the end of clap causing a downward momentum jet. Moreover, clap and fling causes the formation of a massive LEV which also improves lift production [64].
Tip Vortices: Tip vortices is a phenomena that occurs in fixed wings as well as flapping wings, and is usually associated with a decrease in lift and induction of drag. However, in unsteady flows, Tip Vortices can have a positive influence on the total force exerted on the wing. The Tip Vortices creates a low-pressure region near the wing tip. Moreover, the Tip vortices interacts with the with the Leading Edge Vortices as well as the root vortex, thus enhancing the aerodynamic lift.

2.3.3. Aerodynamic Models

There are many aerodynamic models that try to predict the aerodynamic loading that occur from the aerodynamic mechanisms described earlier. [16] compared several aerodynamic models, including Reynolds Average Navier Stokes Method (RANS), Unsteady Methods, panel methods, quasi steady methods and steady methods, in terms of accuracy, computational and implementation efforts. The results is shown in fig 2.7

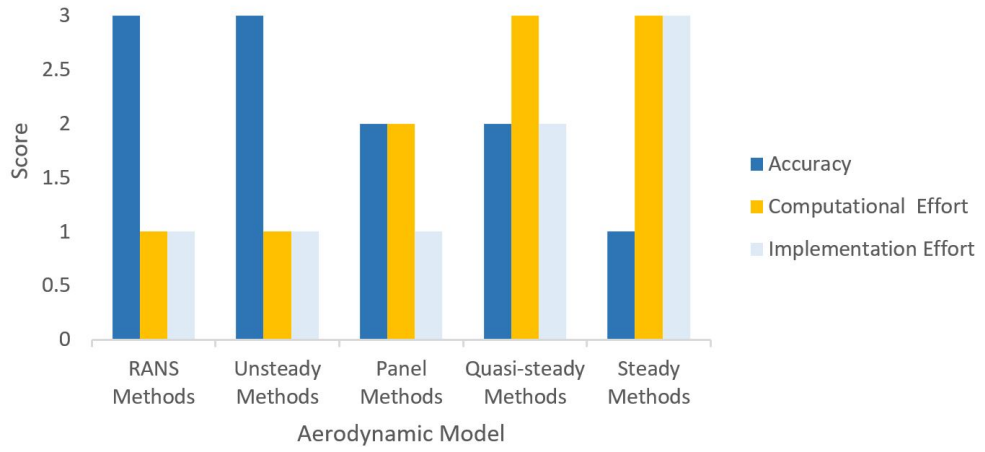


Figure 2.7: Aerodynamic model comparison [16]

RANS Methods: RANS method has been used to predict flow structure on flapping insect wings. The disadvantage of this method is the complexity involved in modeling the flow vortices, making solving the equations difficult. Moreover, there discretization of the mesh is difficult as the mesh needs to be able to handle large deformations for a compliant wing. Thus this methods is fairly accurate however, it is challenging in implementation and require a high computational effort.

Unsteady Methods: Another fairly complex class of models are the Unsteady models. These models focus on the flow separation at the leading and trailing edges and the wake formed by the flapping wing. An unsteady model by Ansari [5] combines two unsteady flow component, which are the leading edge vortex and the trailing edge wake with two quasi steady components, namely, the free stream flow and the unsteady motion of the wing. The methods is 2-D and the total load is calculated by integrating along the span width. The method is able to predict the flow structure and the loads on the wing to a high level of accuracy.

Panel Methods: The basic assumption that characterizes the panel methods is the non viscous flow assumption. In this method we divide the wing into a group of 3-D and 2-D descriptions in a series of flat panels. Similar to boundary elements, vortex sheets are added to the panels after which a Kutta condition is imposed on the circulation of the total of the vortex sheets. These methods have the advantage of efficiency as only the surface needs to be meshed. However, due to inviscid assumption, they cannot model viscous drag forces, which is significant at this scale.

Steady Methods: On the other end of the spectrum there are steady models, which are the simplest in terms of implementation and is based on momentum jet theory used for helicopters. They have the property of being independent of the geometry of the wing, which means that it can be used to give a first estimate of the power consumption and forces generated on a wing of a certain size and frequency. However, of course it cannot be used in the design optimization of the wing.

Quasi-steady Methods: Quasi steady models try to model the unsteady aerodynamics by making the assumption that the instantaneous aerodynamic forces depend on the instantaneous velocity and acceleration of the wing motion. Sane and Dickinson [60] developed an empirically corrected quasi steady model, this method relies on fitting data from kinematically scaled wings. This method was further developed by Wang [74] to calculate the coefficients analytically. He decomposed the flapping motion to take into account the forces that occur due to transitional motion, rotational motion, coupling of both motions as well as added mass effects. Quasi steady models have shown to provide accurate load estimation, without much information on the flow structures. Combined with blade element method, these methods can provide a 3-D model. Quasi steady models can be implemented in optimization while not sacrificing accuracy. Therefore , this method is most popular in flapping wings analysis.

3

Flapping Wing Designs and Design Approaches

In the last chapter the physics of FW wing mechanics, including the shape description, kinematics and aerodynamic aspects of it. In this chapter we present more concrete description on how the flapping design problem is tackled in the literature, and comparing the approaches found. First the morphology of natural flyers wings is examined in order to get an insight on the desired mechanical behaviour of the wing. Then some examples of morphing wing MAVs with avian kinematics are introduced. Although having different wing motion than our desired, we will examine the wing construction to get insight on designing deformable, passive pitching wings. Then the design methodology of FWMAVs with similar kinematics will be investigated. Most commonly top down approach could be found in the literature, however, also some attempts to come up with designs based on analytical models are discussed for rigid as well as deformable wings.

3.1. Bio Inspiration in Flapping Wing Design

Scientists have been amazed by nature's design and try to study and understand the working principles behind it's very intricate mechanisms that have developed through a very long process of natural selection and evolution. They have observed that birds, bats and insects alter the wing shape and projected area while flying in an active and passive manner. An increase in projected area of the wing due to the deformation improves the performance, as the aerodynamic forces changes [64]. This is specially true in insects,as their slender structure can deform to a large extent passively. Bat wings, on the other hand, are made of a thin membrane attached to their finger bones and arm which can contract reducing the span by about 20 percent [65].At a certain speed the flexible wing start to flap, spontaneously, which creates an attached LEV during the downstroke, thus enhancing lift [24]. Insects wings are anisotropic in nature due to the membrane vein structures with a varying thickness[46]. This structure causes the wings bending stiffness is 1 to 2 orders of magnitude more than the torsional stiffness stiffness [21]. A common feature among insect wings is a reinforced leading edge, although the aspect ratio varies among different species[22]. An interesting feature that some insects exhibit such as the dragonfly wing are local variations structural composition and corrugations. These corrugation contributes to the warping rigidity and flexibility [6], however, the aerodynamic advantages are still not very clear[45]. Regarding the kinematics of flight, flies can actively alter the stroke deviation using a set of steering muscles [70][43]. Most insects show U-shaped [34][59] or figure eight flapping motions [44][26] The coupling of anisotropic wing structures, unsteady aerodynamics and kinematics of the wings is a challenging yet to be solved [65].

A closer look into the structure of insect wings

Insect wings are made of a thin chitin membrane which is supported by a system of veins the are running along the span of the wing. The veins are sometimes connected to each other by a number of cross veins. The membrane is usually folded radially outwards from the root. The veins are present either on the crest (convex) or the troughs (concave) of the folds 3.2. The wings is divided into series

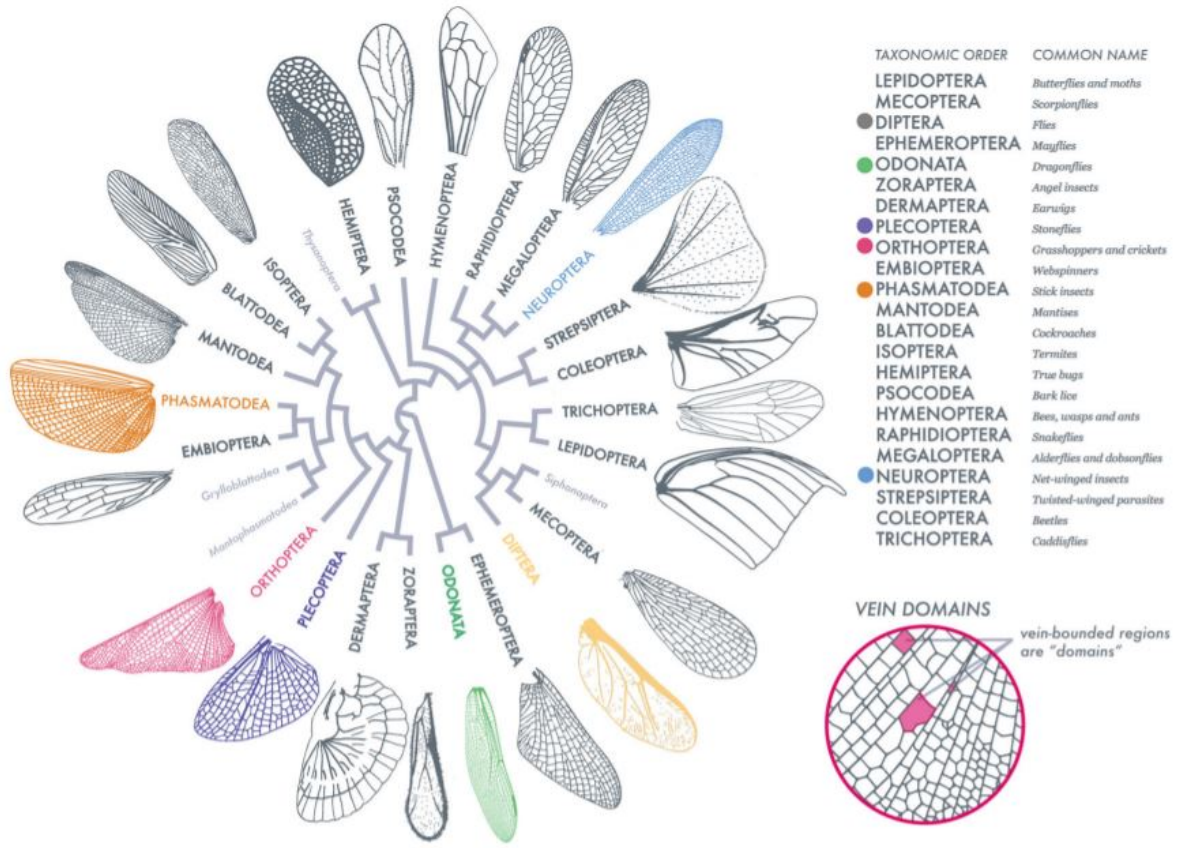


Figure 3.1: Insect wing venation patterns, wing contour and shapes of vein-bounded domains. [2]

of cells of cells by the veins. A cell completely surrounded by veins is called a closed cell, and is called otherwise. In some insects a small region of high density pigment is present on the leading edge of the wing called the pterostigma as can be seen in the wasp wing in figure 3.3. It is thought to decrease flutter and to enhance the passive pitching behaviour of the wing. Due to the nano scale structure the wing, its colour may appear to change with angle of illumination or angle of view.

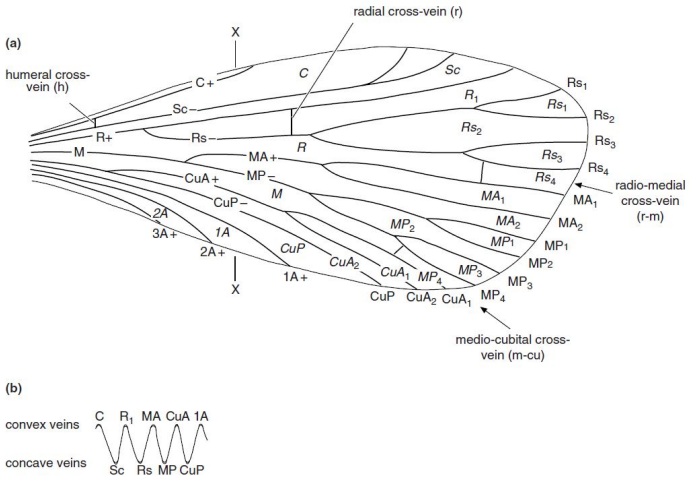


Figure 3.2: Wing venation. Diagram (a) of wing venation shows the main cross-veins and the names of the cells (italicized) enclosed by the veins. Diagram (b) shows a section at X–X in (a) showing the concave and convex veins with an exaggerated depth. [18]

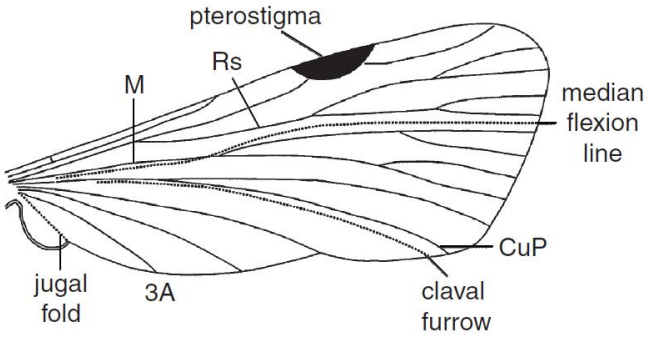


Figure 3.3: A wing of wasp, showing main flexion lines and the pterostigma[18]

3.2. FW Design Approaches

The design of flapping wing MAVs can be approached from two ways. The first one and the most common one is the top down approach, where the design of the MAV is done on larger scale, then attempting step by step to reduce the size of the MAV. This approach is usually done because of lack of knowledge of the system and difficulty of modeling FWMAV discussed earlier. The other approach is the bottom up approach where we build and test the small parts necessary to make a functioning MAV. We try to understand the aspects that influence the design and come up with new understanding and techniques. The top-down approach have limitations that it is time consuming and might not recognize significant parameters in the design. While the bottom up approach might be focusing on detailed aspects that might not be important for having a flying system. The wing construction is very important in determining its performance and the design approach. A common construction of the wing is a PET foil reinforced with carbon fibre polymer rods. This choice of construction has the downside problem that the manufacturing process cannot be automated. Moreover, this construction leads to limited the design options. For these limitations, other methods have been researched that rely on MEMS manufacturing or 3D printing.

3.2.1. Morphing Avian Wings

Morphing flapping wings have been mostly researched and applied in larger MAV with avian kinematics. Despite the difference in kinematics and scale from our desired design, insight can be drawn from the working principles in achieving passive deformation. In such designs, it is desirable to achieve a nonlinear behaviour for the wing, with high stiffness during the downstroke, while being flexible during upstroke. Wissa [78] designed a bird like robot, with a wing design that managed to achieve a 45% power saving. The wing is supported by a spine made of a series of compliant hinges. The compliant hinges have are constrained in one direction and free to deform in the other, which leads to the desired non linear force deflection behaviour mentioned before. Another design by Billinsgley [10] where he tried to achieve less air resistance during the upstroke, through reduction of effective surface area, by incorporating a torsional spring at the middle of the leading edge spar. The design have shown an increase of 300% of the next lift, however, with an increase in thrust as well which was undesirable. Lentink [67] also developed a bat inspired wing that unfolds passively after a number of flapping cycles. By controlling the folding actively and the unfolding passively, the MAV is be able to achieve variable wing span size on demand with reduced energy requirement.

3.2.2. Experimental Design approaches with similar FW kinematics

Experimental design, which is a top down approach, is the most common approach in current operating MAVs. Although being time consuming procedure and doesn't lead to optimal designs, this method is popular because it provides a design that is guaranteed to work as expected, and eliminates the need to model the complex aeroelastic behaviour of the wing. The Delfly,[36] being one of the most successful operating MAV's wing design is worth investigating. The Delfly II base design is made of 5 μm thick mylar renforced with 0.28 mm diameter carbon rods . The wing has straight trailing edges as seen in Fig 3.4 to create tension in the wing to resist forces induced during flapping.

In their optimization, they tried to systemically vary the stiffness of the wing by optimizing the position

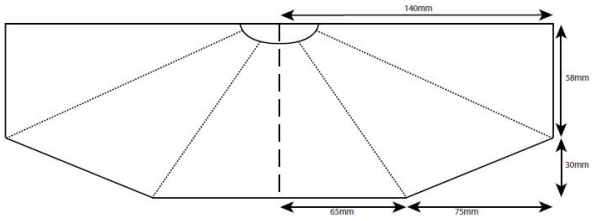


Figure 3.4: Delfly II wing, dashed lines represent the carbon rods position [36]

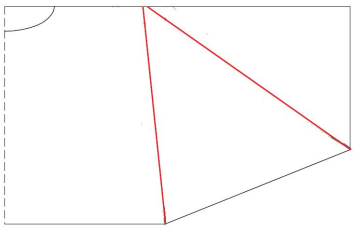


Figure 3.5: Optimized Delfly wing stiffeners orientation [36]

and angle of the 2 stiffener spars, while keeping the wing span and area constant.The ratio of the power to lift was then measured to determine the performance of the tested wings designs. Tests have shown that a stiffeners converging towards the leading edge have better performance. The Optimal configuration is shown in Figure 3.5 having the first and second stiffeners has an angle of 84° and 35° with the horizontal.

For the humming bird of TAM University, Coleman [19] used an experimental wing design approach with an objective of maximizing deformation , due to the relation with minimizing power consumption. They tested 50 different designs with slight variations to the base line design, and the deformation was recorded using a strobe light. The design has a flexible hinge at the root to further increase the twist of the wing.They discovered that the most influential parameters, on the the lift are the stiffness of the leading edge spar and the existence of a cross spar. If the leading edge spar is too compliant, it will cause the wing to bend out of plane and degrade performance. They also hypothesised that the existence of cross spar increased the deformation due to the inertial loading it creates during stroke reversal. The base line design and optimized design can be seen in figure 3.6.

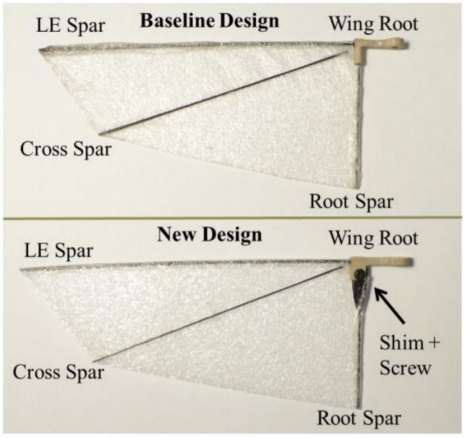


Figure 3.6: Basline design vs. optimized design with flexible hinge [19]

Another humming bird MAV [50] optimized the wing for power generation by varying the slackness of the wing, its aspect and taper ratios and surface area. Their optimization process indicated that the camber angle, which was defined as the angle between the wing root edge and a normal to the leading edge as critical parameter. They related increasing the camber angle to the foil becoming slacker, thus affecting the twist and camber distribution along the wing span. They ended up with a trapezoidal wing

design with a straight leading edge and aspect ratio of 9.3.

A third MAV inspired by a humming bird was developed by [40] Defense Advanced Research. They attempted to design a wing that is durable, reliable to manufacture, having fast stroke reversal and produces low noise. The wing design involved two phases in the wing design: First a computational step to obtain a baseline design with an initial planform and twist distribution, which is followed by an experimental phase, during which 300 iterations were performed to improve the performance and approach optimality. In all the trials span-wise main spar and a chord wise root spar were made of carbon fibre, while trying different membrane materials and spar diameters. This tests showed that wings having span wise main spar and a chord wise root spar and diagonal stiffeners have optimal perfomance. An example of a nominal wing is shown in Fig 3.7.

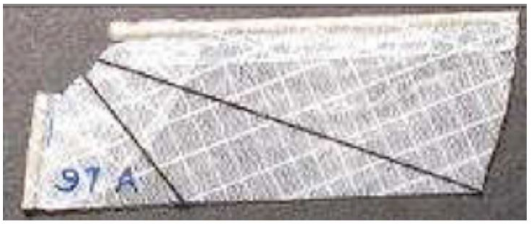


Figure 3.7: Nominal Wing Design of Humming bird Nano [40]

The final example is the KU Beetle [55], which used the Unsteady Blade Element Method to evaluate different designs performance with the aim of to obtain high lift to power ratio. This model was also validated experimentally, and shown that wings with veins placed outboard in the certain locations can cause a improvement in lift production and less power consumption.

3.2.3. Analytical Design approaches with similar FW kinematics

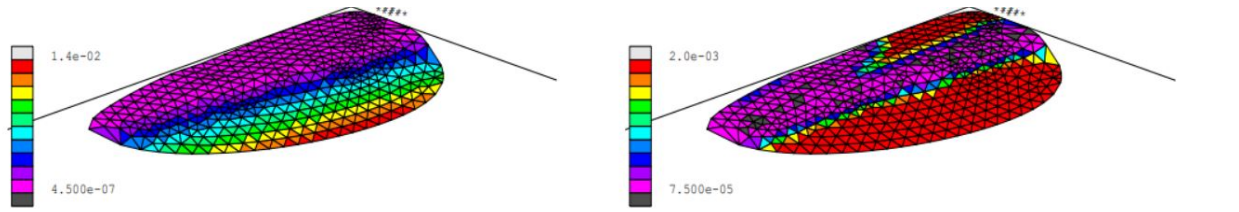
Several attempts have also been made to try to develop analytical models that can be used in optimizing the parameters of the wing to achieve better performance. However, there is still a lot of work to be done in this field as there has been no complete attempt to achieve a functional, optimal flapping wing up till now. Some of these attempts will be discussed in this section, which are divided into two main categories namely, rigid and flexible wings.

In the Rigid Wings modeling approach, the wing is assumed to be rigid, with a stiffness at the root that will allow the wing to achieve the desired pitch angle. Bolsman [16] did an optimization of the wing root torsional stiffness. He assumed that nonlinear root stiffness has a cubic relation with angle, and then optimized the root stiffness coefficient that provides a passive pitching motion closest to sinusoidal. He calculated the forces on the wing using the quasi steady model and assumed sinusoidal sweeping motion and no heaving motion.

In order to improve the efficiency of the wing by including the deformation of the wing, some models try to include the flexibility of the wing. Qi Wang [75] tried to design a wing that produces optimal twist, by minimizing the power required for hovering. He used a quasi steady force model [74] and coupled it with an analytical model of the twist to achieve the required required design. He performed his analysis on twistable wings and rigid wings with root stiffness, and came up with optimal values for wing stiffness and flapping frequency.

Stewart et al.[66], performed a plan form shape and thickness optimization of flapping wings with the a multi-objective optimization . They performed a Fluid, structural analysis, where the plan form was parameterized by the modified Zimmerman method and the thickness having polynomial distribution.

In his MSc. thesis, Anirudh [51] tried to achieve a design with continuous stiffness, thus eliminating the stiffness at the root, while still trying to achieve the required angle of attack. He used the quasi steady model developed by Qi Wang to estimate calculate the average load at 2 time instances, during stroke reversal and during mid stroke, then interpolated the force along the wing to get a distributed load. He then set up and optimization problem, where he used the thickness of the elements as design variable, and an objective to maximize the deformation at the tip with a constraint on bending, thus achieving twist. Two different designs came from the optimization for the two different load cases. Shown in Figure 3.8 the design obtained at stroke reversal.



(a) Average Displacement [m] plot of the obtained design. (b) Thickness distribution [m] plot of the obtained wing design.

Figure 3.8: Thickness optimization results by Anirudh for the stroke reversal load case [51]

Another similar research was conducted by Anul and Sunil [4], formulated the problem as an optimization problem, with the goal of mimicking the deformation of hawkmoth wing.

3.3. Concluding Remarks

The purpose of the complex morphology of the insect wings is difficult to decode, but some information could be inferred from the global behaviour. From the structural point of view the wings, have a peculiar feature. It seems to be optimized for stiffness in bending, while being compliant in torsion. We can see that different attempts to design FW MAVs having this property, either by design or by optimization and testing. Most wings we have discussed share common features like stiff leading edge to support the wing in bending, a chord-wise spar to provide inertia for rotation and cross spars to support tension in the membrane. A flexible root is also implemented when possible to increase the effective angle of attack. However, there are problems associated with the current designs related to the manufacturing, reliability, and optimality.

Most of the designs were made of Mylar sheet with carbon rod reinforcement. This type of construction makes it impossible to achieve optimal wing planform and pitching axis location discussed in the previous chapter. With the current construction, the leading edge needs to be straight and needs to to coincide with pitching axis, Moreover, the trailing edge needs to be made of straight segments to support membrane, thus the wings cannot be having the desired optimal geometry. From the structural perspective, the available wings are very fragile, making them susceptible to breaking if mishandled or in the case of a minor impact. They are also not durable as they only operate for a number of cycles after which they have to be replaced because of the wear that cause drastic decrease in efficiency [23]. Another major issue is the inability to reproduce identical wing characteristics during the manual assembly of the wing. It is very difficult to tune the tension in the Mylar sheet [36], precisely place the carbon rods as well and accurately tune the stiffness of the root[16][57][72]. A slight deviation can cause a big impact on the performance of the wing and also as the wings need to be identical for stability during hover.

Anirudh FEM modeling approach [51] on the other hand allowed to create wings with optimal kinematics and shape, and resulted in desired deformation behaviour at certain load case. Such a design also eliminated the need to add the root stiffness element which was shown to be problematic, in an attempt to achieve the pitching behaviour with deformation within the wing itself. However, thickness optimization method showed that it still suffers from certain limitations. For example, at lift maximizing load case with no inertial loading it failed to achieve the required angle of attack.The reason is that his method relied heavily on inertial loading due to varying thickness rather than change in moment of inertia of the structure. Anirudh used shell finite elements to model the wing. Shell structures have a very interesting feature, which is that by changing the curvature of the shell, the properties of the shell can vary drastically, thus their exists space for design optimization. Shape optimization is well known and developed area in structural mechanics, in which we achieve a certain mechanical behaviour by changing the geometrical parameters of the structure. If we apply this technique to shell structures with the goal of achieving the mechanical properties mentioned earlier, we could achieve a wing shape with a corrugated pattern similar to the one that was observed on insect wings. Thus exploiting the properties of shells to achieve the mechanical behaviour we want while maintaining minimum weight, just like in insects wings.

4

Structural Optimization of Flapping Wings with a Finite Element Model

In this chapter, the modelling of the mechanical behaviour of the wing as a continuous deformable structure is discussed, as well as how its design can be formulated as a structural optimization problem. The main aspects required to perform such an optimization and the methods applied in the literature is reviewed and compared. Finally some examples of shape optimization of shell structures are shown. These examples have been chosen as they resemble a similar optimization model and strategy to the one the author intends to use in his research.

4.1. Shell Structures

Shells can be considered as a generalization of an isotropic homogeneous plate. A plate is structure whose dimensions in plane is much larger than the thickness direction. It is defined by its mid plane, thickness and material properties. The mid plane in a plate is flat, while it can curved in shell. A shell has a low thickness to minimal radius ratio (less than $\frac{1}{50}$). Like plates, when shells are subjected to out of plane loading it causes larger displacements than in plane loads. However, due to the initial curvature that shells have it allows it to transfer the loads in plane thus having a more efficient structural performance [12]. This advantageous structural performance combined with advancement in numerical methods for the analysis of shells makes it attractive for use by engineers in their designs. However, some basic knowledge of the mechanical behaviour and the underlying theories is needed. Due to its simplicity membrane theory is often used to describe shell behaviour. However, in some cases, particularly at boundaries, bending needs to be accounted for to compensate the distributed membrane field as seen in figure 4.1.

4.1.1. Finite Element Modeling of the Wing

The wing geometry represents a membrane like structure having a relatively small thickness compared to its surface area. Such structures can be modelled by Shell finite elements. Shell structures are common in engineering applications due to their efficient load carrying capacity [53]. There are many types of shell elements developed, varying in shape, number of nodes, number of degrees of freedom and the underlying mathematical model. Bathe [17] proposed these four criteria for a shells to be applicable to be used in modeling engineering problems.

- Reliability
- Computational effectiveness
- Generality i.e should be applicable to non linear analysis, thick thin shells and any shell geometry
- Mechanistically clear and simple enough to make the elements suitable for engineering analysis.

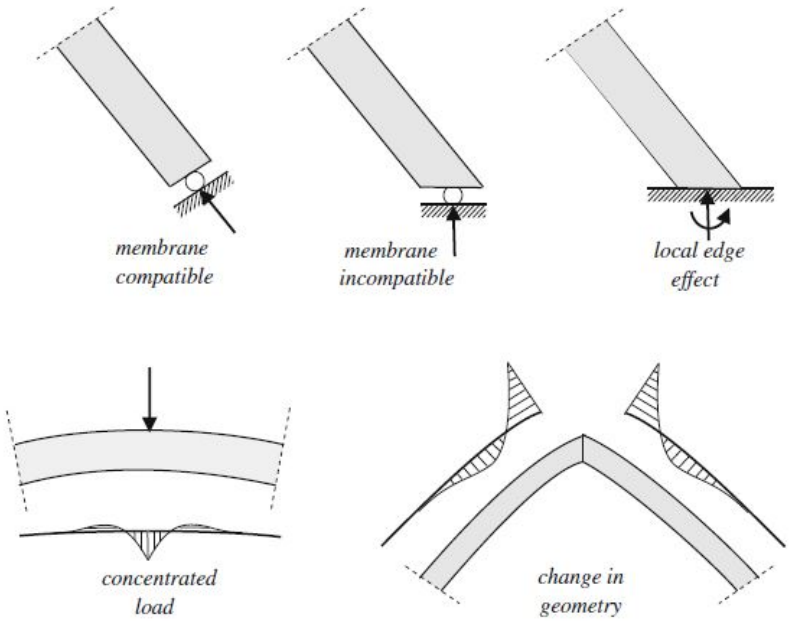


Figure 4.1: Membrane and bending conditions[12]

A common problem faced by shell elements is the phenomena of membrane and shear locking. Remedies of such problems include reduced order integration [38] and spurious mode control [7]. Van Keulen [71] developed an element based on the simple facet element with 12 nodal degrees of freedom, namely 9 translations of the nodes and 3 rotation about each side (Figure 4.2). This element has been established by combining constant strain triangle, and the well known Kirchhoff-Love and Mindlin–Reissner plate bending. This element doesn't suffer from shear locking and satisfy the requirements mentioned earlier.

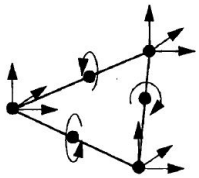


Figure 4.2: Nodal degrees of freedom of triangular facet element [42]

4.2. Shell structures FE Modeling in COMSOL

COMSOL is commercial software that is used to conduct multi-physics simulations. COMSOL has optimization module which is able to do shape and topology optimizations. In the most recent update COMSOL 5.5 added shell shape optimization feature which will be the main tool used in this research for the wing design.

The shell is described by providing its thickness, a possible offset, and the material properties. The shell element is of a Mindlin-Reissner type, which means it accounts for the shear deformation and can be used for thicker shells. The shell has a MITC formulation (Mixed Interpolation of Tensorial Components). It does not take the strain components directly from the shape functions of the element. Instead, carefully selected interpolation functions are used for the individual strain components. The values of the interpolated strains are then at selected points in the element tied to the value that would be computed from the shape functions. The interpolation functions and tying points are specific to each element shape and order[49]. The dependent variables are the displacements u_i in the global directions x_i , as well as the displacements of the shell normals a_i also defined in the global directions.The degrees

of freedom represent the displacements on the reference surface.

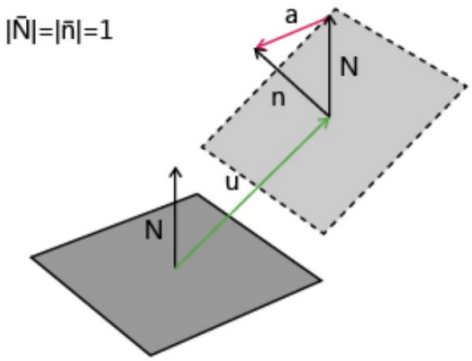


Figure 4.3: The degrees of freedom in the shell interface. N is the normal vector in the original configuration and n is the normal in the deformed state. [49]

4.2.1. Strain calculation

We define **r** to be the position of the mid surface. The surface local curve linear coordinates ξ^i and **n** to be the local normal to the surface and the thickness of the shell is given the variable **d**. ξ^1 and ξ^2 are are defined on the surface of shell, with ξ^3 is normal to the shell. The position of the deformed midsurface is given by **r**+**u**, and deformed normal is calcualted as **n**+**a**. To keep the normal a unit vector the condition |**n**+**a**| = 1 needs to be satisfied. The rotation vector is related to the surface normal displacement and is defined as:

$$e_\theta = \frac{\mathbf{n} \times \mathbf{a}}{|\mathbf{n} \times \mathbf{a}|}. \tag{4.1}$$

A lagrange basis function is used to interpolate the vectors **r**, **u**, **a**, and **n**.With the assumption that the position of a point within the shell after deformation depends linearly on ξ^3 coordinate which gives

$$\mathbf{x}(\xi^1, \xi^2) = \mathbf{r}(\xi^1, \xi^2) + \mathbf{u}(\xi^1, \xi^2) + \xi^3(\mathbf{n}(\xi^1, \xi^2), \mathbf{a}(\xi^1, \xi^2)). \tag{4.2}$$

The in-plane Green-Lagrange strain in the local co-variant components is expressed as

$$\epsilon_{\alpha,\beta} = \frac{1}{2}\frac{\partial(\mathbf{r}+\mathbf{u}+\zeta^3)}{\partial\xi}.\frac{\partial(\mathbf{r}+\mathbf{u}+\xi^3)}{\partial\xi} - \frac{1}{2}\frac{\partial(\mathbf{r}+\mathbf{u}+\xi^3)}{\partial\xi}.\frac{\partial(\mathbf{r}+\mathbf{u}+\xi^3)}{\partial\xi}, \tag{4.3}$$

with indices α and β ranging from 1 to 2. This gives equation 4.4,

$$\epsilon_{\alpha,\beta} = \gamma_{\alpha\beta} + \xi^3\chi_{\alpha\beta} + (\xi^3)^2\kappa_{\alpha\beta}, \tag{4.4}$$

where

$$\gamma_{\alpha\beta} = \frac{1}{2}[\frac{\partial\mathbf{u}}{\partial\xi^\alpha}\frac{\partial\mathbf{r}}{\partial\xi^\beta} + \frac{\partial\mathbf{r}}{\partial\xi^\alpha}\frac{\partial\mathbf{u}}{\partial\xi^\beta} + \frac{\partial\mathbf{u}}{\partial\xi^\alpha}\frac{\partial\mathbf{u}}{\partial\xi^\beta}], \tag{4.5}$$

$$\chi_{\alpha\beta} = \frac{1}{2}[\frac{\partial\mathbf{r}}{\partial\xi^\alpha}\frac{\partial\mathbf{a}}{\partial\xi^\beta} + \frac{\partial\mathbf{a}}{\partial\xi^\alpha}\frac{\partial\mathbf{r}}{\partial\xi^\beta} + \frac{\partial\mathbf{u}}{\partial\xi^\alpha}\frac{\partial\mathbf{n}}{\partial\xi^\beta} + \frac{\partial\mathbf{n}}{\partial\xi^\alpha}\frac{\partial\mathbf{u}}{\partial\xi^\beta} + \frac{\partial\mathbf{u}}{\partial\xi^\alpha}\frac{\partial\mathbf{a}}{\partial\xi^\beta} + \frac{\partial\mathbf{a}}{\partial\xi^\alpha}\frac{\partial\mathbf{u}}{\partial\xi^\beta}], \tag{4.6}$$

$$\kappa_{\alpha\beta} = \frac{1}{2}[\frac{\partial\mathbf{a}}{\partial\xi^\alpha}\frac{\partial\mathbf{n}}{\partial\xi^\beta} + \frac{\partial\mathbf{n}}{\partial\xi^\alpha}\frac{\partial\mathbf{a}}{\partial\xi^\beta} + \frac{\partial\mathbf{a}}{\partial\xi^\alpha}\frac{\partial\mathbf{a}}{\partial\xi^\beta}, \tag{4.7}$$

While the transverse shear strain is given by

$$\epsilon_{3\alpha} = \epsilon_{\alpha 3} = \frac{1}{2}[\frac{\partial}{\partial\epsilon^\alpha}(\mathbf{r}+\mathbf{u}+\xi^3(\mathbf{n}+\mathbf{a})).(\mathbf{n}+\mathbf{a}) - \frac{\partial}{\partial\xi^\alpha}(r+\xi^3\mathbf{n}).\mathbf{n}] = \zeta_\alpha + \xi^3\omega_\alpha, \tag{4.8}$$

where ζ_α and $\omega_{\alpha\beta}$ are given by:

$$\zeta_\alpha = \frac{1}{2}[\frac{\partial \mathbf{r}}{\partial \xi^\alpha}.\mathbf{a}] + \frac{\partial \mathbf{u}}{\partial \xi^\alpha}.\mathbf{n} + \frac{\partial \mathbf{u}}{\partial \xi^\alpha}.\mathbf{a}], \tag{4.9}$$

$$\omega_{\alpha\beta} = \frac{1}{2}\frac{\partial \mathbf{n}}{\partial \xi^\alpha}.\mathbf{a} + \frac{\partial \mathbf{a}}{\partial \xi^\alpha}.\mathbf{n} + \frac{\partial \mathbf{a}}{\partial \xi^\alpha}.\mathbf{a}. \tag{4.10}$$

One can observe the terms responsible for non linearity, namely the products between u, a, and their derivatives. The contributions from the parts $\kappa_{\alpha\beta}$ and ω_α can be ignored in the analysis as they have usually small values.

4.2.2. Fold lines

Fold Lines are edges connecting two shell elements at an angle. The convention in COMSOL is that this angle must be greater than 3° to be considered a fold line. At a fold line the displacement of the shell normal is not uniquely defined. An assumption that COMSOL makes with fold lines is that the angle of shell normals connected by a fold lines remains constant before and after deformation. This relationship can be expressed by equation 4.11 shown below

$$n_j.n_k = (n_j + a_j)(n_k + a_k). \tag{4.11}$$

4.3. Optimization of structures

Structural optimization is combining the principles of mechanics and mathematics to come up with a design that is optimal according to some criteria defined by the designer. It usually follows a cycle as shown in the Figure 4.4. The loop usually starts with an initial design, after which a sequence of procedures is performed on the design in order to update this design. The aim is to incrementally update design so that it outperforms the previous design, until we eventually reach a design that is optimal.

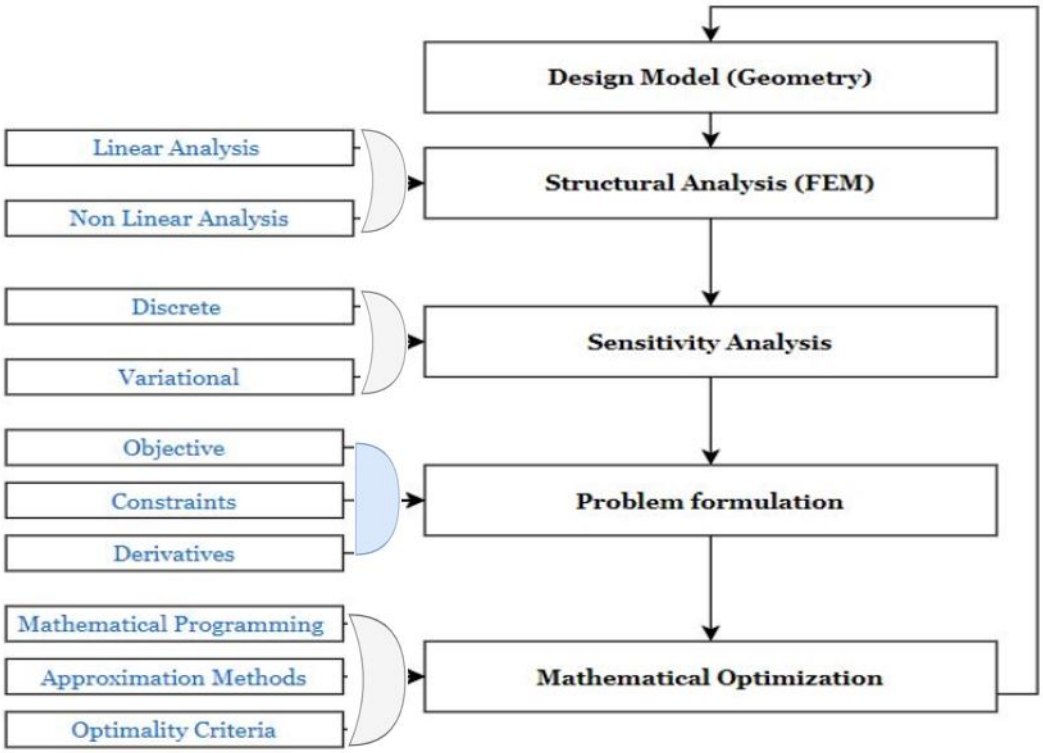


Figure 4.4: Optimization Loop [56]

4.3.1. Problem Formulation

Structural Optimization problems are formulated the following form:

$$Minimize \quad f(\mathbf{s},\mathbf{u}), \qquad \mathbf{s} \in R^n \tag{4.12}$$

$$Such\ that \quad g_i(\mathbf{s},\mathbf{u}) \leq 0, \qquad i = \{1,..,n\} \tag{4.13}$$

$$h_j(\mathbf{s},\mathbf{u}) = 0, \qquad j = \{1,..,m\} \tag{4.14}$$

$$\mathbf{s}_l \leq \mathbf{s} \leq \mathbf{s}_u \tag{4.15}$$

f being the objective function, *g* the inequality constraint, *h* the equality constraint, **s** is the design variable vector, **u** the state variable vector (eg. displacement), $\mathbf{s}_u$ and $\mathbf{s}_l$ are upper and lower limits of the design variable **s**.The objective function can be compliance, displacement of certain point. Constraints can include stress and buckling. The objective and constraint equations can be reformulated into a single function called the Lagrangian function . .

$$L(\mathbf{s},\mathbf{u},\lambda,\mu) = f(\mathbf{s},\mathbf{u}) + \sum_{i=1}^{n} \lambda_i \cdot g_i(\mathbf{s},\mathbf{u}) + \sum_{j=1}^{m} \mu_j \cdot h_j(\mathbf{s},\mathbf{u}); \quad \lambda_i > 0, \quad \mu_j \neq 0, \tag{4.16}$$

The Lagrangian function provides the basis for many constrained optimization algorithms.

4.3.2. Design Parameters

Structural design optimization problems can have different types of design variables. The design variable has an influence on the choice of the objective function and constraints as well as the mathematical optimization algorithm chosen. Typical design variables in structural optimization problems include sizing, material, shape and topology (Figure 4.5). Sizing optimization is usually related to a change in dimension in one geometrical aspect of the structure or a constituent of it. An example would be thickness optimization of the finite elements that make up the structure. Material Optimization is the process of changing the mechanical behaviour of the structure by changing its properties. An example would be changing the young modulus of the finite elements or changing the orientation of fibres in a composite structure. Shape optimization is optimization by altering the shape of the structure, while maintaining the same topology. Examples include altering the nodal coordinates of finite elements, control point coordinates of CAD models. In Topology optimization the design space and the boundary conditions of the structure are specified by the designer and the optimizer calculates the optimal material distribution within this space. The most famous topology optimization method is SIMP [8].

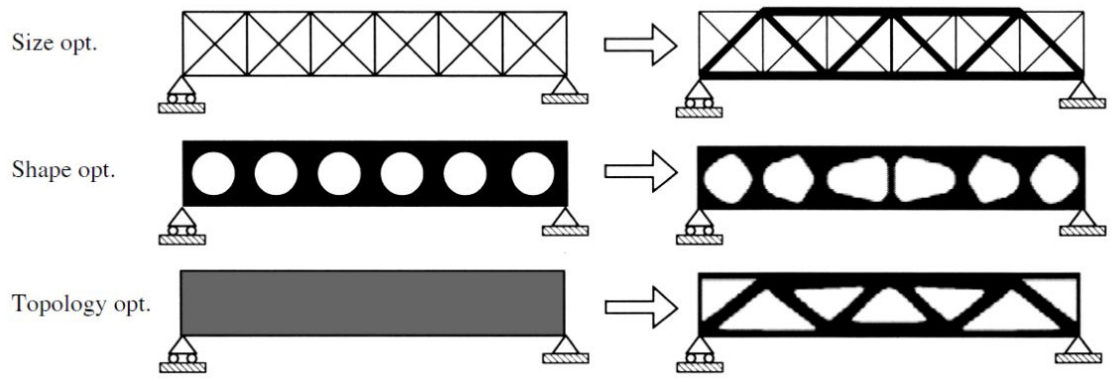


Figure 4.5: Design Variables of Structural Optimization Problems [3]

4.3.3. Sensitivity Analysis

Sensitivity analysis is the change of the response function with respect to the design variable. It provides the direction and in which the optimizer should move towards. It allows us to use gradient based optimization methods, which are much more efficient compared to zeroth order methods. Moreover, knowing the influence of changing each design variable on the objective function provides insight for the designer. There are 2 basic approaches for sensitivity analysis, namely the variational and discrete approaches. In the variational approach the continuum equations are differentiated before discretization. On the other hand in the discrete approach we calculate the derivative after the discretization. For each approach we can calculate the sensitivity directly or using the adjoint formulation.

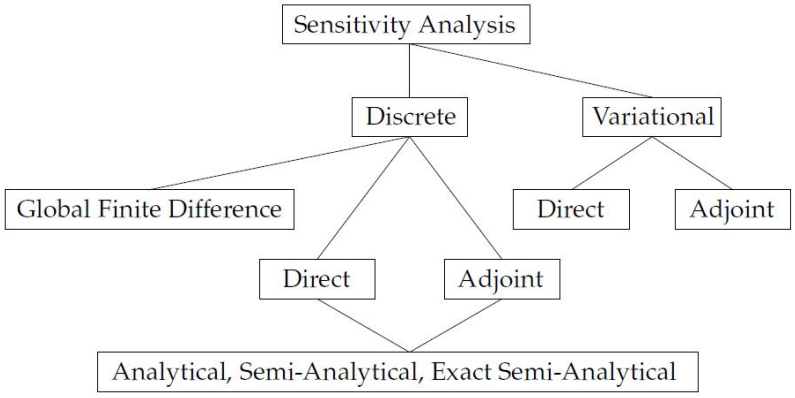


Figure 4.6: Sensitivity Analysis Methods [31]

Analytical sensitivities algorithms are efficient and accurate but have the disadvantage of being difficult to implement. Work on analytical sensitivity analysis of shells can be reviewed in [79]. Global finite difference is the application of forward or centre finite difference method to compute the sensitivity. It is easy to implement and can be used to compute the sensitivities for response functions which we are not able to differentiate analytically. The disadvantage of this method is that it requires a high computational effort and that it suffers from approximation errors. This makes it usually applied when the number of design variables is small.

4.3.4. Discrete Sensitivity Analysis

The discrete approach can be derived in the direct and the adjoint formulation. In the direct sensitivity analysis, the state derivative is computed explicitly for each design variable. This leads to the need to solve a number of equations equal to the number of design variables, making it very inefficient for the case of large number of design variables, therefore the adjoint method is introduced.

The derivation of the state derivative for linear and non linear finite element analysis is presented below, which is important as it is used in calculating both the direct and adjoint sensitivities. We present the semi analytical method, which we use to compute the state derivatives derived. The semi analytical method is based on applying the finite difference method for the calculation of the derivatives of the stiffness and load. A corrected formulation is presented to account for large rotations. Then the adjoint method is presented for non linear FEM problem for the efficient calculation of the sensitivity of the response function *h*.

State derivative calculation

The discretized governing equations of Linear elastic Finite Element models are written as:

$$\mathbf{f}^{ext}(\mathbf{s}) = \mathbf{K}(\mathbf{s})\mathbf{u}(\mathbf{s}), \tag{4.17}$$

where **K** is the global stiffness matrix, **u** is the global displacement vector, and $\mathbf{f}^{ext}$ is the external load vector. Implicit differentiation of equation with respect to the design variables s_i results in the following equation:

$$\frac{\partial \mathbf{f}^{ext}}{\partial s_i} = \frac{\partial \mathbf{K}}{\partial s_i}\mathbf{u} + \mathbf{K}\frac{\partial \mathbf{u}}{\partial s_i}, \tag{4.18}$$

Then we can calculate the state derivative as.

$$\frac{\partial \mathbf{u}}{\partial s_i} = \mathbf{K}^{-1}\left(\frac{\partial \mathbf{f}^{ext}}{\partial s_i} - \frac{\partial \mathbf{K}}{\partial s_i}\mathbf{u}\right) = \mathbf{K}^{-1}\mathbf{f}^{*}, \tag{4.19}$$

where $\mathbf{f}^{*}$ is the pseudo load vector. The derivatives of the element data i.e the Stiffness matrix and load matrix can be calculated efficiently using the semi analytical sensitivity analysis

$$\mathbf{f}^{*}(s_i) = (1/\Delta si)\left(\mathbf{f}^{ext}(s_i + \Delta s_i) - \mathbf{f}^{ext}(s_i) + \mathbf{K}(s_i + \Delta s_i) * \mathbf{u} - \mathbf{K}(s_i) * \mathbf{u}\right). \tag{4.20}$$

However, for elements undergoing large rotations the derivative calculations of the stiffness matrix need to be. Several work has been done to come up with an exact semi analytical method that doesn't suffer from this deficiency which includes the work done by Bletzinger [14]. Using the work of Van Keulen [41][15] we adjust the pseudo load to take into account rigid body rotations as follows:

$$\mathbf{f}^{*} = \frac{\partial \mathbf{f}^{ext}}{\partial s_i} + \frac{\partial \mathbf{K}^{e}}{\partial s_i} * \mathbf{u}^{e}_{de} + \left(\frac{\frac{\partial r_k}{\partial s_i}.\mathbf{K}^{e}.\mathbf{u}^{e}_{de}}{r_k.r_k}\right)r_k + \left(\frac{r_k.\frac{\partial \mathbf{K}^{e}}{\partial s_i}.\mathbf{u}^{e}_{de}}{r_k.r_k}\right)r_k + \alpha^{k}\mathbf{K}^{e}\frac{\partial r_k}{\partial s_i}, \tag{4.21}$$

Where $\alpha^{k} = \frac{u^{e}_{de}.r_k}{r_k.r_k}$. Here $\mathbf{K}^{e}$ is the the element stiffness matrix. r_k is the rigid body mode number k. $\mathbf{u}^{e}_{de}$ is the part of displacement $\mathbf{u}^{e}$ which leads to the deformation of the element. $\frac{\partial r_k}{\partial s_i}$ can be evaluated analytically because the rigid body modes are known as a function of the design variables and $\frac{\partial \mathbf{K}^{e}}{\partial s_i}$ can be evaluated using finite differences. We can repeat the same procedure for the non linear governing equations, which can be represented as:

$$\mathbf{f}^{int}(\mathbf{u},\mathbf{s}) - \mathbf{f}^{ext}(\mathbf{u},\mathbf{s}) = 0, \tag{4.22}$$

Differentiating with respect to **s** we get.

$$\frac{\partial \mathbf{f}^{int}}{\partial s_i} + \frac{\partial \mathbf{f}^{int}}{\partial \mathbf{u}}\frac{\partial \mathbf{u}}{\partial s} - \frac{\partial \mathbf{f}^{ext}}{\partial s_i} - \frac{\partial \mathbf{f}^{ext}}{\partial \mathbf{u}}\frac{\partial \mathbf{u}}{\partial s} = 0, \tag{4.23}$$

Thus the state derivative can the be calculated as

$$\frac{\partial \mathbf{u}}{\partial s_i} = \left(\frac{\partial \mathbf{f}^{int}}{\partial \mathbf{u}} - \frac{\partial \mathbf{f}^{ext}}{\partial \mathbf{u}}\right)^{-1}\left(\frac{\partial \mathbf{f}^{ext}}{\partial s_i} - \frac{\partial \mathbf{f}^{int}}{\partial s_i}\right) = \mathbf{K}_t^{-1}\mathbf{f}^{*}_{nln} \tag{4.24}$$

where $\mathbf{K}_t^{-1}$ and $\mathbf{f}^{*}_{nln}$ are the tangetial stiffness matrix and the non linear pseudo load respectively.

Adjoint method sensitivity analysis for Non Linear FEM

We then proceed with the adjoint method, which is a more efficient method to calculate the sensitivities of the response function *h*. We will be using the non linear state derivative calculated earlier.

$$\frac{dh}{ds_i} = \frac{\partial h}{\partial s_i} + \frac{\partial h}{\partial \mathbf{u}}\frac{\partial \mathbf{u}}{\partial s_i}. \tag{4.25}$$

Substituting the state derivative we get

$$\frac{dh}{ds_i} = \frac{\partial h}{\partial s_i} + \frac{\partial h}{\partial \mathbf{u}} \left(\mathbf{K}_t^{-1} \mathbf{f}_{nln}^* \right) \tag{4.26}$$

This can be rewritten in the adjoint form as:

$$\frac{dh}{ds_i} = \frac{\partial h}{\partial s_i} + \left(\mathbf{K}_t^{-1} \frac{\partial h}{\partial \mathbf{u}} \right)^t \mathbf{f}_{nln}^* = \frac{\partial h}{\partial s_i} + \lambda \mathbf{f}_{nln}^*, \tag{4.27}$$

where $\left(\mathbf{K}_t^{-1} \frac{\partial h}{\partial \mathbf{u}} \right)^t$ is the adjoint variable λ.

After the setting up our problem and calculation of the sensitivities we need to choose a proper optimizer to iteratively update the design. The Method of Moving Asymptotes (MMA) transforms the original optimization problem, which is usually non convex, into a convex problem with asymptotic behavior to the upper and lower boundaries. It doesn't a need feasible starting point and deals with non linear and equality constraints.

4.4. Shell Structures Shape Optimization

Shape parameterization is a popular design variable choice in shell structure optimization problems. This reflects the effectiveness of shape changes on improving the structural performance of a design [37]. In this section FE based shape parameterization will be presented as well as two examples having two different shape optimization approaches for compliance minimization of shell structures.

4.4.1. FE based parameterization

Selecting the Finite elements nodes as a degree of freedom has advantages to other shape parameterization methods such as CAD based and morphing boxes approaches. It can explore larger design space, as well as avoids the needs for re-parameterization. However, it may problems such a a jagged boundaries shown in Figure 4.7 as well as distorted mesh.

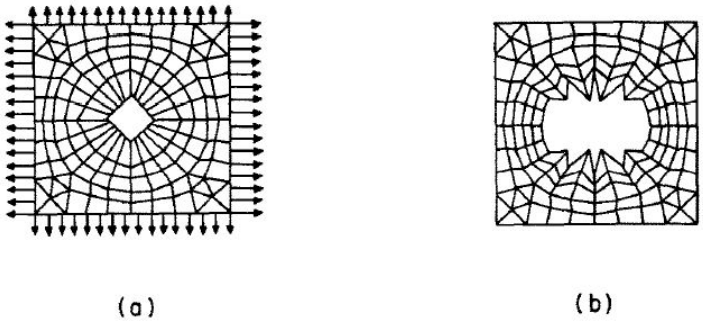


Figure 4.7: Independent node movement technique for a hole in a plate: (a) initial design; (b) final design. [33]

The jagged boundaries is due to non smooth sensitivity field, attempts smoothing of the sensitivities is done by applying a filter on the sensitivity at each node. As for mesh distortion this can be adjusted either by Geometric or mechanical mesh regularisation methods. In geometrical regularization a local mesh improvement criteria is implemented. An example of a simple geometrical regularization technique is called the umbrella operator. This method is one of the Laplace smoother methods. It calculates the optimal position x^* of an inner node using the positions of the surrounding nodes. This relation can be expressed by:

$$x^* = \frac{1}{N} \sum_{n=2}^{N+1} x_i$$

This operator is known to work well for triangular elements that's why it will be used in this research. A schematic of the regularization process by the Laplace smoother is shown in figure 4.8

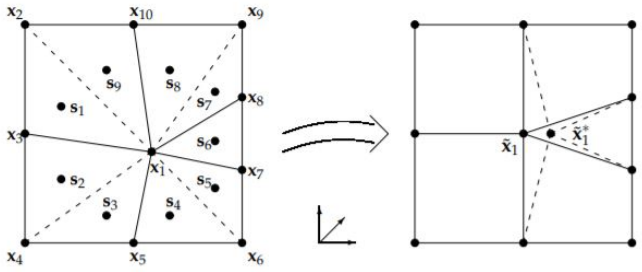


Figure 4.8: Mesh regularization by Laplace smoother [31]

4.4.2. Examples of shape optimizations of shell structures

TUM: At Technical Univeristy of Munch, [32] [48] used FE based parameterization along with mesh regularization techniques for optimization of shell structures. He divided the coordinates of the FE mesh into two groups, denoted by n_i and t_i respectively. n_i, which determines the geometry of the model are chosen as the set of design variables for optimization while t_i, contain the internal and the tangential components which define the shape of the element but not the shape of the component. This coordinates can be shown in Figure 4.9

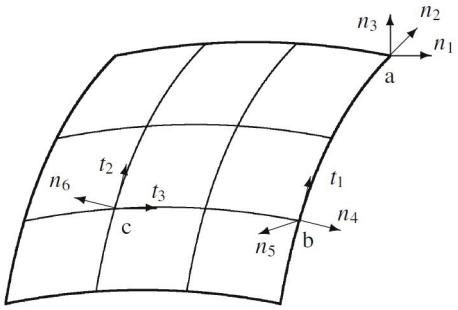


Figure 4.9: FE coordinates definition by Firl [32]

To avoid jaggedness problem discussed earlier, he applied out of plane regularization in the form of convolution integral for the design sensitivities, which is form of filtering process. In-plane mechanical regularization was applied to minimize mesh distortion, by proposing a method based on the Updated Reference strategy method. This approach was tested for several examples including compliance minimization of a simply supported shell structure (4.10. The results show mesh Independence and similar results for linear and non linear analysis.

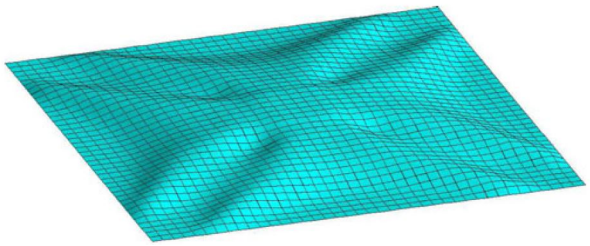


Figure 4.10: Optimal shape of a Shell with simply supported boundary conditions for compliance minimization problem, TUM[32]

Toyota Technological Institute: A research conducted at Toyota [62][47][63] attempted to do shape optimization of shells, by applying a derived shape gradient function in the direction normal to the shell surface. This gradient function is applied as as pseudo external forces to vary the surface and to minimize the objective function which was in this case the stiffness. The optimization procedure is given in the flow chart in figure 4.11. This method was applied to design several shapes of brackets

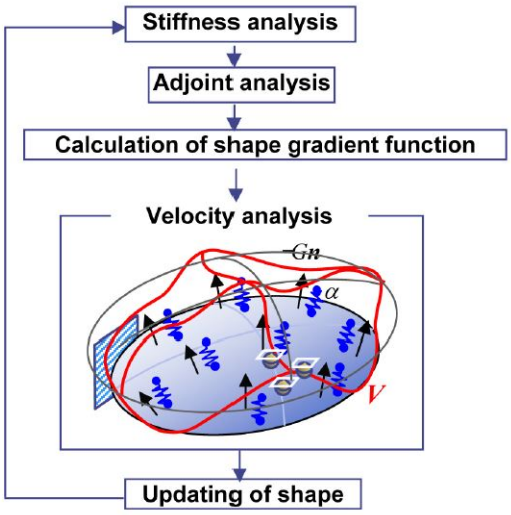


Figure 4.11: Free form optimization procedure by Shimoda[62]

as well as a square plate simply supported at the edges. The intial and final designs are shown in figure 4.12

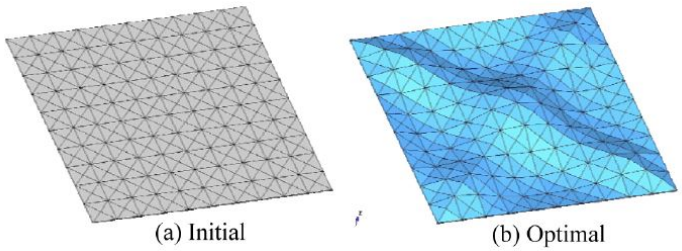


Figure 4.12: Shape Optimization of a Shell with simply supported boundary conditions compliance minimization, Shimoda [62]

5

Shell Shape Optimization Method for Passively Pitching Wings

The intent of this chapter is to implement the shape optimization method to come up with a wing design that will exhibit passive pitching behavior. The desire for passive pitching behaviour is motivated by observations in nature and numerical analysis conducted in the literature, that shows efficient wing flapping for pitching wings. The optimization process is conducted with a static non linear finite element analysis.

Shape Optimization is something observed in in nature specially for thin walled structures to improve performance. An insect wing aeroelastic properties is influenced by the corrugation pattern it exhibits. Shape optimization is also utilized for engineering structures, usually with the purpose of compliance minimization. Figure 5.1 shows a variety of shapes that outperforms a flat sheet of paper in term of rigidity.

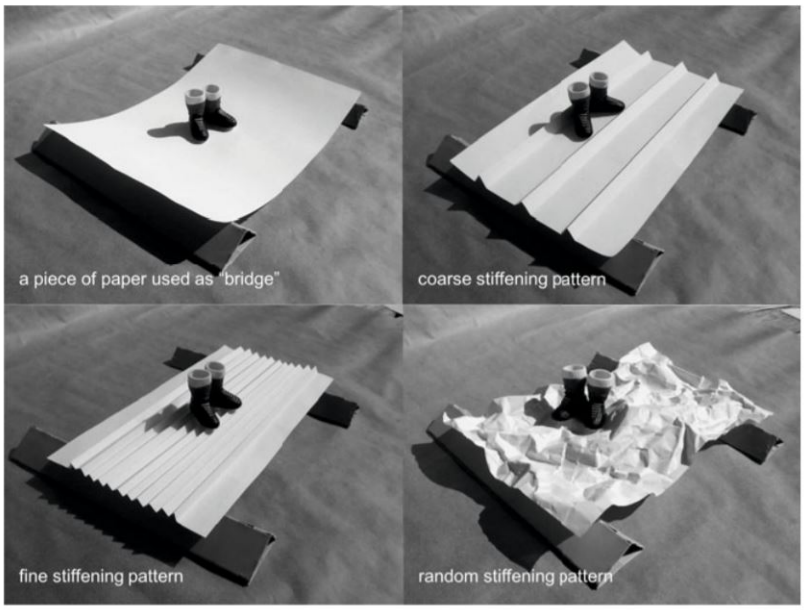


Figure 5.1: [13]

Shell Shape Optimization has the advantage that it can achieve the required mechanical behaviour without an increase in weight, which is a crucial factor in designing an efficient MAV. Moreover, it can be combined with other forms of optimization such as topology or thickness optimization. Some disadvantages of shell shape optimization is that its highly non convex optimization, so might lead to

sub-optimal designs or multiple designs. Moreover, it usually entails a high number of design variables making it computationally expensive. Another difficulty that might arise is the inaccuracies related to the FE modeling of the folds. Due to the high non linearity of the problem, the folded regions result sometimes in discontinuity in the displacement fields,which needs special types of elements to model. This limitation will result in an inaccuracy in the FE results and consequently the optimization.

5.1. Passive Pitching as an Optimization Goal

We would like to select an objective function that will give as a measure of the power efficiency, or in other terms setup a surrogate model. A surrogate model optimization is usually formulated for complex optimization problems where it is difficult to quantify the desired objective. This is common in flapping wing design due the complexity in modeling the aerodynamics, specially for a flexible corrugated wing. In this section we investigate the effect of wing twist and pitching behaviour on the wing performance as a possible candidate for a an alternative objective that we can use in our optimization. Based on the quasi-steady aerodynamic model, translational Lift, which is the main lift mechanism in flapping wings, is given by the following equation:

$$L = \frac{1}{2}\rho U(r)^2 c(r) C_l(\alpha(r)) dr. \tag{5.1}$$

Translational Drag has the same form but with C_d instead of C_l. Force coefficients (C_l and C_d) for a scale model of Drosophila at Re ≈ 100 was determined expirementaly by Dickinson et al. shown in Fig. 5.2. As we can see the maximum Lift is obtained at an angle of attack 45 degrees, while maximum efficiency (C_l/C_d) is achieved at a lower angle. Thus we can already see that for a rigid wing non twisted wing, having a pitching motion is a more desirable kinematics to have.

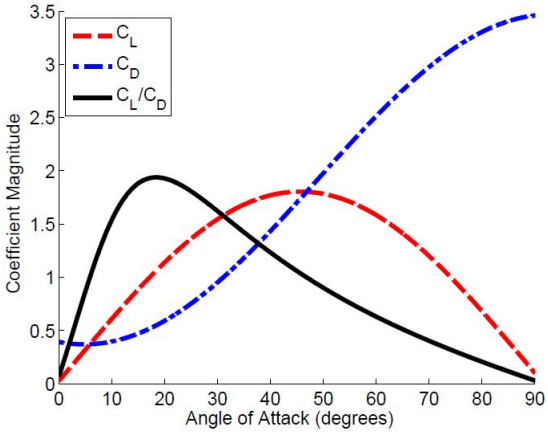


Figure 5.2: [20]

Another aspect that is needed is twist, due to the circular motion of the wing, twist is needed to maintain an optimal angle of attack throughout the span of the blade. Changing the angle of attack of a wing can be achieved by twisting the wing as can seen in figure 5.3.

Wing twist can also be achieved passively during flapping motion due to a flexibility of the wing. This has been observed in many natural flyers including insects and humming birds. This Flexibile twisting behaviour has been proven to be important in efficient flapping.

Du and Sun [27] studied the relation between the deformation of flapping wings and the resulting aerodynamic forces and power consumption. They found that a flexible wing that exhibits a 20°and 6% camber would increase the lift to drag ratio by 20% and result in power savings of 16% . Also, [52] performed an FSI analysis of on a revolving flexible wing with hawkmoth shape and kinematics. It was shown that the wing flexibility can enhance the aerodynamic performance of the flexible revolving wing specially at larger angle of attacks. This effect takes place in the two phases of flapping, acceleration and steady rotation phases. During the acceleration phase, large inertial and aerodynamic forces causes large dynamic deformations which reduce the angle of attack at wing tip. At steady rotation,

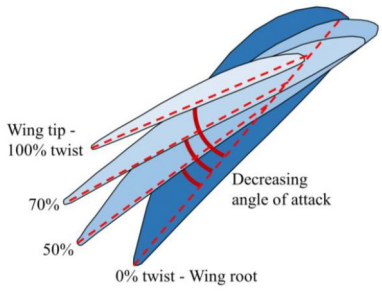


Figure 5.3: Twist profile [20]

the wing deformation is small and the reduction of the angle at the tip is less however it still increases the translational lift at higher angles of attack (40°–60°) while reducing translational drag forces.

[20] used a quasi steady model to find the optimal twist profile which is displayed in figure 5.4.

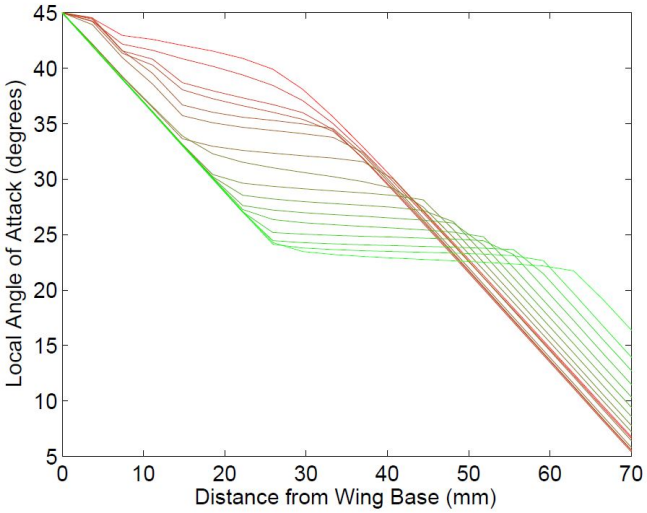


Figure 5.4: Optimal twist using quasi steady model [20]

The curves shows optimal wing twists for wings of different objectives (lift maximization and power minimization). Lower green curve shows the twist with a power minimization objective. As we can observe a trend of having a twisted profile is also shown by this optimization.

One way of achieving wing flexibility is through the root. A flexible root can be used to connect the wing to the MAV body. This root which is present in insect wings as well as synthetic wings will allow the wing to achieve the required high AOA. In most synthetic wings the elastic element is made of spring steel [16] or polymide film. [72] Modeled the root as an elastic element of linear stiffness with pitching angle. However, due to the combined loading conditions and high deformations a more accurate model is needed. According to Qi Wang [72],the design of the root based on a split tube [35] is thought to be worth investigating it can provide rotational compliance while constraining heaving motion of the wing. Meindart [57] has designed a novel X shaped hinge which is capable of achieving the bending and torsional behaviour. However, there remains problems related to the reproducability of the wings due to the manual process involved in their manufacturing.

5.1.1. Problem Formulation

After concluding that passive pitching is important in efficient wing design, we use this information to setup an optimization problem to come up with wing designs that exhibit this mechanical properties. A passively pitching wing should exhibit twisting behavior without comprising bending stiffness. A deformation profile similar to the one shown in figure 5.5 is attempted, with the point P having a high vertical deformation, while the leading edge remain relatively undeformed.

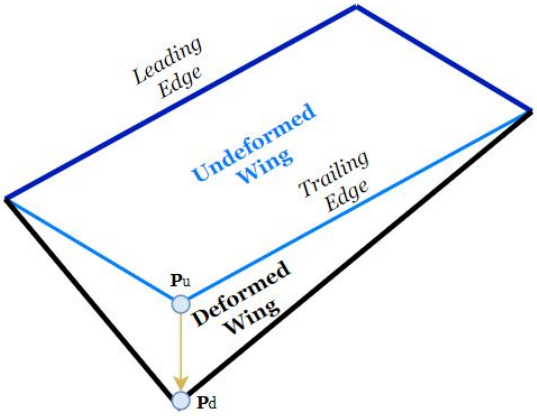


Figure 5.5: Deformation of the wing that we aim to achieve

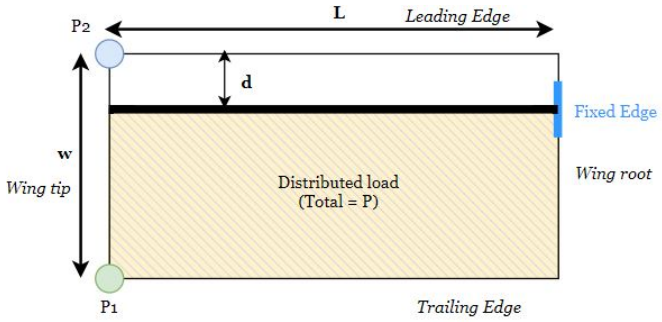


Figure 5.6: Geometry and boundary conditions

In an attempt to achieve this deformation profile, A simple rectangular plate is investigated as seen in fig. 6.1 with with length L, width w and constant thickness t. A fixed edge boundary condition is applied at the root and a constant distributed load, with a sum of total sum of P is applied on the area of the wing below the pitching axis. Due to the high geometric non linearity of problem, load is applied incrementally using an auxiliary sweep. The load is a follower load to the shell surface. Material non linearity is neglected in this analysis. The default solver MUMPS was used for non linear analysis, as for the Optimization, the solver was chosen to be GCMMA. The Optimization was divided into two Models, the first Model is displacement minimization, while the second Model is based on an angle objective

Parameter	Value
Length (L)	1 [m]
Width (w)	0.5 [m]
Thickness (t)	0.005 [m]
Young's Modulus (E)	2.7 [GPa]
Mesh size	0.05 [m]
Filter radius (R)	0.01 [m]
Max displacement of mesh (d)	0.2 [m]

Table 5.1: Model A parameters.

Analysis Settings	Value
Geometrical Non Linearity	Yes
Material Non Linearity	No
Auxiliary Sweep of load P	4-20, step size 2
Equations Solver	MUMPS
Max number of iterations	25
Optimization Solver	MMA
Max number of Model Evaluations	2000

Table 5.2: Shape Optimization analysis settings on COMSOL.

5.2. Model A

For Model A the Optimization problem was formulated as a displacement minimization problem at the trailing edge tip with a constraint on the leading edge tip as shown below.

$$Minimize \qquad u_{p1}, \qquad \mathbf{s} \in R^n, \tag{5.2}$$

$$Such\ that -0.005 \leq u_{p2} \leq 0. \tag{5.3}$$

The objective function and constraints was formulated similar to Anirudh's model [51]. Anirudh managed to achieve a high twist to bending ratio for the MAV wing by having an objective and constraints of the same form. The goal is to achieve high twist angle at the tip, while minimizing out of plane deformation (bending). Very limited deformation is allowed at point p2, this is to achieve the bending stiffness required mainly and also to observe a a large variation from the baseline design. This will be beneficial when analyzing the sensitivities later on. The objective and constraints were implemented on COMSOL as a point sum objective and a point sum inequality constraint respectively. The control variables was the free shell shape optimization of the wing surface, excluding the borders to maintain the overall planform shape of the wing. The optimization parameters chosen are provided in tables 5.1 and 5.2 respectively.

The resulting optimized shape of the wing has chordwise folds that are highest towards the root and flattens out as we move towards the tip. In the spanwise direction the leading edge is highly curved upwards at the root and becoming flat when it reaches the tip. We observe less severe out of plane variation in the spanwise direction for all sections.

We can also observe an effect on the displacement field gradient. The gradient in the initial design is mostly in the x-direction, while the optimized design has a rotated gradient directed towards the trailing edge tip. The results of displacement field and the corresponding angle is shown in the table. The optimized design show a significant improvement in bending angle compared to the flat plate. Even though the displacement gradient is rotated for the optimized design, the torsional behaviour has worsened. The displacement of the leading edge tip is close to the set constraint but it hasn't been satisfied.

	Displacement[m]		Angle [deg]
	Point P1	Point P2	
Initial Design	-0.234	-0.199	3.55
Shape Optimized Design	-0.022	-0.0078	1.61

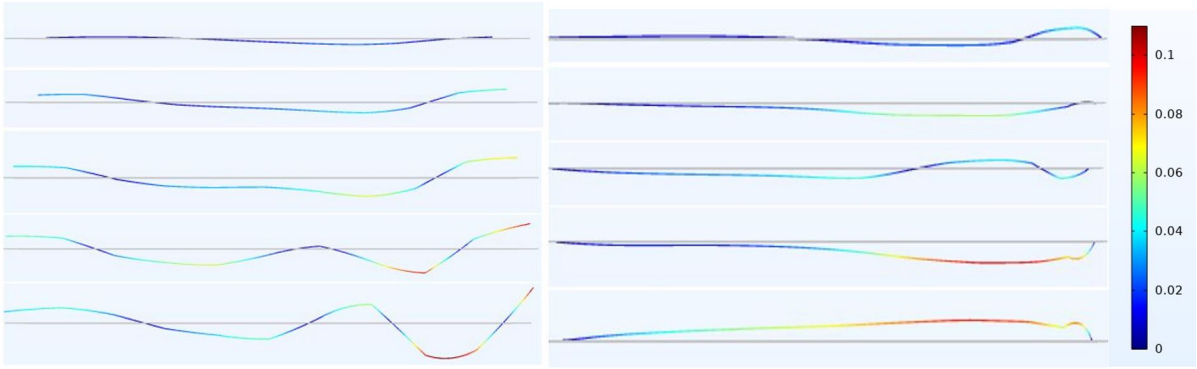


Figure 5.7: Results of shape optimization: On the left span wise cross sections are taken at 0.2 m intervals top to bottom is tip to root. On the right chord wise sections are taken at 0.1m intervals, top to bottom is Trailing edge towards Leading Edge. The colour bar shows the relative out of plane displacement of the surface, 1 being the displacement of the highest point

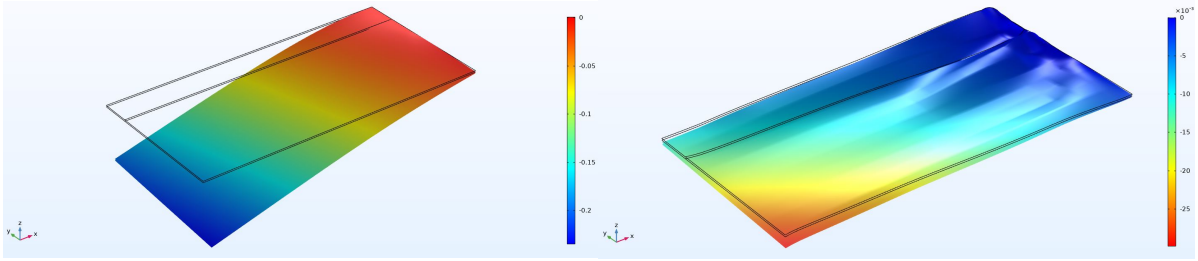


Figure 5.8: Initial Design with displacement field

Figure 5.9: Final Design with displacement field

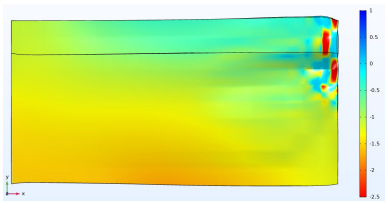


Figure 5.10: Model A Rotation about y axis θ_y [deg]

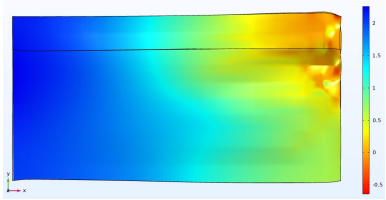


Figure 5.11: Model A Rotation about x axis θ_x [deg]

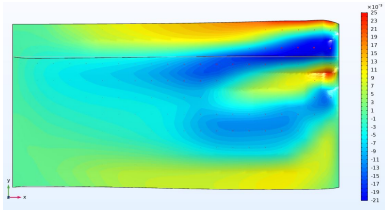


Figure 5.12: Model A Variation in shape from the flat plate in the Z direction [m]

The results of Model A show that the optimized design succeeded in stiffening the beam in bending. However, the pitching behaviour was not achieved. The bending behaviour can be considered satisfactory, because the constraint was too difficult to achieve in the first place. The constraint is not strictly imposed as the optimiser uses a penalisation method for the constraints.
The optimizer produced a design that consists of chord wise folds. This out of plane variation in shape causes the wing shell element to carry load using membrane action thus making this region stiffer. Towards the tip the wing is more flat to allow higher deflection, however, because of the overall stiffness of the wing, the deformation is still very small.
Several problems were faced during the optimization which is believed to have prevented the optimization model from achieving the required angle of attack. The first problem is an over constrained design, the bending constraint provided might be a unrealistic while achieving the required pitching. This can be improved either by eliminating it and replacing it with another objective function for minimizing bending, or by making the constraint comparable to the deformation that the flat plate design will undergo. Another aspect is the objective itself, a better objective would be maximizing the angle at point P2 because unlike the displacement objective, it doesn't worsen the bending objective. The Results show that shape variation near the root at the pitching is important, therefore the shape optimization degree of freedom should be set free. This will not affect the overall planform shape of the wing and will help improve bending behaviour by creating a fold that extends till the root.

Another aspect to consider is how much degree of geometrical non linearity we would like to have.

This is related to the applied loads or/and the thickness chosen for the wing. We will focus on the load while keeping the thickness constant. A sensitivity analysis can thus be performed to observe the effect of the load on the sensitivity field, and consequently on the final design. A higher load comes at the cost of a much more computationally expensive Non Linear analysis, which is a limitation we have in this research. A coarser mesh will improve the computational effort needed, however, the effect of the mesh size on sensitivity field will also need to be studied to ensure mesh in dependant results. Finally the effect of the filter radius will be investigated. A larger filter radius has a smoothing effect, which prevents mesh distortion, however, if a too large filter radius is be applied information will be lost which will lead to sub optimal designs. In the coming sections these problems will be tackled systematically to get a final design with the requirements set.

5.2.1. Sensitivity Analysis

Sensitivity analysis is performed on Model A to understand the effect of some parameters on the final design, without the need to perform the full optimization every time. Sensitivity is the effect of certain variable on the response function, which is part of the optimization process. The sensitivity values are obtained at the initial design. The effect of the distributed load, mesh size and filter radius on the sensitivity field will be investigated.

Load Sensitivity Analysis

The effect of the magnitude of the load is first investigated. The aim is to see the effect of the load on the sensitivity and consequently on the final design. The effect of loads at load steps of 1, 10 and 20 was investigated. 20 being the final load used for the optimization is Model A. The sensitivity field for the three load cases are displayed in figure . For the three load cases we can observe a common feature of a higher ridges at the leading edge and L shape ridge at the trailing edge that extends from the root until approximately mid span. For higher loads we can see a different pattern towards the pitching axis, with double folds emerging instead of a single one. This is related to the degree of non linearity that the forces can achieved. High forces expose non linear behaviour of shells, thus more variation and more folded patterns is achieved.

Mesh Sensitivity Analysis

The effect of the mesh size on the sensitivity is also investigated. Usually we would like the sensitivity to be mesh independent, mesh dependant sensitivity is known when dealing with semi analytical sensitivities of shell structures [14][41]. Although Comsol utilizes analytical derivatives for sensitivities calculation, which shouldn't show this phenomenon the results show mesh dependant results as shown in figures. Here the filter radius was chosen to be equal to the mesh size. The sensitivities failed to converge with decreasing mesh size, even if we reached extremely small values of mesh sizes.

Filter Radius Sensitivity

Filter radius sensitivity will be studied to examine its effect. In a compliance minimization example by Firl [31] shown that the curvature of the optimal geometry decreases when the filter radius increases. Thus, application of a large filter radius yields to smooth geometries whereas a small filter radius allows for wavy geometries. We would like to have a smaller filter radius to exploit non linear behaviour of folds, however, very sharp angles can lead to discontinuity in shell finite elements , which is difficult to model by current shell elements. This is even bigger problem for coarser mesh. Sensitivity studies results are shown with filter radius of 0.1 0.05 and 0.01. The results show that the for larger filter radius causes a smearing effect of the sensitivities. This effect diminishes for smaller filter radius. Studies of filter radius less than 0.01 produced identical sensitivity field to a filter radius of 0.01. This indicates that decreasing the filter radius beyond the element size is unnecessary and will not produce a deign with more kinks and folds.

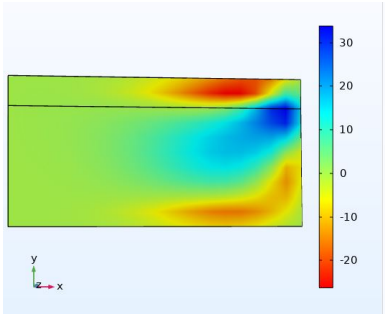


Figure 5.13: F=1 N

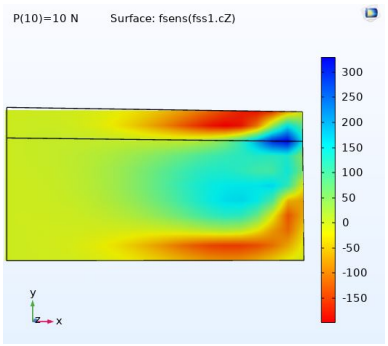


Figure 5.14: F=10

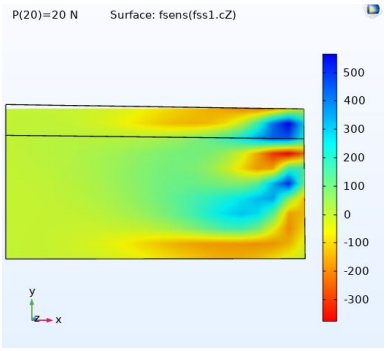


Figure 5.15: F=20

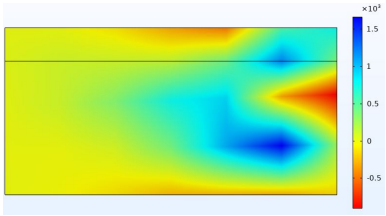


Figure 5.16: Coarse Mesh

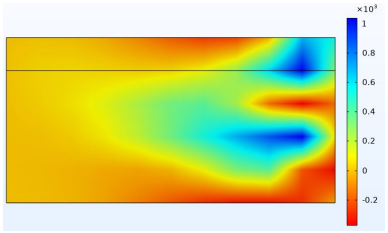


Figure 5.17: Normal Mesh size

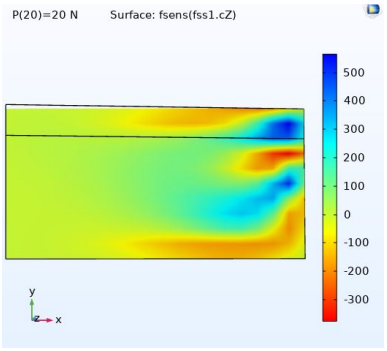


Figure 5.18: Fine Mesh Szie

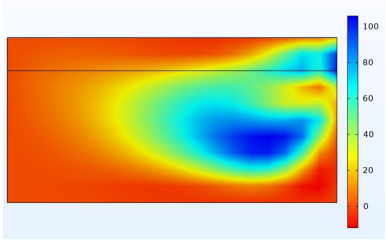


Figure 5.19: Filter Radius = 0.1

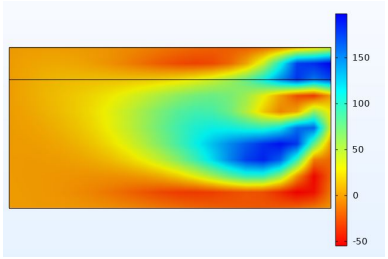


Figure 5.20: Filter Radius = 0.05

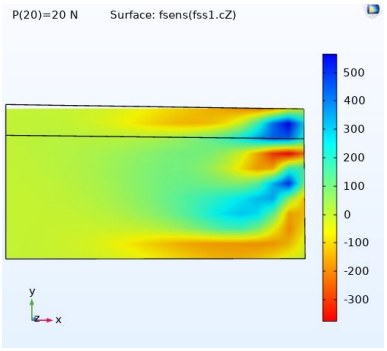


Figure 5.21: Filter Radius =< 0.01

5.3. Model B

In this model an improved version of the design of the initial model is provided, with an angle objective, instead of a displacement. It is a direct measure of the objective, therefore, we expect improved designs and faster convergence. For this Model, constrained and non constrained optimization will be attempted. For the Non constrained optimization Model B1, the objective will be the minimization of the bending angle at the leading edge tip and maximizing the twist at the trailing edge tip. For constrained optimization, angle and displacement constraint were simulated on the leading edge tip. Due to very high computational time a coarser mesh will be used. The importance of including a highly non linear analysis is shown in the previous sensitivity study, therefore a load which causes significant deformation will be applied. Filter radius is chosen to be less than the element size to eliminate the smearing out effect and end up with more distinct features in the final designs. A summary of different optimization models is shown in figure 5.22

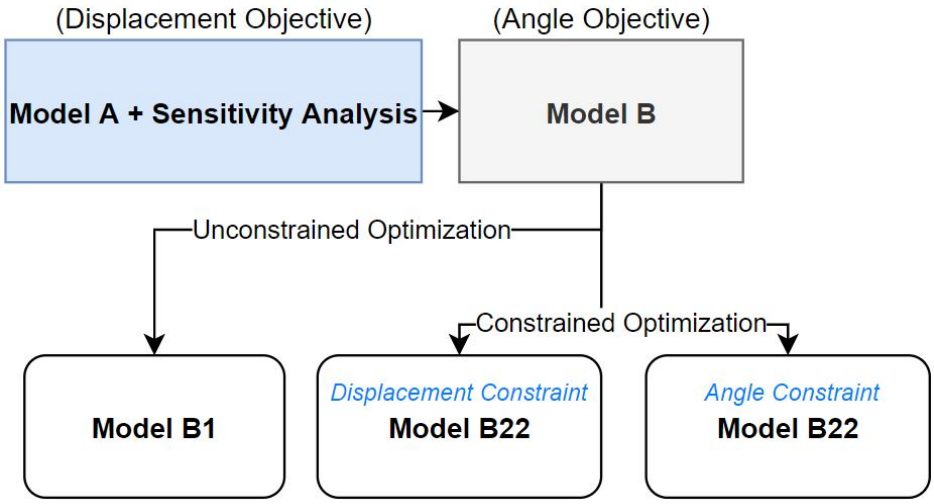


Figure 5.22: Optimization Models Flow Chart. Information about the optimization parameters were inferred from previous analysis of Model A as well as sensitivity analysis performed.

5.3.1. Model B1 - Non constrained Optimization with angle objective

In this model, the constraint on the leading edge tip is replaced by a bending angle objective (rotation about Y axis) is implemented. After applying different weights to the the optimization study a twist to bending ratio of 5 was selected as it maximizes twisting behaviour while still achieving bending stiffness.

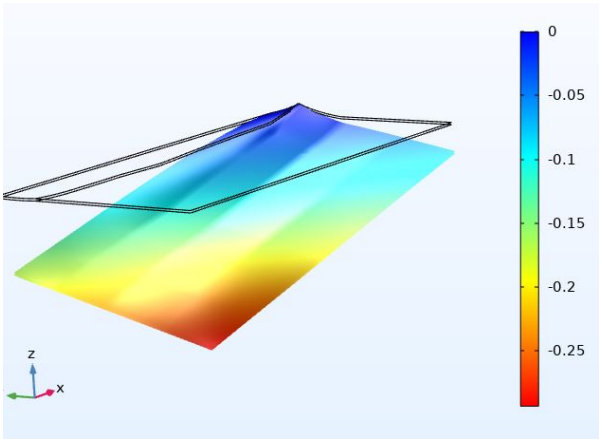


Figure 5.23: Model B1 vertical displacement field with 2 points fixed at the root

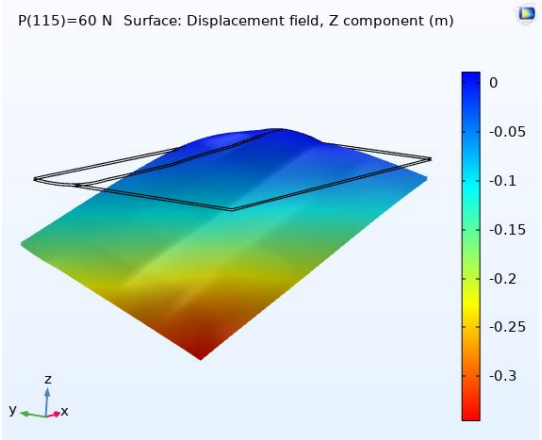


Figure 5.24: Model B1 vertical displacement field with 2 points fixed at the root

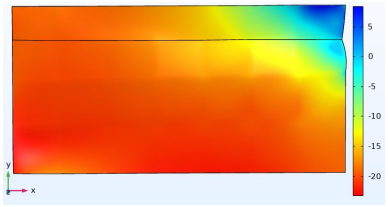


Figure 5.25: Model B1 Rotation about y axis θ_y [deg]

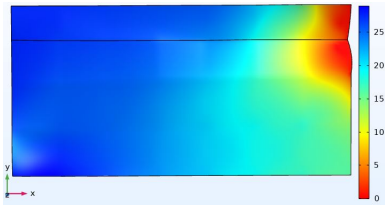


Figure 5.26: Model B1 Rotation about x axis θ_x [deg]

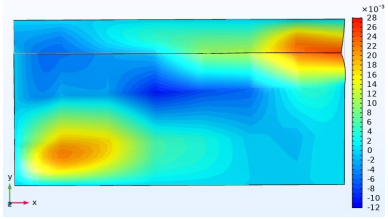


Figure 5.27: Model B1 Variation in shape from the flat plate in the Z direction [m]

Model B1 shows a significant improvement on than twist the previous model. However, the bending angle is still too large. The excess displacement of the leading edge can be attributed to the need to change the fixed boundary conditions used at the root. When using a coarser mesh, only 2 points are fixed along the fixed edge. This leads to the rotational behaviour (figure 5.24), instead of achieving bending behaviour (figure 5.23) . In order to mitigate such behaviour we add a an extra point along the fixed edge. The results we adjusted B.C shows a better bending performance without compromising twist too much as seen in figures 5.24, 5.25 5.26. The shape obtained (figure 5.27) doesn't contain smaller features as observed in Model A. The shape is optimized for being compliant along the diagonal direction, with not much stiffness support. We can observe that the flat region near the (green) corresponds to a weak diagonal line where the deformation gradient is highest. An upward curved fold line near the leading edge that extends towards two thirds of the wing span provides bending stiffness. A dome shape structure is produced at bottom left of the wing, which provides local stiffness for transmitting the torque responsible for the pitching of the wing. A computational time of 3 hours and 47 minutes was needed to reach convergence which is the highest run time of all models used.

5.3.2. Model B2 - Angle Objective, with constrained leading edge

The previous models shows a significant improvement in bending and torsional behavior compared to a flat plate. However, The bending is too high therefore, they need to be constrained. For the first model 9 hours and 3 mins computational time was taken. A moderate constraint for bending is chosen for preventing too stiff designs and allow significant twisting.The results of this optimization is shown in figure below . The results shows a design which is much stiffer than model B, however, the still achieving some twisting behavior. If we examine the the results of the shape optimization of this model, we can observe three distinct regions. We can observe a fold along the leading edge which signifies a stiff leading edge, another fold can be observed that extends diagonally from the tip of the leading edge towards the root. This fold is responsible for reinforcing the leading edge tip and at the same time act as a hinge about tip can rotate. At the tip a double curved structure is observed, which maintains high stiffness of the region. A similar result is shown by Anirudh Flapping wing optimization[51]. Anirudh tried to achieve a similar behaviour of the wing by thickness optimization of the finite elements. His design shows that thick leading edge, signifying a stiff leading edge, a thin diagonal section, signifying a hinge like behaviour and a thick region towards the tip for a stiff region.

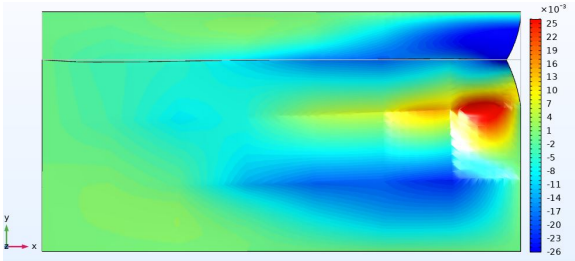


Figure 5.28: Displacement Constraint Shape

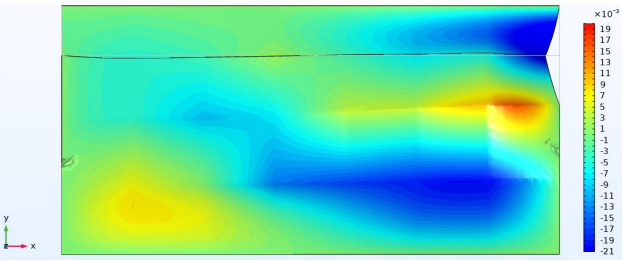


Figure 5.29: Angle Constraint Shape

A final optimization was attempted with having a point load instead of a distributed load. The reason is that a distributed load acts directly on the folds, thus doesn't allow the optimizer to go towards higher folded regions. Therefore a similar optimization to the previous one was conducted with point load instead of a distributed load. This study showed the best performance among previous models, with

a twist to bending angle ratio of 2. The design shows a clearly visibly horizontal fold line, the wing can easily rotate about this fold line, which a downward curvature at the root maintains the bending stiffness. The optimization took 13 hours 56 minutes to converge, 7 hours 10 minutes.

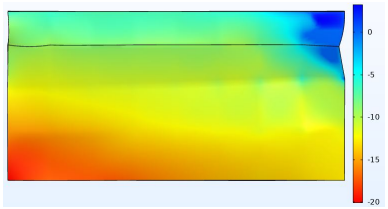


Figure 5.30: Point Load, Coarse mesh, bending Angle

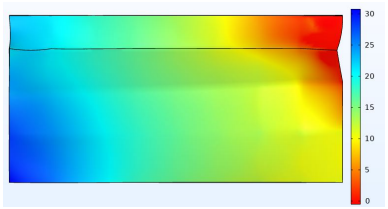


Figure 5.31: Point Load, Coarse mesh, Twist Angle

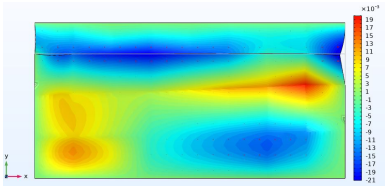


Figure 5.32: Point Load, Coarse mesh, Final Shape

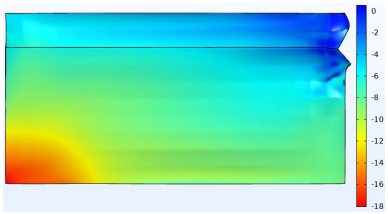


Figure 5.33: Point Load, Fine mesh, bending Angle

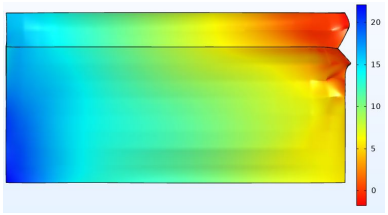


Figure 5.34: Point Load, Fine mesh, Twist Angle

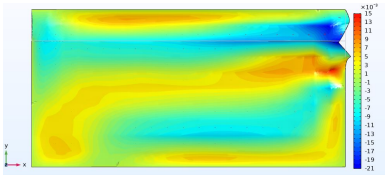


Figure 5.35: Point Load, Fine mesh, Final Shape

Model B22 with fine and coarse meshes have proven to be the ones providing highest Twist and Bending to Twist Ratio. The results will be tested against a finer mesh size to check for convergence. The results are summarized in the table below:

	Direction 1			Direction 2		
Model	Twist	Bending	T/B	Twist	Bending	Average T/B
Flat Plate	21	52.7	0.4	X	X	0.4
Model A	17.7	7.7	2.3	24.7	15.5	1.95
Model B1	33.6	22.0	1.53	21.3	15.5	1.84
Model B21	23.6	13.5	1.75	30.0	19.4	1.64
Model B22C	30.4	10.8	2.8	23.9	14.2	2.24
Model B22F	24.6	6.1	4.0	28.3	12.7	3.11

Table 5.3: Twist and Bending results comparison for different models

Several models were investigated for shape optimization to achieve optimal twisting to bending ratio. The results have shown that it is possible to achieve such a mechanical behaviour without the need to add a root stiffness. Although such a mechanical behaviour is motivated by observation of natural flyers, as well as proven by aerodynamic analysis, a better performance is not guaranteed due to the large number of variables that might affect the performance. This includes the planform shape of the wing, mass distribution and the kinematics. All these parameters might have an influence on the performance of the wing. In order to make a fair comparison, we need to find a wing that was aerodynamically proven to be optimal, and that has similar kinematics and size to our desired wing. In the next section we find a a better objective function, namely a least square objective function using a known optimal wing design by Qi Wang [75] where we attempt to mimic the static load displacement field of this optimal wing.

5.4. Optimization to achieve Qi Wang's Wing Optimal Mechanical behaviour

Qi Wang has found the optimal twistable wing, by performing a computationally efficient FSI analysis. He coupled non-linear twist mechanical model to model the deformable wing, to a quasi steady aerodynamic model and found the optimal distributed stiffness, root stiffness and flapping frequency. If we can mimic the static load deflection behaviour of such a wing with shape optimization, it is possible to achieve the same twist profile during flapping, and thus the same desirable aerodynamic characteristics of the wing.

5.4.1. Qi Wangs Model

Qi Wang developed an efficient Fluid Structure Interaction model based on an improved quasi steady aerodynamic model and a analytical plate mechanical model. This model enables optimization of wing parameters and wing twisting behaviour. The mechanical model approximates the wing twist along the spanwise direction by a polynomial function. A linear rotational root stiffness models the stiffness of the connection between the wing and body. The quasi steady aerodynamic model includes analytically derived coefficients which allows the model to be used in a fully automated optimization process.

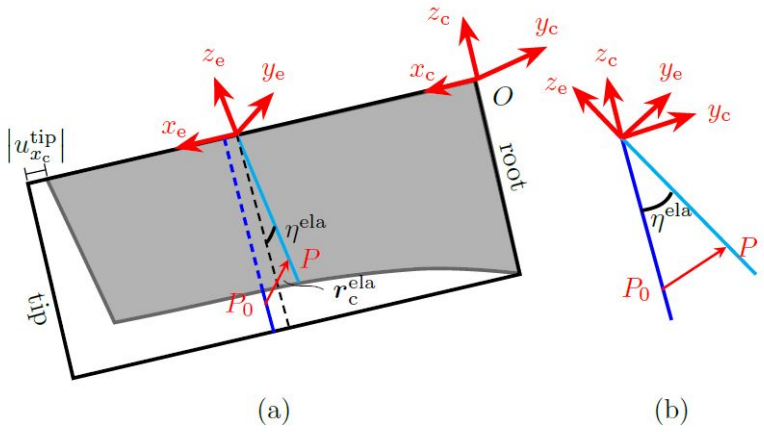


Figure 5.36: Schematic diagram of the elastic displacement of a twisted rectangular wing. The elastic frame $x_e y_e z_e$ is generated by first translating the co-rotating frame $x_e y_e z_e$ along the leading edge and then rotating by the local twist angle. P_0 and P indicate the positions of an arbitrary point at the mid-plane before and after twist. The spanwise tip displacement and the local pitching angle are denoted as $u^{tip}\ x_c$ and η^{ela}, respectively. $u^{tip}\ x_c$ will be negative due to the shortening effect. (a) 3D view of the untwisted and twisted wing. (b) 2D view of the local chord when observed from the wing tip.[75]

Qi Wang optimized the root and distributed stiffness of the wing as well as the flapping frequency for power minimization.The optimization showed that an optimized rigid and twistable wing can achieve similar power efficiency. It was also shown as seen figure 5.37 for different root stiffness values we can achieve similar performance given that there is enough flexibility in the distributed wing stiffness.

Based on this result we attempt to design a wing that exhibits similar mechanical behaviour of this wing, while eliminating all together the root stiffness. This means that the root stiffness will be modeled as an infinitely stiff connection, with the pitching angle along the wing obtained entirely from the wing deformation.

5.4.2. Qi Wang Wing Optimal Wing static FE load analysis

The Wing model of Qi Wang is replicated using FE element model, to perform static load analysis and check the static behaviour of the wing. Wang performed this analysis to check the validity of his twist model. Here we use this analysis to get the deformation profile that will be used as an obejctive for our optimization analysis. The wing is modeled using shell elements, with E=10^5. The leading edge y and z displacements are fixed, while the root side is fixed in z and x. Two loads are applied which represent the inertial load and the aerodynamic load. The inertial load is applied as a force per unit area and is linear, starting from zero at the root and taking the valuo B_0 at the tip. The aerodynamic

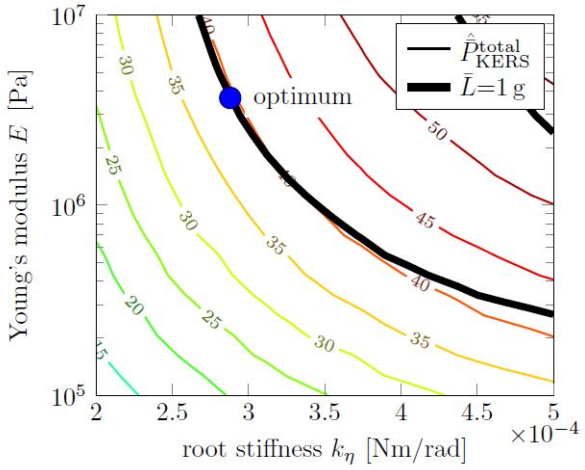


Figure 5.37: Contour plots of the lift and the power consumption as a function of the root stiffness and Young's modulus. The lift acts as a constraint in the optimization. The lift constraint is included as a thick solid line. The blue dot represents the wing stiffness of the optimized twistable wing based on the full optimization.[75]

dynamic load is an edge load (force per unit length) which acts a distance of 0.4c from the leading edge and is represented by a quadratic function, with a load value of A_0 at the tip. The B.C's and applied loads are shown in figure 5.38.

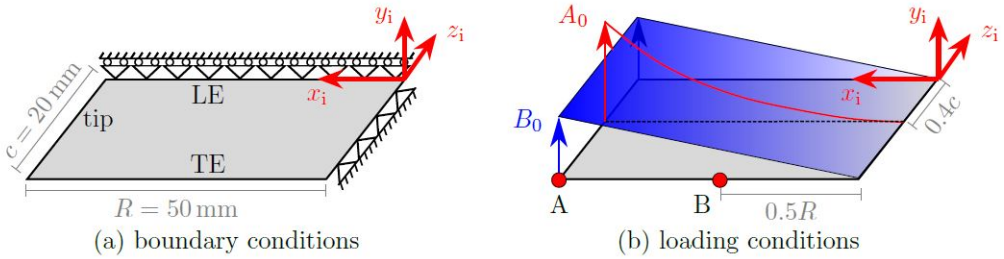


Figure 5.38: Boundary conditions and applied loading on Qi Wang Wing. In blue the the inertial load is applied linearly from root to tip with amplitude B_0. In red the aerodynamic load is approximated as quadratic with amplitude A_0. The roller support B.C is applied at the leading edge to prevent out of plane deformation and a hinge support is applied at the root. [75]

The deformation is captured along the trailing edge at 5 equidistant point at 0.01 mm distance from each other. Table 5.4.2 shows this deformation profile obtained.

Distance from root [m]	Displacement in z direction [m]
0	8.57E-04
0.01	0.001332
0.02	0.0017974
0.03	0.0022517
0.04	0.0027035
0.05	0.0031279

5.4.3. Least Square Objective Optimization

The deformation of Qi Wang will be used as an least square objective for our optimization problem.

$$Minimize \qquad (u_i^* - u_i)^2, \qquad \mathbf{s} \in R^n$$

$$Such\ that - 0.0001 \leq u_{le},$$

Here i corresponding points along the spanwise direction of the wing which we want the deformation profile to match. u_i^* is the deformation obtained from the FE analysis of Qi Wang wing. u_i is the target displacement of our design that the optimizer tries to achieve. The leading edge tip displacement u_{le} is

constrained at -0.0001 which keeps it at a deformation less than 10% the tip deformation of the trailing edge that we obtained by the Finite element analysis of the model.

The obtained design is shown in figure 5.39.

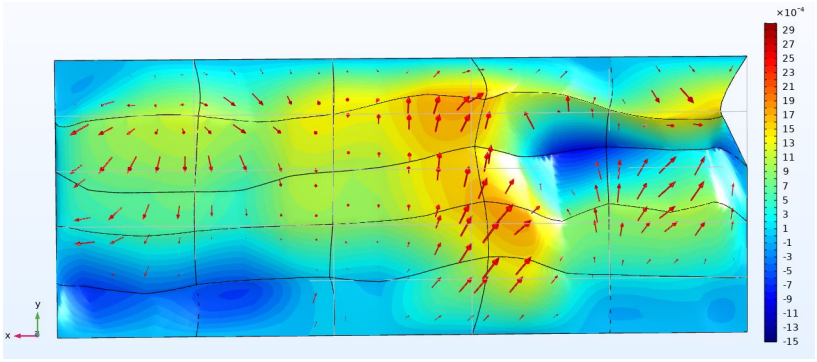


Figure 5.39: Design 2 obtained with least squares optimization. The red arrows represents the boundary displacements in x y and z directions. Longer arrows indicate more in plane distortion of the mesh from the original configuration

The plot of the displacement of wing's leading edge and trailing edges is shown in figure 5.40. The results shows that there is close resemblance between the two wing displacement profiles at the trailing edge and leading edge. Thus this design is used as a potential candidate for our flapping wing.

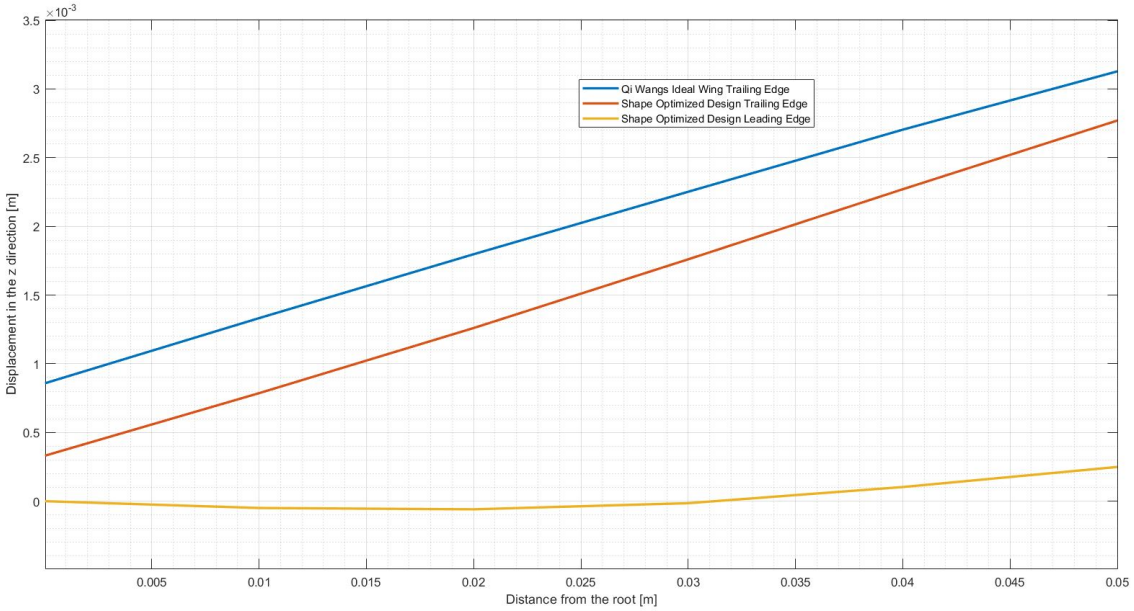


Figure 5.40: Displacement profile comparison between design 2 and Qi Wang optimal wing. The Trailing edge displacement is measured for both designs which shows that both have approximately the same slope and are close in values. The leading edge shows a positive displacement till 3 cm then a negative displacement

6

Aerodynamic Analysis and Validation of Corrugated Wing Designs

In this chapter a time dependant study, simulating a simple flapping motion of the wing is performed on the obtained wing designs. We check the passive pitching and heaving behaviour of the obtained designs and compare them to a flat plate. The deformation obtained allow us to qualitatively and quantitatively compare their performance and determine if this approach is beneficial to pursue in flapping wing design. Finally the Wing is manufactured and tested to check the actual resulting pitching angle.

6.1. Dynamic Analysis

In this section the transient behaviour of the flapping wing is simulated. First a dynamic analysis in vacuum is performed, then artificial damping is added to stabilize the simulation. Then a quasi steady aerodynamic model will be added to analyze the performance of the wing.

For the dynamic analysis 2 models is be tested. A wing design (D1) which based on the optimal twist to bending ratio optimization performed in the previous chapter (ModelB22F) scaled by a factor of 20. A geometrically similar initial design with the same optimization settings will result in the same wing shape. This result is similar to the scaling of a cantilever beam, where the bending angle is the same for geometrically similar scaled designs with scaled loads. The second design which is based on the least square optimization performed in the previous chapter (D2) will not be tested. A model of a flat plate fixed at the root edge will be analysed (FP) as a benchmark to check how much improvement we get by performing our shape optimization.

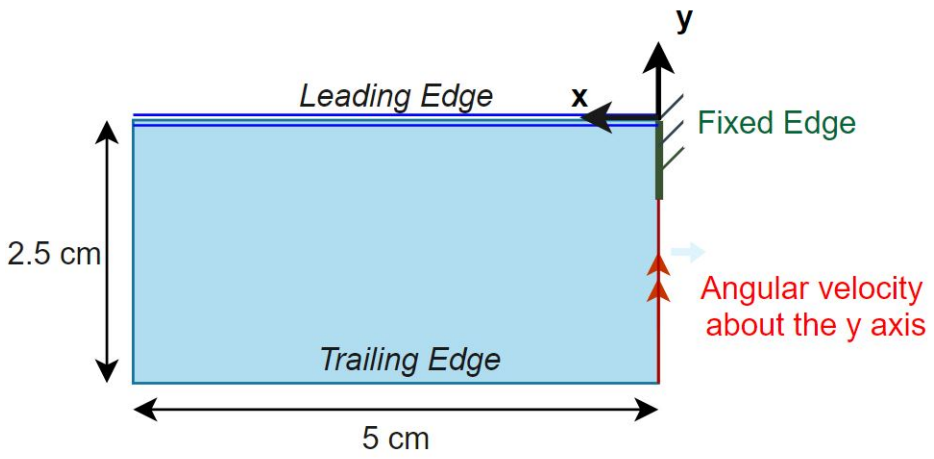


Figure 6.1: Dynamic Analysis setup for different wing models.

The dynamic analysis conducted only considers the inertial loads. This is enough to get an estimate of the behavior, as inertial loads are dominant at this scale. An angular velocity is applied below the fixed root of the wing which represents the wing sweeping motion driven by the actuator. The displacement in the Z direction is measured at the tip of the leading and trailing edges in order to measure the amount of twist and bending. The wing model is shown in figure 6.1.

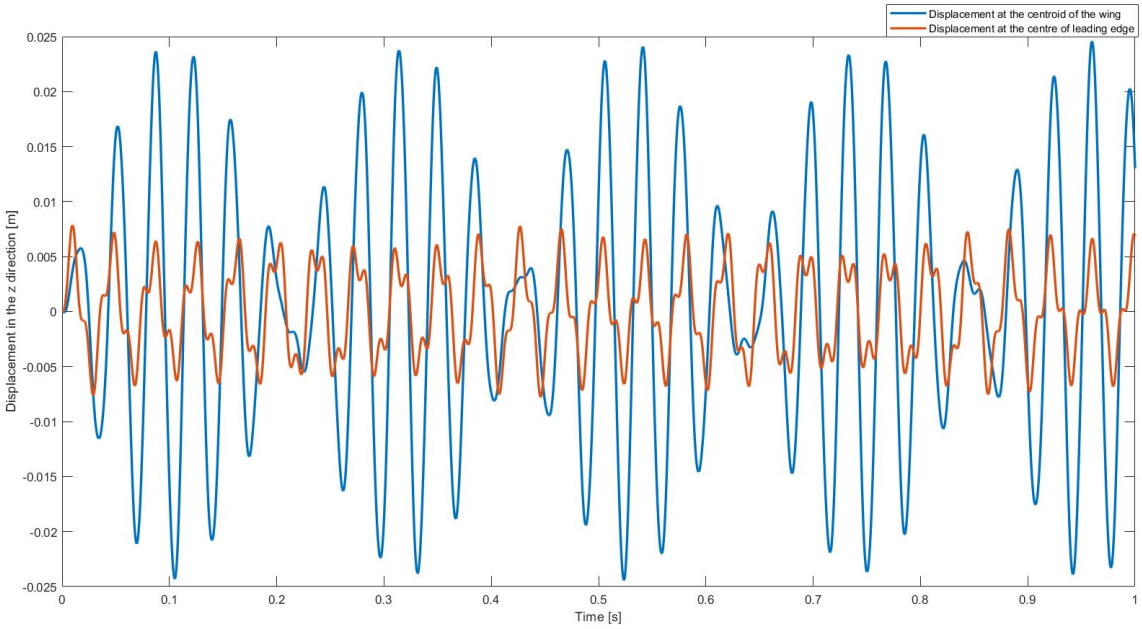


Figure 6.2: Displacement at the tip vs. time for design 1 in vacuum

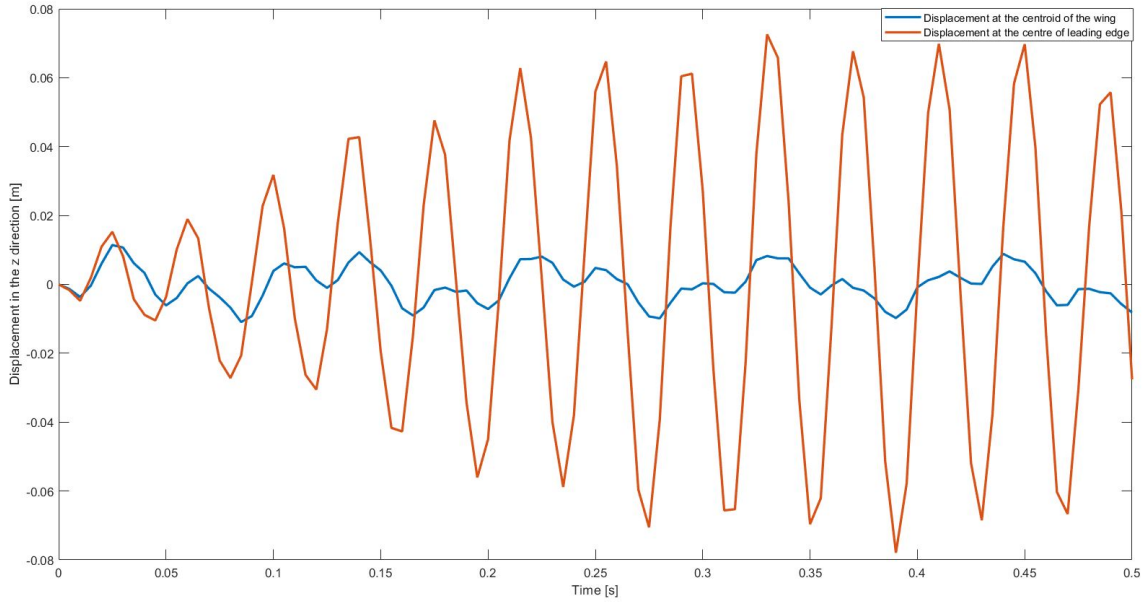


Figure 6.3: Displacement at the tip vs. time for a flat plate in vacuum

The time dependant study on COMSOL was performed for design 1. A time step was chosen to be 0.0005 seconds. This time step is chosen as it balances between a reasonable computation time and accuracy of the results. The displacement of two points at the central section of the wing is plotted in Figure 6.2 as representation of deformation of the whole wing. The first point is the centre of the chord while the second is at on the leading edge. The plot shows that there is a significant difference

in amplitude of both points, due to the optimized properties of the wing. However, due to to the lack of damping the oscillations doesn't reach steady state. In the flat plate model on the other hand the amplitude of displacement of the centroid is less than the leading edge which is undesirable. 6.3. Moreover, the the oscillations exhibit the same unstable behavior and doesn't reach steady state.

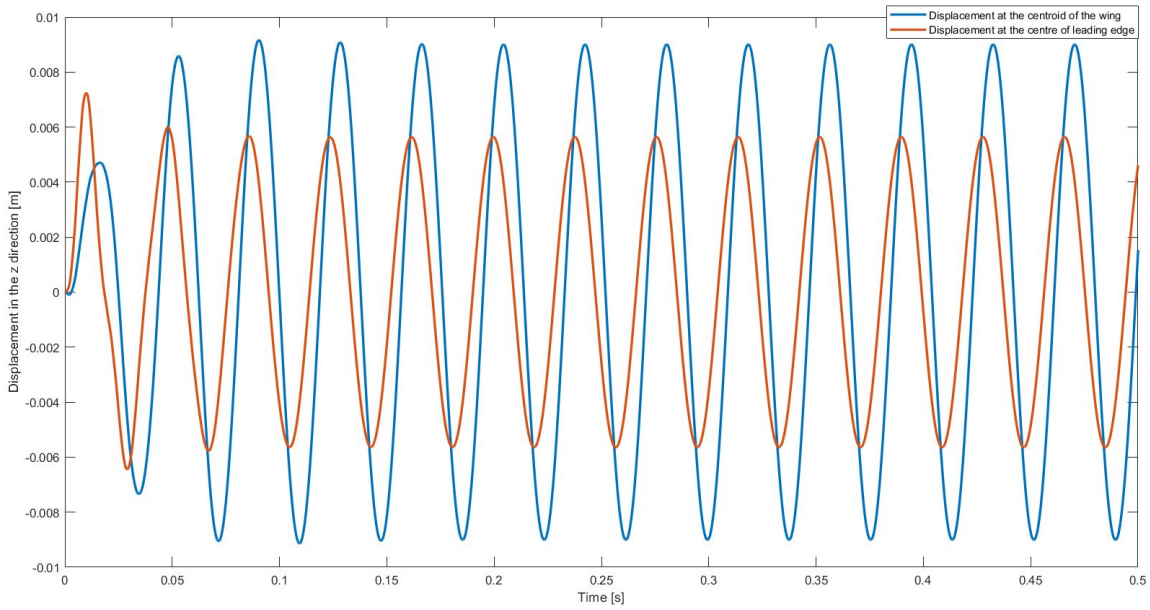


Figure 6.4: Displacement at the tip vs. time for design 1 after applying viscous damping

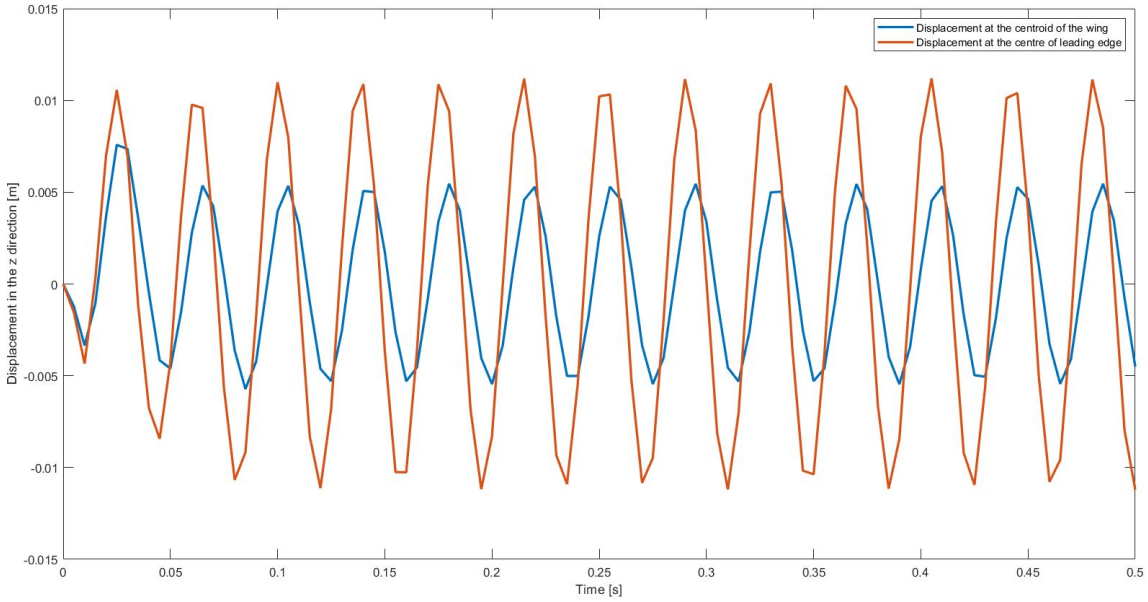
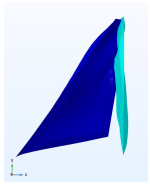


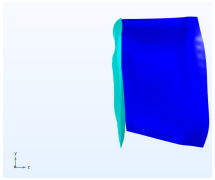
Figure 6.5: Displacement at the tip vs. time for a flat plate after applying viscous damping

The instability can be mitigated by adding a damping model. A simple viscous damping acting on the wing surface, having a magnitude of 100Ns/m was shown to stabilize the simulation and get the expected dynamic behaviour.

The displacement curves is shown again for both the wing design and the flat plate in figures 6.4 and 6.5. Snapshots at different time instances for a side view of the flapping wing are displayed in figure 6.6. The dynamic analysis qualitatively shows a desired twist behavior similar to natural flyers,



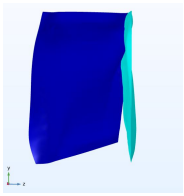
(a) Middle of the upstroke, time = 0.418s



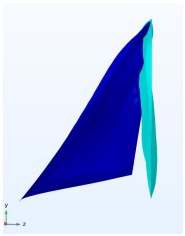
(b) End of the upstroke, time = 0.428s



(c) Middle of the downstroke, time = 0.4375s



(d) End of the downstroke, time = 0.447s



(e) Middle of the upstroke, time = 0.4565s

Figure 6.6: Side view of the flapping cycle results form the dynamic simulation at different time instances. The cyan edge represents the wing at the initial position. The blue surface is the dynamic deforming wing.

such as insects and humming bird. On the other hand, the plate dynamic simulation shows multiple mode shapes appearing in the flapping motion. This is due to the overall low value of stiffness, causing it to flap close to resonance frequency. Generally, this behaviour is undesirable in flapping flight as it causes less efficient flapping motion.

In the next section the performance of the wing design will be evaluated quantitatively by applying an quasi-steady aerodynamic model. Moreover the kinematics of the wing will be compared to the optimal wing design developed by Qi Wang [72].

6.2. Aerodynamic Model

The model chosen for this analysis was the one by semi-empirical quasi steady model by Berman and Wang [9]. This model is one of the simplest models to implement and popular model in the literature. Since the analysis purpose is just to give a rough estimate of the performance, the inaccuracies of this model is not of big concern.

6.2.1. Kinematics

In original model, the wing is modeled as a rigid plate which can have three in dependant rotations, namely the sweeping angle ϕ, heaving angle θ and the pitching angle η. z is defined as the vertical axis, y is aligned with forward direction and x is acting in the horizontal plan perpendicular to y. This gives the following relations. The visualisation of the euler angles is shown in figure 6.7.

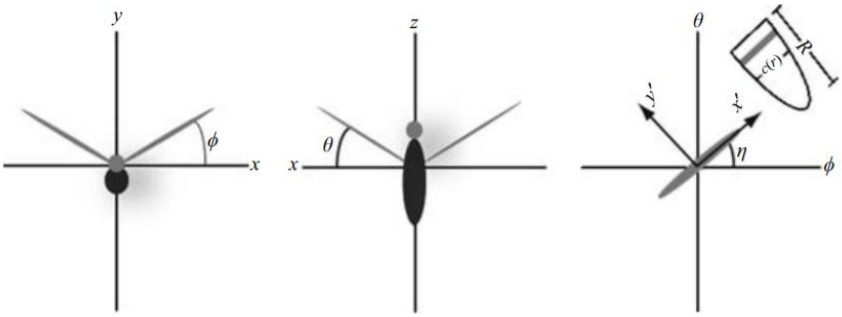


Figure 6.7: Angles Definition[9]

The velocities and the accelerations can be defined on the co-moving coordinate system x' and y'. This transformation can be obtained by writing the position of a cross section of the wing in spherical coordinates, then applying a rotation through the pitching axis η.

$$v_{x'} = r(\dot{\phi}cos(\theta)cos(\eta) + \dot{\theta}sin(\eta)), \tag{8.1}$$

$$v_{y'} = r(\dot{\theta}cos(\eta) - \dot{\phi}cos(\theta)sin(\eta)), \tag{8.2}$$

$$a_{x'} = r([\ddot{\phi}cos(\theta) + \dot{\theta}(\dot{\eta} - \dot{\phi}sin(\theta))]cos(\eta) + (\ddot{\theta} - \dot{\eta}\dot{\phi}cos(\theta))sin(\eta)), \tag{8.3}$$

$$a_{y'} = r([\dot{\theta} - \dot{\phi}sin(\theta)) - \ddot{\phi}cos(\theta)]sin(\eta) + (\ddot{\theta} - \dot{\eta}\dot{\phi}cos(\theta))cos(\eta)). \tag{8.4}$$

The kinematics of the wing are time dependant and a function of the flapping frequency, f, and the amplitude of rotation. The main rotational motion, which is the sweeping motion and is the one applied by actuator, can be generally defined as

$$\phi(t) = \frac{\phi_m}{arcsinK} arcsin(Ksin(2\pi f t), \tag{8.5}$$

where ϕ_m represents the sweeping amplitude. K is a parameter that determines the shape of the cyclic motion of the wing and it can take value between 0 and 1. As K approaches 0, $\phi(t)$ tends to take a sine shape and takes the triangular wave form as K approaches 1.

6.2.2. Aerodynamic load model

The aerodynamic loads are calculated based on the quasi-2 dimensional load model. The Blade element method assumption is used, where the wing is divided into strips along the span, each strip is of infinitesimal width dr and the total load is calculated by summing over all strips. A strip at distance r is shown in figure 6.8. The model neglects the curvature of the motion of the wing. It also neglects span wise velocity components of the loads on the wing. However, this assumption is corrected slightly by using semi-empirical terms in the formulation.

The loads and the torque on an infinitesimal slice of the flapping wing in the co-rotating frame are given by:

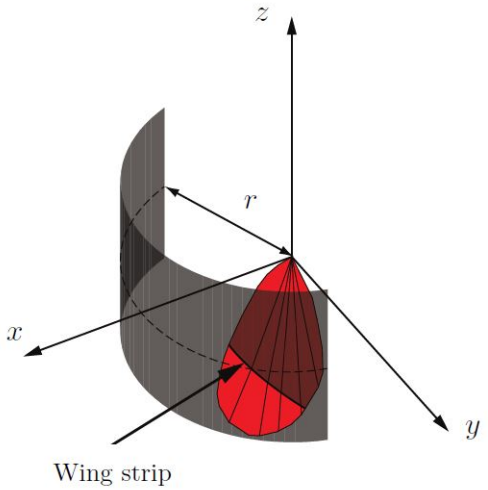


Figure 6.8: A wing strip at a distance r, used for mapping three dimensions to two dimensions for the wing movement.[16]

$$dF_{x'} = [\frac{c(r)}{cR}M_{wing} + m_{22})v_{y'} * \dot{\eta} - \rho_f \Gamma v_{y'} - m_{11}a_{x'})dr - dF_x^v, \tag{8.6}$$

$$dF_{y'} = [-(\frac{c(r)}{cR}M_{wing} + m_{11})v_{x'}\dot{\eta} + \rho\Gamma v_{x'} - m_{22}a_{y'}]dr - dF_y^v, \tag{8.7}$$

$$d\tau_\eta = [(m_{11} - m_{22})v_{x'}v_{y'} - I_a\ddot{\eta}]dr - d\tau^v, \tag{8.8}$$

where

$$\Gamma = -\frac{1}{2}C_T c(r)|\mathbf{v}|sin(2\alpha) + \frac{1}{2}C_R c^2(r)\dot{\eta}, \tag{8.9}$$

$$F^v = \frac{1}{2}\rho_f c(r)[C_D(0)cos^2(\alpha) + C_D(\pi/2)sin^2(\alpha)]|\mathbf{v}|\langle v_{x'}, v_{y'}\rangle, \tag{8.10}$$

$$d\tau^v = \frac{1}{16}\pi\rho_f c^4(r)[\mu_1 f + \mu_2|\dot{\eta}|]\dot{\eta}dr], \tag{8.11}$$

$$m_{11} = \frac{1}{4}\pi_f b^2, \qquad m_{22} = \frac{1}{4}\pi_f c^2(r), \qquad I_a = \frac{1}{128}\pi_f[c^2(r) + b^2]^2, \tag{8.12}$$

Γ given by equation 8.9 is the circulation around the wing and ρ_f is the density of the surrounding air. m_{11}, m_{22} and I_a in equation 8.12 are added mass terms. These terms represent virtual mass, added to the system because the body should displace some of the surrounding fluid. α here is the angle of attack, c(r) is the chord length at a distance r from the wing root, C_T, C_R and $C_D(\alpha)$, are experimentally obtained coefficients and are included to increase the accuracy of the model. C_T and C_R are the translational and rotational lift coefficients of the wing respectively, $C_D(\alpha)$ is the wing's drag coefficient as a function of the angle of attack. The coefficients μ_1 and μ_2 are dimensionless and are determined by the fluid viscosity. b is the thickness of the wing and f is the flapping frequency.

The first term in equations 8.6 and 8.7, represent a Coriolis term that appears due co-rotating co-ordinate system. The third term represents the inertial forces of the added mass. dF_x^v, dF_y^v and τ_η are viscous dissipation terms on the wing strip. The velocity and acceleration terms in the equations above are calculated using the equations from the previous section. The lift and drag forces acting on wing can then be calculated by transforming the load vectors back into the inertial frame. They are given by equations 8.13 and 8.14 respectively.

$$F_{lift} = F_{x'}sin(\eta) + F_{y'}cos(\eta), \tag{8.13}$$

$$F_{drag} = F_{y'}sin(\eta) - F_{x'}cos(\eta), \tag{8.14}$$

where $F_{x'}$ and $F_{y'}$ are the summation of the $dF_{x'}$ and $dF_{y'}$ forces of all wing strips along the wing.

6.2.3. Angle of Attack

The angle of attack, which appears in the equations of the aerodynamic load model, is defined as the angle between the incoming air and the chord of the airfoil. The velocity can be considered as the sweeping velocity of the wing as this is the main motion of the wing. The angle of attack is related to the pitching angle, but since the velocity vector direction changes, this needs to be adjusted. The angle of attack can be calculated from the pitching angle using the relation in equations 8.15 and 8.16.

for $\dot{\phi} <= 0$

$$\alpha = -\eta, \tag{8.15}$$

for $\dot{\phi} > 0$

$$\alpha = -(\eta + \pi). \tag{8.16}$$

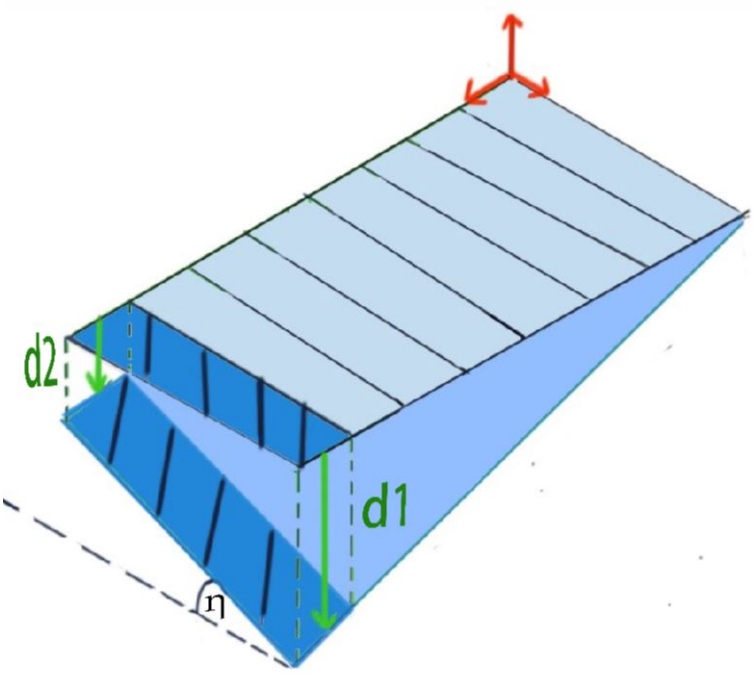


Figure 6.9: Depiction of the assumption of deformation occurring on the wing and the corresponding pitching angle η.

6.2.4. Adjusting model for deformation

The model needs be adjusted for the deformation occurring during flapping motion on the wing. Two points will be used to represent the deformation occurring on the wing at the middle of the span of the wing. These points are the same points which were used to analyze the dynamic behaviour of the wing, which are the leading edge of the middle chord section and the centroid. Based on the deformation, the euler angles, and angular velocities and accelerations can be calculated as can will be shown in this section. Some assumptions are made when calculating the pitching angle from deformation of two points.

- The chord lines is assumed to be a straight line. This suggests that there is no camber.
- The local corrugations of the wing are ignored.
- The pitching and heaving angles of the wing is approximated at the mid span chord of the wing
- The load is calculated at the centre of the wing

It should be noted that these assumptions are in addition to the initial assumptions mentioned earlier regarding the quasi-steady model itself. The angles are calculated at each strip, the overall approximation of the deformation that is used in the quasi steady model is depicted in figure 6.9.

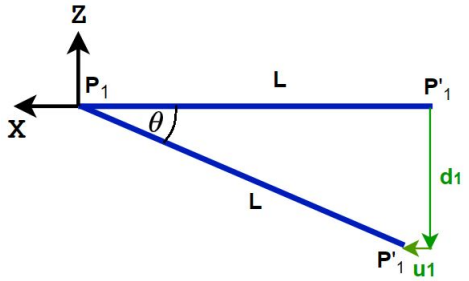


Figure 6.10: Heaving angle calculation

$$\eta = \arccos(\frac{d1}{L}) \tag{8.15}$$

$$\theta = \arcsin(\frac{d2}{L}) \tag{8.16}$$

The pitching and heaving angular velocities and accelerations, $\dot{\eta}$ and $\ddot{\eta}$, $\dot{\theta}$ and $\ddot{\theta}$, are calculated using backward finite difference scheme. For the the velocities it can be calculated for the first time step, while the accelerations need to be calculated from the second time step. The initial values of the velocities and accelerations are assigned zero values.

$$\dot{\eta}_{t1} = \frac{\eta_{t1} - \eta_{t0}}{\Delta t} \tag{8.17}$$

$$\dot{\theta}_{t1} = \frac{\theta_{t1} - \theta_{t0}}{\Delta t} \tag{8.18}$$

$$\ddot{\eta}_{t1} = \frac{\eta_{t2} - 2\eta_{t1} + \eta_{t0}}{(\Delta t)^2} \tag{8.19}$$

$$\ddot{\theta}_{t1} = \frac{\theta_{t2} - 2\theta_{t1} + \theta_{t0}}{(\Delta t)^2} \tag{8.20}$$

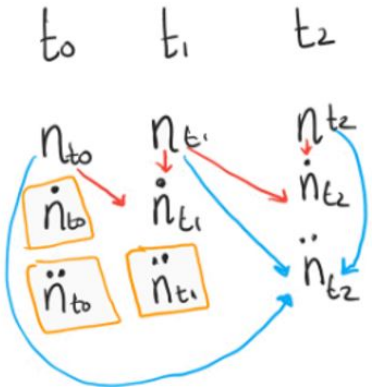


Figure 6.11: Calculation of the pitching velocities and accelerations. Red arrows represent values of η used to calculate angular velocities, while blue arrows are used for angular accelerations. The terms highlighted in orange are unknown at initial conditions and at $t = t_1$. They are assumed to be zero in this case since the flapping motion starts from rest.

6.3. Aerodynamic Model Verification

To verify the adjusted aerodynamic model the average Lift and Drag will be calculated for different situations. Here only the mid-span section of the wing will be considered. The deformation of the leading edge and trailing edge will cause an effective pitching and heaving motion of this section during flapping motion.

The first test will be fixing point P2 while assuming a harmonic deformation profile of $d1 = -Dcos(2\pi ft)$ for point P1, the heaving angle will be constrained and the deformation will only cause pitching. Here we will first determine the optimal value of the deformation amplitude D, by sweeping over all values as shown in figure 6.12.This results shows that for a harmonic pitching deformation Optimal lift is achieved as expected at D=0.02, which corresponds to α=37 degrees.

After verifying the simple case of pure pitching motion and calculating optimal D we perform the second test. The second test involves deformation of point P2 which is set to be equal $\frac{d1}{3}$, while point P1 will have the optimal deformation amplitude calculated form the previous test. Here the heaving angle contribution will not be added.

Finally test 3 will include heaving as well as pitching and deformation of both points. The average Lift and Drag will be compared for the three cases at D= 0.02 to verify the implementation was performed correctly and that the model outputs realistic results.

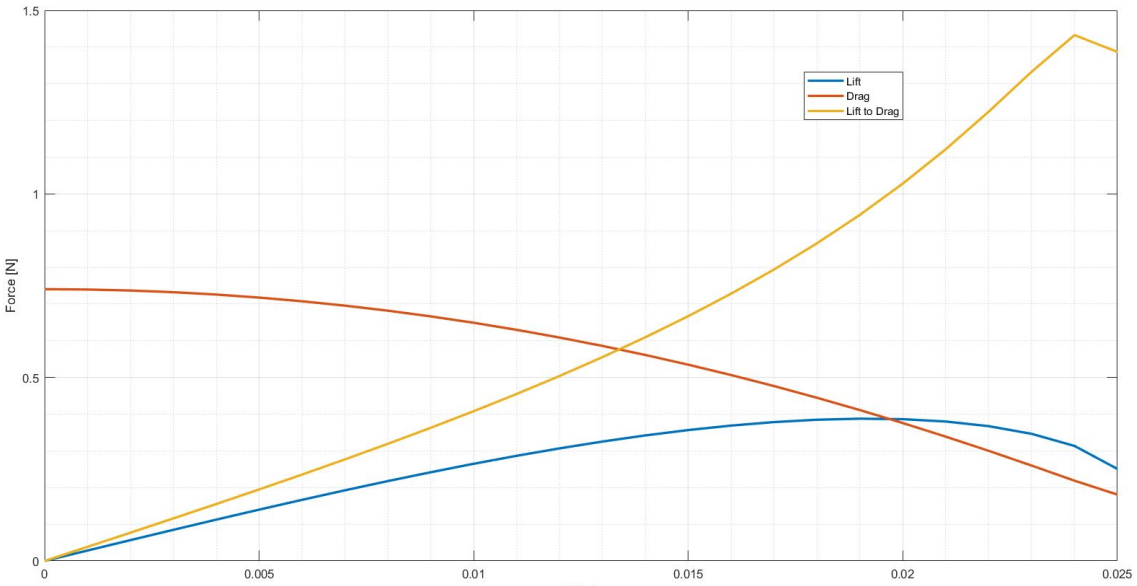


Figure 6.12: Lift and Drag forces with changing pitching amplitude D

	Lift [N]	Drag [N]	Lift to Drag ratio
Test 1	0.106	0.101	1.05
Test 2	0.091	0.157	0.583
Test 3	0.086	0.148	0.583

Figure 6.13: Lift and Drag with different test cases for the model

Table shown in figure 6.13 shows the average lift and drag for the 3 cases. The results shows that the lift Test 1 has the highest lift and highest lift to drag ratio, which is expected since it has the highest effective pitching angle due to the constraint of the leading edge tip. Test 2 which doesn't have the heaving effect has more lift and drag than test 3. The effect of less lift for including the heaving angle is a result of the lift force being inclined thus some of the effective goes in the spanwise direction. The drag however, reduces because the effective area is at an angle to the flow rather than being perpendicular in Test 2.

6.4. Aerodynamic Analysis of the wing design

Using the relation between the deformation and pitching and heaving angles derived earlier we can calculate the equivalent euler angles due to deformations for our design during one flapping cycle. Figure 6.14 shows the passive pitching behaviour during one cycle at the midspan of the wing. The pitching behaviour which is detrimental in aerodynamic performance, shows a typical pitching behaviour of natural flyers. The angle of attack of the midspan approaches $60\mathrm{deg}$ at the mid stroke, which is close to optimal values required. Moreover, an early stroke reversal can be seen which is also quite similar to the insects behaviour. This is known to have a positive effect on the aerodynamics, however, the exact optimal stroke reversal timing is a topic of research. Figure 6.15 shows the lift and drag forces for during a flapping cycle on the mid span of the wing while figure 6.16 shows it for the flat plate.

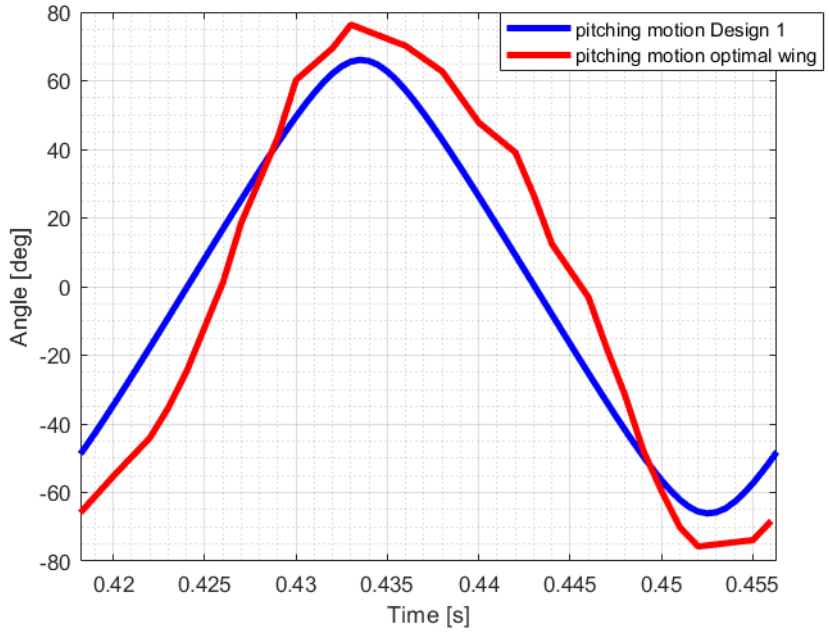


Figure 6.14: pitching angles comparison with optimal wing during one flapping cycle

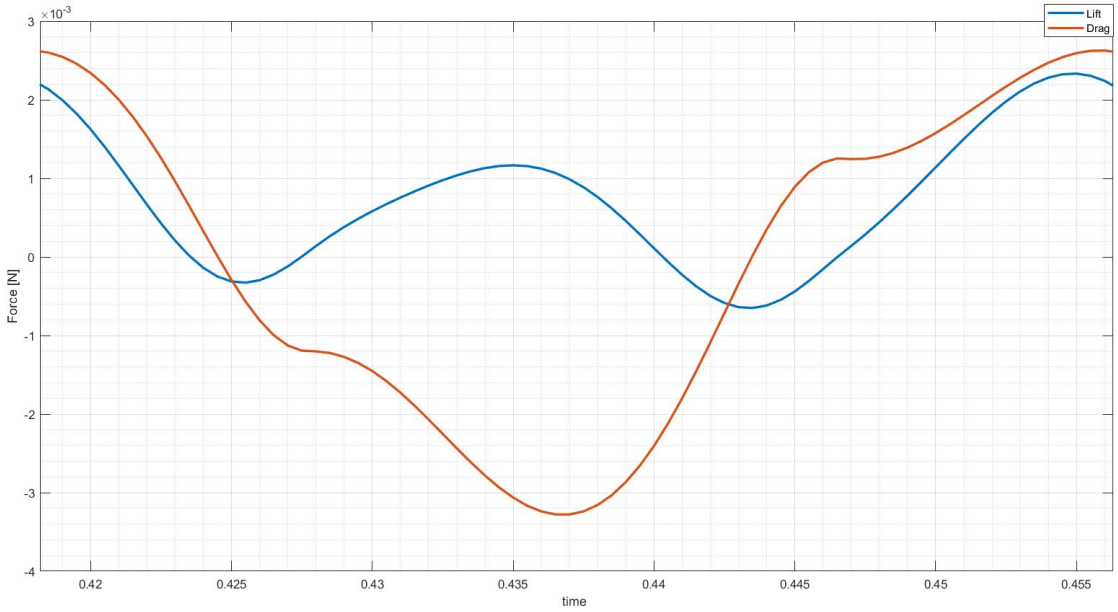


Figure 6.15: Lift and Drag D1

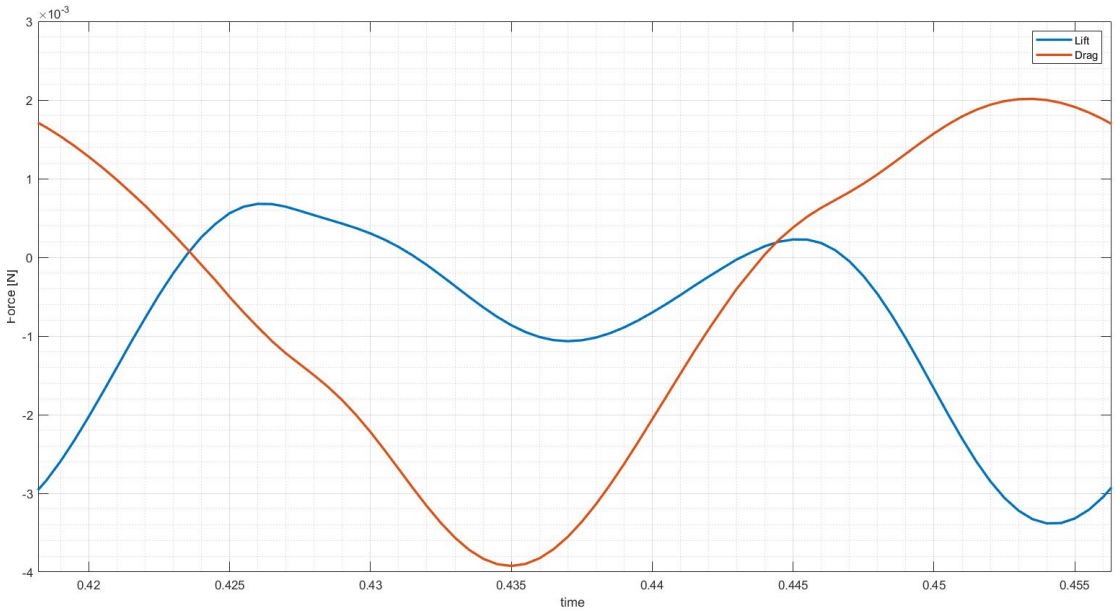


Figure 6.16: Lift and Drag plate

6.4.1. Evaluation of the Wing Design

In order to evaluate the performance of the designs the lift and drag were calculated using the adjusted aerodynamic model. The displacement of the leading edge and trailing edge were extracted from the dynamic simulation using a point probe at 10 equidistant locations. This displacement is then used to calculated the euler angles and angular rates and consequently the aerodynamic loads at each section. These loads are then summed to get the equivalent contribution along the wing. The Lift and drag is then calculated for one flapping cycle. The lift contribution is summed directly, while the drag is summed if it is opposite to the velocity vector other wise it is subtracted. The data for the displacement of the leading edge and trailing edge of design1 is shown in Appendix B. The matlab code used for the calculation of lift and drag is available in Appendix A.

The results are summarize in the tables in figures 6.17 and 6.18. Design 1 shows a total lift of 0.0105N and a total drag force 0.01379N, with a Lift to to Drag ratio of 0.761. While for the flat plate the total lift was found to be -0.0041N and the 0.019N with a L/D ratio of -0.218.

Strip Number	Strip position along length [m]	Lift Sum over cycle [N/cycle]	Drag sum over cycle [N/cycle]
1	0.0025	0.001	0.001
2	0.0075	0.004	0.016
3	0.0125	0.011	0.046
4	0.0175	0.023	0.090
5	0.0225	0.042	0.146
6	0.0275	0.069	0.213
7	0.0325	0.106	0.289
8	0.0375	0.153	0.375
9	0.0425	0.209	0.478
10	0.0475	0.273	0.607
	Total per cycle [N/cycle]	0.89	2.3
	Avg [N]	0.012	0.029
	Lift to Drag Ratio	0.39	

Figure 6.17: Lift and drag calculation D1

Strip Number	Strip position along length [m]	Lift Sum over cycle [N/cycle]	Drag sum over cycle [N/cycle]
1	0.0025	0.002	0.001
2	0.0075	0.011	0.016
3	0.0125	0.011	0.040
4	0.0175	0.036	0.092
5	0.0225	0.017	0.143
6	0.0275	0.068	0.229
7	0.0325	0.015	0.313
8	0.0375	0.100	0.427
9	0.0425	-0.003	0.549
10	0.0475	0.128	0.694
	Total per cycle [N/cycle]	0.39	2.5
	Average [N]	0.005	0.033
	Lift to Drag Ratio	0.15	

Figure 6.18: Lift and drag calculation PW

6.5. Corrugated Wing Manufacturing

The manufacturing of the wing design is a challenge due to the small size features required. Moreover, a high level of accuracy is required due to the sensitivity of the performance of the wing to the shape change. This has to be done while maintaining a constant thickness and material properties. All this puts limitation on the possible manufacturing processes that can be used to obtain the required design.

6.5.1. Hot compression molding

A manufacturing process similar to compression molding is chosen to be investigated. An upper and a lower mold having the features of the wing and are negatives of each other is 3D printed. A sheet of PETG of the required thickness and material properties is chosen and heated till glass transition temperature to make it easy to form. The heated sheet is then sandwiched in between in the mold upper and lower part with a small pressure applied to the mold to keep it in place. The sheet is then removed and the wing is cut out of the sheet. The configuration of the molds and the wing is shown in fig 6.19.

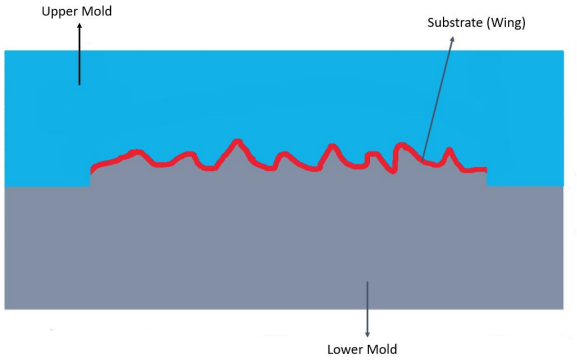


Figure 6.19: Manufacturing process of the wing

6.5.2. Mold design

In order to create the STL files of the molds the following process was followed (figure6.20):

(a) First the Mesh of the wing design was exported as an STL file from COMSOL to autocad mesh mixer.

(b) The wing is extruded to create thickened part of the wing while keeping the same features.

(c) The root part is extruded to create an extended part for clamping the wing

(d) The wing is subtracted from a cuboid of a slightly larger dimensions to create the negative of it, this is the upper mold.

(e) The upper mold is then subtracted from a cuboid of equivalent size to create the lower mold.

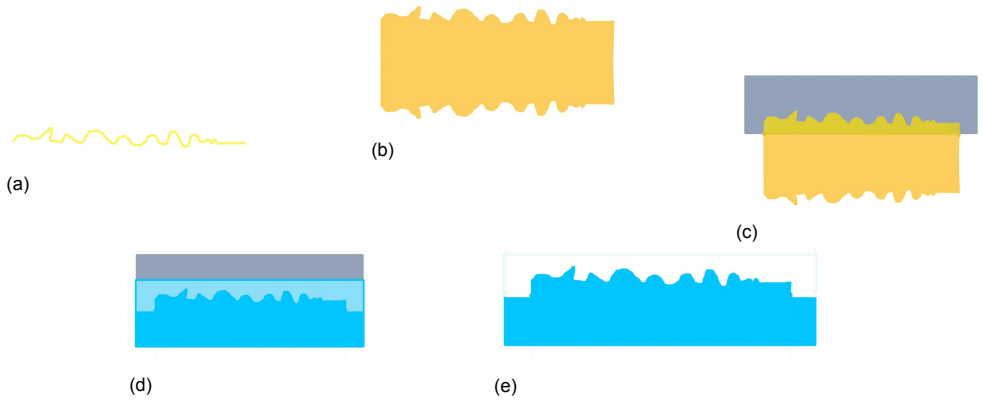


Figure 6.20: Process for creation of the STL files of the upper and lower molds for 3D printing

The resulting STL designs are then 3D printed to create the upper and lower mold parts. Figure 6.21 shows the 3D printed upper and lower molds for wing design 1.



Figure 6.21: 3D printed mold

6.5.3. Vacuum forming

The compression molding method for manufacturing the wings didn't result in the desired wing manufacturing accuracy. The reason is that the very thin plastic sheets cool very quickly and by the time they are put in the mold they will are at some regions have cooled too much to be able to form. Another problem is the need to apply tension on the sheets while pressing them between the mold, as they become slack due to the heating. This can be done by clamping the sheets, but its still a challenge to do this at the very short time window we have between getting the sheet out of the oven and putting it inside the mold. For these reasons a second method was investigated which is vacuum forming, this method doesn't suffer from the problems mentioned, as heating is done uniformly and the time between the stop of heating and shaping is very small. Moreover, the very high uniform pressure makes sure that the plastic sheet closely matches the mold shape. The vacuum forming setup used is shown in the figure 6.22 .

The vacuum forming method used with 0.3 mm PETG plastic, resulted in the following samples, which visually look of a much higher quality than the previous method.

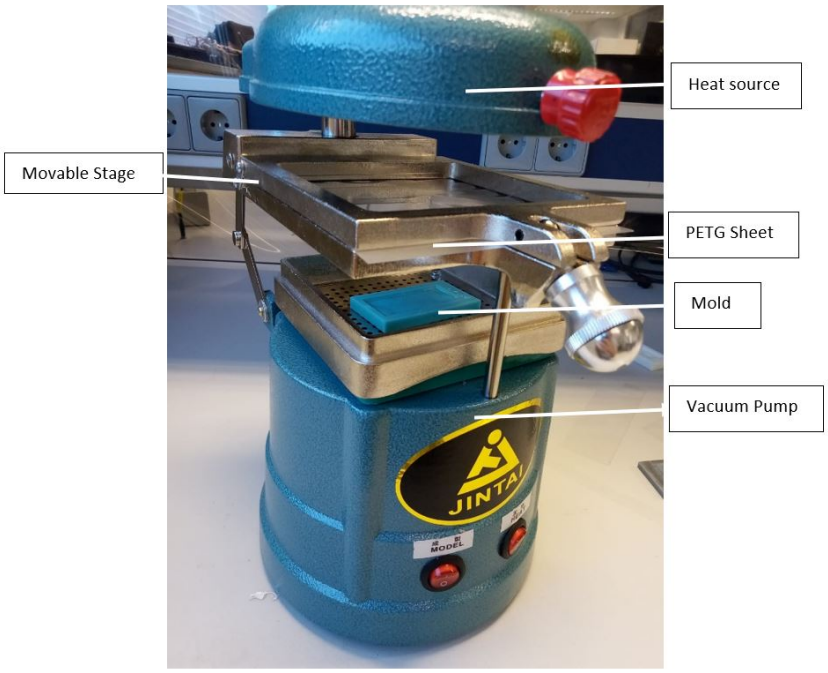


Figure 6.22: Vacuum Former Setup. The PETG sheet is clamped inside a movable stage and heated till glass transition temperature. After heating the movable stage slides down on the vertical rod towards the mold, after which the the vacuum pump is activated for the sheet to take the shape of the mold.

6.5.4. Wing root connection manufacturing

With the current wing we cannot clamp it directly to the body as it damage the corrugated part at the root. Therefore a part that at the root of the wing needs to be added to the wing so that it can be clamped to the body. This part, which is basically a block that surrounds the wing fixed edge can be manufactured using casting process. A silicon mold is manufactured from the 3-D printed wing mold that the wing sits while epoxy is cast ed from an opening in the middle of the mold. The manufactured silicon mold can be seen in figure 6.23

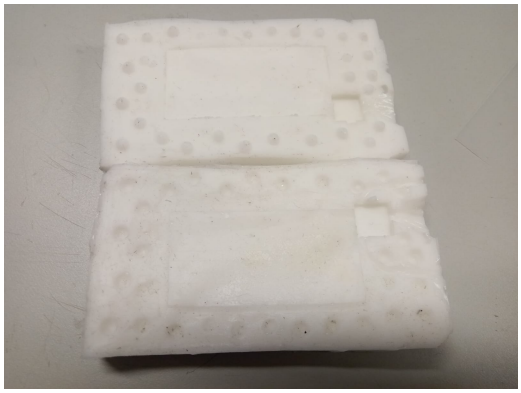


Figure 6.23: Silicon mold for making the root connection

Finally the wing and the wing attachment can be manufactured. The two wing designs were manufactured are shown in figures 6.24 and 6.25.



Figure 6.24: Wing Design 1

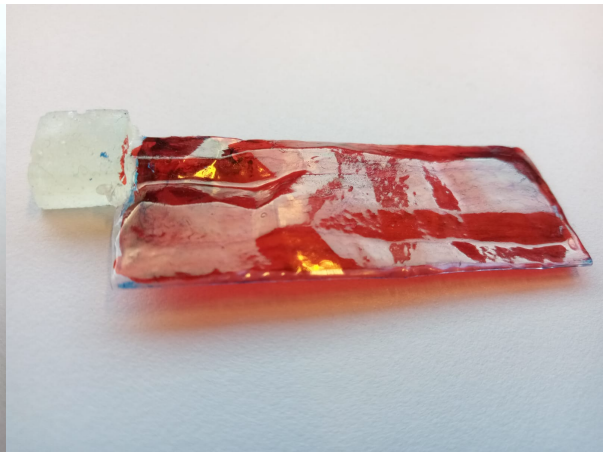


Figure 6.25: Wing Design 2

6.6. Wing Design Experimental Validation

6.6.1. setup

In order to validate the dynamic simulation performed on the wing, an experimental setup was used (figure 6.27) to simulate the flapping motion, where the obtained the wing prototypes is attached and the obtained deformation is recorded. A D.C motor is actuating a 4 bar mechanism where the the wing is attached to the end of the rocker to achieve the flapping motion. The wing motion is captured using a high speed camera with 300 fps. The voltage is controlled in the power source to get the desired RPM at the motor. The setup is shown in figure 6.27

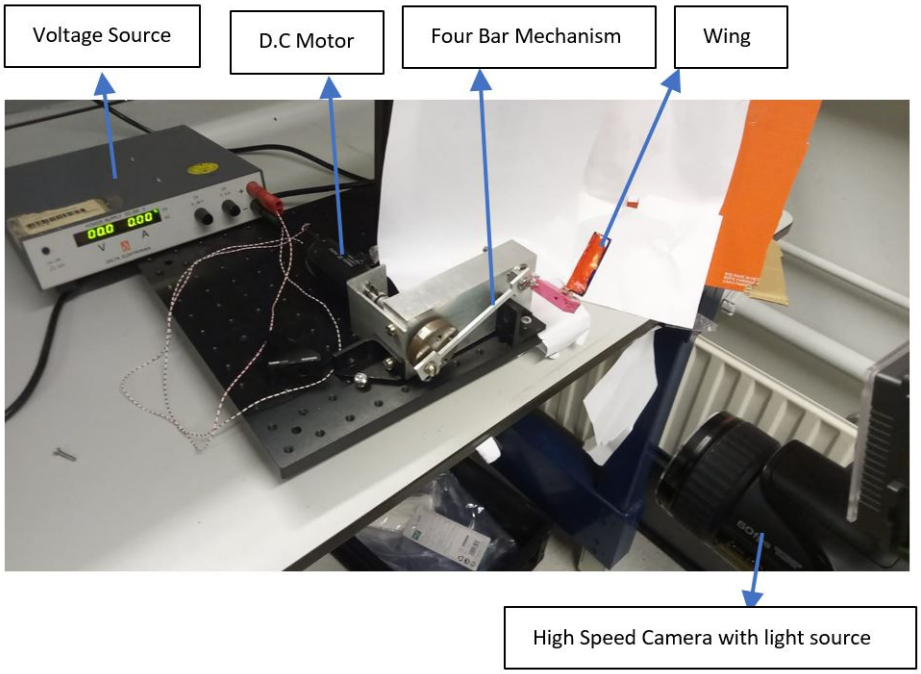


Figure 6.26: Experimental Setup

The camera angle is adjusted to capture the out of plane deformation of the wing. The experiment was conducted to measure the deformation of wing 1. For this test, the sweeping motion is provided at an rpm of 1000 and the amplitude is 60 degrees. The results of the wing cycle is shown in figures .

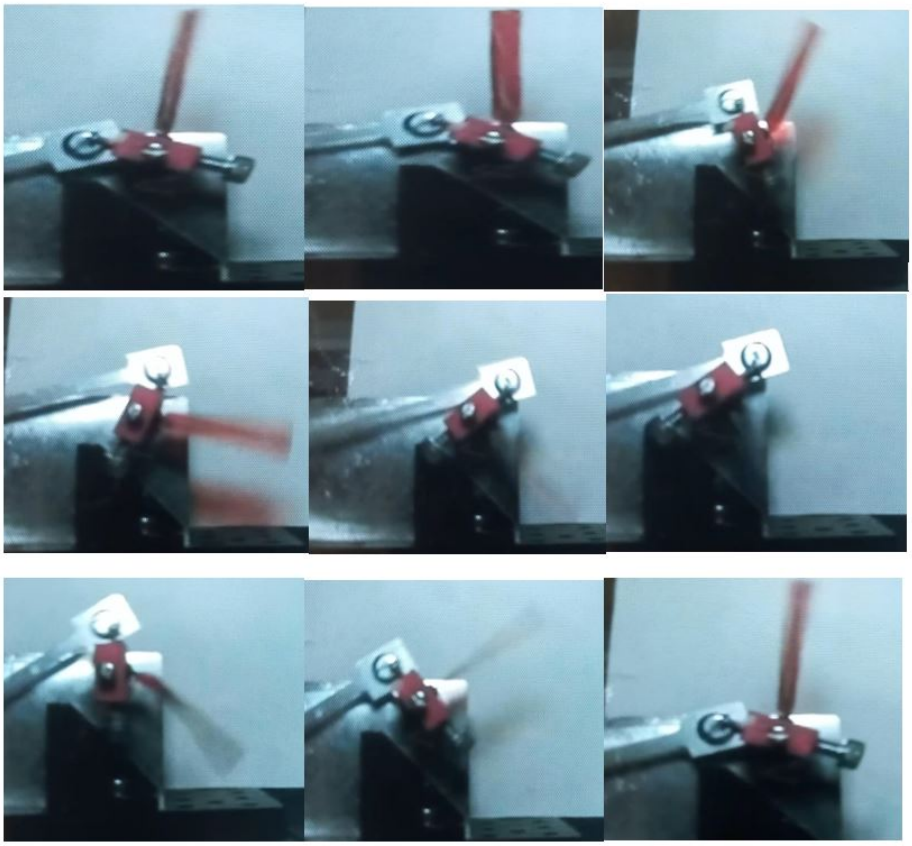


Figure 6.27: Camera Capture for the wing flapping cycle using the high speed camera. The figure shows 9 frames from top left to bottom right

6.6.2. Measured pitching behaviour

The measured kinematics is shown in figure 6.28. The results show that the pitching motion follows a non symmetric harmonic motion. During the middle of the first half cycle the pitching amplitude is 34 degrees, while during the the other half the amplitude is 24 degrees. Also a phase shift is observed of approximately 60 degrees between the sweeping and pitching motions. The results shows that the non symmetric behaviour observed in the static analysis shows up during flapping motion. The results in the desired kinematics in an approximate sense, however, the amplitude and phase shift should be improved for a better performance. There is a discrepancy between the dynamic simulation results for the pitching motion and the experimental results. There can be many reasons attributed to this. Some errors are related to the simulation, others are related to the physical realization and testing procedure of the wing.

Related to making the wing, one reason can be attributed to the shape inaccuracies that occurred during manufacturing as mentioned earlier. However, this reason should be minor. Another error is related to the testing, as during the flapping test, the flapping mechanism doesn't provide an ideal harmonic oscillation, which will effect the passive pitching motion of the wing. Major causes of discrepancy, however, are thought to be related to the dynamic simulation. For example viscous damping is applied instead of an aerodynamic load, which can effect the results significantly due the small thickness of the wing. Another major cause of inaccuracy is related to the type of analysis in the dynamic simulation which was conducted. The dynamic simulation is a linear one, however, this can be quite inaccurate since the problem is highly non linear due to high displacements and strains in this problem. This is attributed to the slender structure of the wings and the folding pattern it posses. Thus a linear analysis can only be as good as an approximation to the actual deformation profile that is occurring which can only be measured by experimentation.

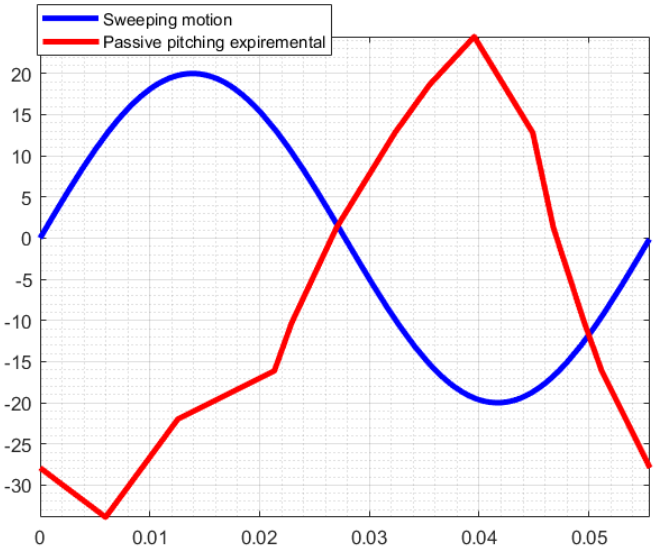


Figure 6.28: Wing kinematics obtained from experiments

7

Retrospection and Discussion

In this paper, shell shape optimization as a method for flapping wing design was investigated. A first design was obtained by formulating the design problem as a twist maximization optimization with bending constrain. A second design was obtained using an objective of minimizing the difference in deformation between the design and an aerodynamically optimal ideal wing. The first design dynamic behaviour was investigated in simulation, and the performance of the wing is measured in terms of lift and drag using an adjusted quasi steady model. The wing was manufactured using a vacuum forming process. Having the physical wing, this wing is attached to flapping mechanism, through which we can observe the passive pitching motion using a high speed camera. The results showed an overall desired behaviour, however, it doesn't match exactly the simulation. Finally a strong, light wing was obtained using a reproducible and robust process that shows promising wing design. A summary of the work done in this study is shown in figure 7.1.

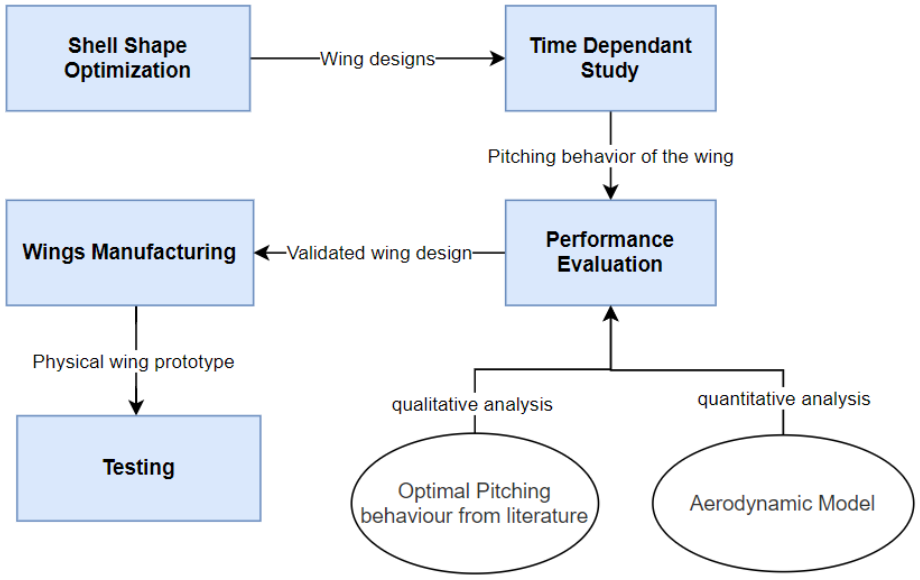


Figure 7.1: Summary of the work done in this study

7.1. Shell Shape Optimization

Different Optimization models were attempted to find the optimization settings for achieving the best performance. The effect of different parameters such as filter radius, load magnitude and type of loading on the results was also measured qualitatively using sensitivity analysis and by varying them from one model to another. Mesh sensitivity analysis showed that this this type of optimization is mesh sensitive. Model B22F was shown to have best Twist to bending ratio, as well as a high degree of symmetrical behaviour for loading in the two directions. There is still non symmetric behaviour that can be seen. Non symmetric behaviour is a feature that is observed in insects wings. The designs share some similarities in terms of structure 7.3 and behaviour of insect wings.

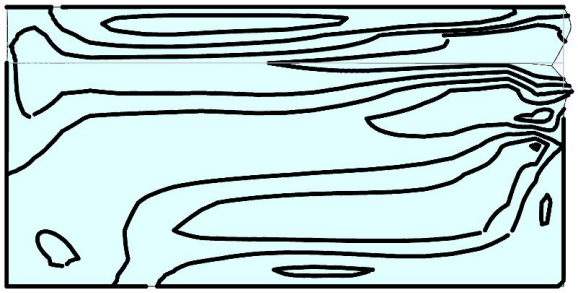


Figure 7.2: Wing Design 1

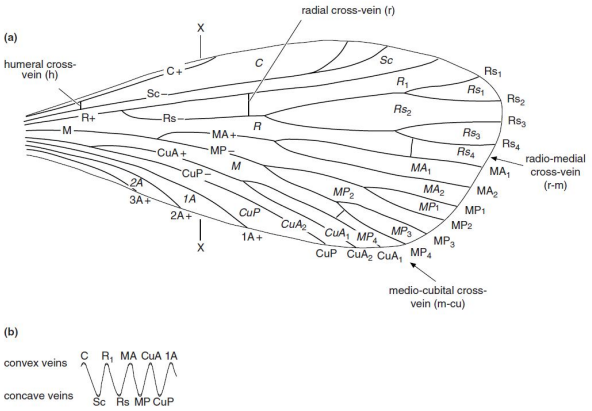


Figure 7.3: Insect Wing

The vein structure of the wing which act on the folds can be seen in the optimized wing designs 7.2. A network of veins extend from the root radially outwards. The density of the veins increases as they move outwards. In terms of deformation profile we can observe the presence flexion lines, which are lines of higher deformation gradient in the regions where the folds are less concentrated. Due to the known non convexity of this type of shape optimization, different initial designs can result in different shapes of the wing. This analysis does not guarantee achieving the required dynamic behaviour, therefore, further analysis was needed to be performed on the designs to show this.

The initial wing design is chosen to be a flat rectangular plate with arbitrary thickness. The overall shape is constrained to avoid designs that are difficult to realize. However, as shown by Wang [76] the chordwise area distribution has a significant effect on the pitching behaviour. Therefore, exploration of optimal planform might help us achieving the desired mechanical behaviour.

In this study the wing designs are obtained from a the high fidelity F.E mechanical model. However, the finite elements analysis have limitations specially when dealing with this type of shape optimization. The corrugation pattern is limited by the the fold angle limit imposed due to the type of elements used. This elements cannot handle discontinuous displacement fields, which can occur due to the high fold angles. This results FE analysis results with limited accuracy. The sensitivity analysis shows that this type of optimization is mesh dependant, which means that for different initial mesh we can get different final design, thus the final design is not really global optima. With the current COMSOL capabilities, shape optimization is only possible within static analysis, so extending it for a dynamic flapping cycle is not straight forward.

7.2. Dynamic Analysis

The dynamic analysis is essential to capture the inertial effects associated with flapping motion. For the dynamic analysis a boundary condition that resembles a rotating wing root is chosen to simulate the flapping motion of the mechanism. The dynamic analysis is a computationally expensive analysis, and to get accurate results, we need step sizes that will result in computational time that is too large for our study. Therefore, a convenient time step was chosen to run the analysis in a reasonable amount of time. For time dependant analysis on COMSOL, a non linear analysis did not converge. Therefore, a linear analysis is performed within the time dependant study. This of course will also limit the accuracy of the information that we obtain from dynamic analysis.

It was attempted to couple the aerodynamic model to the dynamic analysis, however, the simulation didn't stabilize. This can be attributed that the time dependant solver takes smaller steps within the analysis, without calculating the corresponding aerodynamic loads. Viscous damping was therefore added as replacement to the aerodynamic model. The value of the viscous damping was chosen in an arbitrary fashion. Further experimentation needs to be done to choose a realistic damping coefficient. Moreover, the accuracy of the adjusted quasi steady aerodynamic model needs to be evaluated through experimentation. In this study, the dynamic analysis was performed for wing design 1 only, even though wing design 2 could be a better candidate for the wing design.

7.3. Wing Manufacturing

Although the manufacturing process of corrugated wings has shown potential to automate the wing manufacturing process and make it more reproducible and faster, it is still a work in progress. Vacuum forming has shown potential as an alternative to manual hot pressing method, there are some difficulties that were faced during the manufacturing of the wings. The main difficulty is the burning of PETG at small thickness before reaching glass transition temperature. Getting the timing correct for stopping the heating is difficult to achieve.

The current wing designs has a thickness of 0.3 mm which is much larger than the desired design wing thickness of 0.1 mm. This resulted in difficulty to compare the simulations with experiments.

Even though the vacuum forming process is as close as it gets to the mold design. There is still in accuracy that builds up in the predeceasing steps in the process, that is in creating the Mold Model and the manufacturing of the Mold. The inaccuracies is shown in the steps taking to create the physical wing from the optimized design shown in figure 7.4.

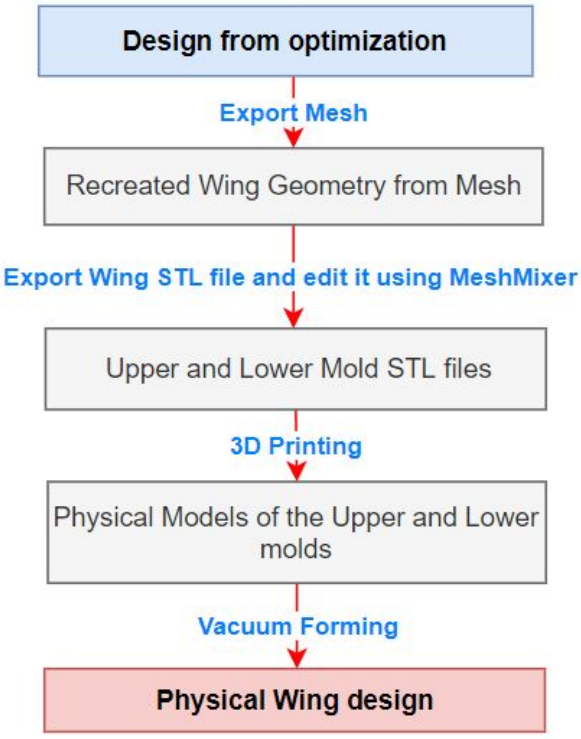


Figure 7.4: Manufacturing process of the wing with errors in the process

Due to the errors mentioned, we need to quantify how far is the manufactured wings from our optimized designs. This can be done by using white light interferometry. This technique can measure features in sub micro accuracy, making it a good method to measure the obtained wing shape. The shape of the wing is measure along several lines as shown here.

7.4. Testing

In FWMAV wing design experimental validation and testing is of utmost importance due to the simplifying assumption made in simulations. Due to a number of reasons it was difficult to replicate simulation results. First of all the thickness of the wings used was much higher than the simulation, which will hinder the twisting behaviour of the wing. Moreover, the inaccuracies mentioned in the manufacturing process can be in issue due the very small scale we are dealing with. Another major influence can be the position of the fixed edge of the wing, which is determined by the manufacturing accuracy of the connecting block to the wing. This fixed edge is approximated to be straight edge for ease of manufacturing, however, the actual boundary condition is at an angle. The dynamic analysis has some inaccuracies mentioned such as time step size, but the most influential aspect is the linear dynamic analysis assumption. This assumption failed to show the fact that the wing buckles at the desired flapping frequency, which was only shown in experimentation. At a lower frequency, the behaviour of the wing has shown pitching behaviour to some extent. The measurement of the pitching was done using a high speed camera, where the images were analyzed at certain time instances during the flapping cycle. The pitching angle was estimated using a fine grid on the obtained images, by counting the number of squares at the leading edge spans as a ratio to the length of the wing (fig 7.5).

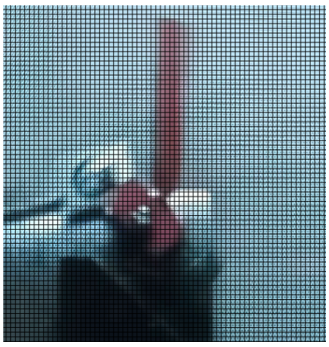


Figure 7.5: measurement of pitching angle

The top view was chosen to measure the pitching angle because its always perpendicular to the wing motion, unlike the front view, which was chosen for the simulation. It should be mentioned that errors during testing, such as parallax error during camera placement, should be avoided or minimized.

8

Final Remarks

8.1. Conclusion

- Shell shape optimization has shown it has potential to output wing designs that can achieve complex deformation profile required for passive pitching wings.
- This type of optimization was known to be non convex, therefore needed multiple models to explore the possible design space and thus approaching a global optimum design.
- Model B22 of the wing, that has a angle objective for the trailing edge tip and an angle constraint for the leading edge tip was shown to produce the wing with highest twist to bending ratio.
- Finer mesh resulted in better performance, as well as applying a point load rather than a distributed load.
- This method has shown convergence problems when dealing with multiple objectives, such as the one used for design 2, however, due to the nature of gradient based methods the obtained design has shown a deformation profile close to the required one.
- A qualitative analysis of the wing performance performed by measuring the passive pitching motion of the wing resulting from a dynamic simulation of flapping has shown that it mimics optimal pitching behaviour. Quantitative analysis of the lift and drag forces on the wing by applying an approximate aerodynamic model also confirmed this.
- Manufacturing the wing prototype has shown that manufacturing process of corrugated thin small scaled sheets is possible and can be more accurate and reproducible manner than current common wing manufacturing methods like cut and glue.
- Experimental testing of the physical prototype has shown that the dynamic analysis of the wing designs can be not very reliable, mainly due to neglecting the non linear effects. However, passive pitching behaviour is still achieved by the tested wings.

8.2. Future Work

The simulation results backed up with the experimental results shows that this wing design has potential to be used for flapping wing design. However, there is still some work to be done in different aspects, which was touched up on by this research that needs further investigation.

- A straight forward extension of this research is to combine the shell shape optimization with topology or thickness as extra design variables. This has the potential to get a higher twist to bending ratios. Another aspect also related to the static load case optimization is to try to optimize the twist to bending ratio in both loading direction, thus achieving more symmetric pitching behavior and better performance.

- A more complete optimization to be investigated is including the dynamic behaviour in the optimization and maximizing the pitching behaviour during the whole cycle, or mid-stroke for instance. Starting with viscous damping as the aerodynamic load, then including the deformation dependant quasi steady load. Two problems arises in such attempt, first the computational cost is much higher than for the optimization under static load, so some simplification needs to be done in the objective and the modeling to make the computational cost feasible. Another difficulty is related to the implementation on COMSOL as this type of optimization is generally not available, so access to the source code might be needed.
- Another goal can be obtaining an efficient aerodynamic model that takes into the account wing camber. This is one of the major in accurate assumption that was done when adjusting the quasi steady model for the deformation. A model which takes camber and corrugations into account can more accurately predict the performance of the obtained designs, and may even be used in the dynamic optimization to obtain the wing design.
- Another research can be done focusing on the manufacturing of the wing, since the method used was attempted for the proof of concept, a more robust and reproducible method can be obtained. For example [69] showed that laser ablation technique can be used to create wings with corrugated patterns up to micrometer accuracy.
- Finally more investigation on experimental testing can be done with the obtained wings. For example, the lift and drag forces and be measured by attaching a sensitive accelerometer to the available setup. Moreover, the wings can be integrated to the MAV and a first flight can be attempted using the available wings. A comparison between the performance of the available wings designs can then performed and documented.

A

Quasi steady model Matlab code

A.1. Main Function

```
clear all
clc


k=1;
f=26.3;
syms t1

D=0;

rr=0.02;
Fld=0;
m=1;
kk=0:0.001:0.025;
kk=-kk;

kk=-0.01;
mm=0:0.0005:0.04;
%A = xlsread('disp_pw.xlsx');
%t=A(:,1);
%w2=A(:,11);
%w1=A(:,21);
Ft=0;
m=1;
AvL=0;
AvD=0;
Lift=[];
Drag=[];

rad=0.0025:0.005:0.0475;
rad=0.025;
D=-0.02;
for rr=rad
    Ft=0;
    Fld=0;
    k=1;
for tt=mm
```

```
38
39  d1=D*cos(2*pi*f*t1);
40  d2=(D/3)*cos(2*pi*f*t1);
41
42  d=subs(d1,t1,tt);
43  dd=subs(d2,t1,tt);
44  %dd=0;
45  %d=double(d);
46  %d2=0;
47  %dd=0;
48  %w2=A(k,1+m);
49  %w1=A(k,11+m);
50  %d=w2;
51  %dd=w1;
52  %dd=d/3;
53  %dd=0;
54  [eta,etad, etadd,alpha2,heaving,hd,hdd,Fl,Fd,vd] = Lift_h(tt,d,dd,rr);
55
56  %Fd1(k)=Fd;
57  eta1(k)=eta;
58  alpha1(k)=alpha2;
59  Fl1(k)=Fl;
60  Fd1(k)=Fd;
61
62
63  Fld=eta+Fld;
64
65  heaving1(k)=heaving;
66  hd1(k)=hd;
67  hdd1(k)=hdd;
68  etad1(k)=etad;
69  etadd1(k)=etadd;
70
71  syms TT
72  Phi=66*sin(2*pi*26.3*TT);
73  Phid=diff(Phi,TT);
74
75
76      vel=vd;
77
78
79          AvL=Fl1(k)+AvL;
80
81
82      if Fd1(k)*vel>=0
83         AvD=AvD+abs(Fd1(k));
84      else
85
86         AvD=AvD-abs(Fd1(k));
87
88      end
89
90
91  k=k+1;
92  end
93  Lift(m)=AvL;
```

```
Drag(m)=AvD;


AvD=0;
AvL=0;









%eff(m)=Fld;
Fld=0;
m=m+1;
end

%tt=mm;
%set(gcf,'color','w');

%plot (-kk,eff,'LineWidth',5)
%xlabel('Displacement Amplitude')
%ylabel('Lift to Drag ratio')

%hold on
n=1;
for aa=mm
    if Fl1(n)>0
    LD(n)=abs(Fl1(n)/Fd1(n));
    else
        LD(n)=-abs(Fl1(n)/Fd1(n));
    end
    n=n+1;

end

eta1=eta1*180/pi;
alpha1=alpha1*180/pi;



AvD=0;
AvL=0;
syms TT
Phi=66*sin(2*pi*26.3*TT);
Phid=diff(Phi,TT);
q=1;
rr=1;
for hh=mm
    vel=subs(Phid,TT,hh);
    vel=double(vel);

        AvL=Fl1(q)+AvL;
        rr=rr+1;

```

```
    if Fd1(q)*vel>=0
       AvD=AvD+abs(Fd1(q));
    else

       AvD=AvD-abs(Fd1(q));
       TotD=AvD;
    end


    q=q+1;
end
TotL=AvL;
AvL=(AvL*1)/rr;
%AvD=AvD/length(Fd1);

set(gcf,'color','w');

plot (mm,eta1,'LineWidth',2)

hold on
plot (mm,alpha1,'LineWidth',2)
%hold on
%plot (mm,hd1(1:2001),'LineWidth',2)
%fplot(Phi,[0.4 0.5],'LineWidth',2)
%fplot(Phi/400000,[0.4 0.5],'LineWidth',2)

legend('Lift','Drag', 'theta','phi')
xlabel('time ')
%xlim([0.4182 0.4563])
ylabel('Force [N]')



%{
set(gcf,'color','w');
plot (mm,alpha1,'LineWidth',2)
hold on
plot (mm,eta1,'LineWidth',2)
ylabel('Displacement in z direction [m]')
xlabel('time [s]')
legend('Middle of Leading Edge ','Centre of the Wing')
xlim([0.4182 0.4563])
%}
```

A.2. Called Function

```
function [eta,etad,alpha2,theta,thetad,Fl,Fd]=quasi(tt,d1,d2)
persistent etat0 etat1 thetat0 thetat1
d=d1;
f=26.3;
Mw=47*10^-6;
A_phi=60.5*(pi/180);
A_eta=58*(pi/180);
ph_et=-90*(pi/180);
c_b=0.025;
```

```
R=51.9*10^-3;
Ct=1.678;
Cd0=0.07;
Cdpi=3.06;
Cr=pi;
mu1=0.2;
mu2=0.2;
rho=1.29;
b=0.0001;
dt=0.0005;
rr=0.0475;
syms t1
phi=A_phi*sin(2*pi*f*t1);

eta1=pi/2;
etad= 0;
etadd=0;

L=0.025;
% Eta calculation

eta=-acos(d/L);

if tt==0
d0=d;
hakim=-acos(d/L);
end

phid=diff(phi,t1);
theta=0;
phidd=diff(phid,t1);
thetad=0;
thetadd=0;

phid=diff(phi,t1);
theta=0;
phidd=diff(phid,t1);
thetad=0;
thetadd=0;

%Numerical Calculation of velocity and acceleration
if tt>1*dt
etad=(eta-etat0)/dt;
else
etad= diff(eta,t1);
end

if tt>=2*dt
etadd=(eta-2*etat0+etat1)/dt^2;
else
etadd=0;
end

%Heaving
dh=d2;
```

```
theta=asin(dh/(0.025));
if tt>1*dt
thetad=(theta-thetat0)/dt;
else
thetad= diff(theta,t1);
end

if tt>=2*dt
thetadd=(theta-2*thetat0+thetat1)/dt^2;
else
thetadd=0;
end

r=rr;

vx=r*(phid*cos(theta)*cos(eta)+thetad*sin(eta));
vy=r*(thetad*cos(eta)-phid*cos(theta)*sin(eta));
ax=r*((phidd*cos(theta)-thetad*(etad+phid*sin(theta)))*cos(eta)-...
(thetadd+etad*phid*cos(theta))*sin(eta));
ay=r*((thetad*(etad-phid*sin(theta))-phidd*cos(theta))*sin(eta)+...
(thetadd-etad*phid*cos(theta))*cos(eta));
vx = subs(vx, r, rr);
vy = subs(vy, r, rr);
ax = subs(ax, r, rr);
ay = subs(ay, r, rr);
v=(vy.^2+vx.^2).^0.5;
c=c_b;
m11=0.25*pi*rho*b^2;
m22=0.25*pi*rho*c.^2;
Ia=(1/128)*pi*rho*(c.^2+b^2).^2;

%% alpha
phid=subs(phid,t1,tt);
if phid<=0
        alpha2=-eta;
else
        alpha2=-(pi+eta);
end
circ=-0.5*Ct*c.*abs(v)*sin(2*alpha2)+0.5*Cr*c.^2*etad;
DFxv=(0.5*rho*c.*(Cd0*(cos(alpha2))^2+...
Cdpi*(sin(alpha2))^2)*abs(v)'.*vx)*(R/10);
DFyv=(0.5*rho*c.*(Cd0*(cos(alpha2))^2+...
Cdpi*(sin(alpha2))^2)*abs(v)'.*vy)*(R/10);
dFx= (((c/(c_b*R))*Mw+m22).*vy*etad-rho*circ.*vy-m11*ax)*(R/10)-DFxv;
dFy=(-((c/(c_b*R))*Mw+m11).*vx*etad+rho*circ.*vx-m22.*ay)*(R/10)-DFyv;


dTv=((1/16)*pi*rho*c.^4*(mu1*f+mu2*abs(etad))*etad) *R/10;
dT=((m11-m22).*vx.*vy-Ia*etadd)*R/10-dTv;
Fx=sum( dFx , 'all' );
Fy=sum( dFy , 'all' );
Fxv=sum( DFxv , 'all' );
Fyv=sum( DFyv , 'all' );
Tv=sum( dTv , 'all' );
Circ=sum( circ , 'all' );
```

```
120 Fl=dFx*sin(eta)+dFy*cos(eta);
121 Fd=dFy*sin(eta)-dFx*cos(eta);
122
123
124
125 k=(tt/dt)+1;
126 if k==0
127     etat0=eta;
128     thetat0=theta;
129 else
130     etat1=etat0;
131     etat0=eta;
132     thetat1=thetat0;
133     thetat0=theta;
134 end
135 dFy1=subs(dFy,t1,tt);
136 dFy2=double(dFy1);
137 Fd=subs(Fd,t1,tt);
138 Fd=double(Fd);
139 Fl=subs(Fl,t1,tt);
140 Fl=double(Fl);
141 theta=double(theta);
```

B

Design 1 Deformation Data

B.1. Trailing Edge

Time (s)	ppb2 (m)	ppb3 (m)	ppb4 (m)	ppb5 (m)	ppb6 (m)	ppb7 (m)	ppb8 (m)	ppb9 (m)	ppb10 (m)	ppb11 (m)
0.412	-0.0038049	-0.0056825	-0.0075774	-0.0095109	-0.011461	-0.013432	-0.015394	-0.017276	-0.019007	-0.020867
0.4125	-0.0039382	-0.0058912	-0.0078647	-0.0098877	-0.011933	-0.013994	-0.01604	-0.017985	-0.01974	-0.021566
0.413	-0.0040445	-0.0060597	-0.0080982	-0.010197	-0.012323	-0.014461	-0.016576	-0.018572	-0.020339	-0.022117
0.4135	-0.0041233	-0.0061868	-0.0082765	-0.010437	-0.012628	-0.014829	-0.017	-0.019033	-0.020799	-0.022518
0.414	-0.004174	-0.0062718	-0.0083983	-0.010605	-0.012848	-0.015096	-0.017307	-0.019363	-0.021117	-0.022765
0.4145	-0.0041961	-0.0063139	-0.0084628	-0.010702	-0.01298	-0.01526	-0.017497	-0.019561	-0.021291	-0.022856
0.415	-0.0041897	-0.006313	-0.0084696	-0.010725	-0.013023	-0.015319	-0.017567	-0.019626	-0.021319	-0.022792
0.4155	-0.0041546	-0.006269	-0.0084186	-0.010675	-0.012978	-0.015275	-0.017517	-0.019557	-0.021203	-0.022572
0.416	-0.0040912	-0.0061822	-0.0083102	-0.010552	-0.012844	-0.015126	-0.017347	-0.019355	-0.020941	-0.022198
0.4165	-0.0039999	-0.0060532	-0.0081451	-0.010357	-0.012622	-0.014874	-0.01706	-0.01902	-0.020537	-0.021673
0.417	-0.0038813	-0.005883	-0.0079243	-0.010092	-0.012315	-0.01452	-0.016655	-0.018556	-0.019992	-0.020999
0.4175	-0.0037362	-0.0056726	-0.0076496	-0.0097574	-0.011923	-0.014067	-0.016138	-0.017965	-0.019311	-0.020183
0.418	-0.0035657	-0.0054235	-0.0073226	-0.0093565	-0.01145	-0.013519	-0.01551	-0.017251	-0.018499	-0.019229
0.4185	-0.0033708	-0.0051374	-0.0069457	-0.0088918	-0.010898	-0.012878	-0.014776	-0.01642	-0.01756	-0.018143
0.419	-0.0031529	-0.0048162	-0.0065214	-0.0083664	-0.010273	-0.012149	-0.013942	-0.015477	-0.016501	-0.016934
0.4195	-0.0029134	-0.0044622	-0.0060525	-0.0077839	-0.0095772	-0.011337	-0.013012	-0.014428	-0.01533	-0.015609
0.42	-0.0026542	-0.0040777	-0.0055424	-0.0071483	-0.0088162	-0.010448	-0.011994	-0.013281	-0.014054	-0.014178
0.4205	-0.0023768	-0.0036655	-0.0049945	-0.006464	-0.007995	-0.009488	-0.010893	-0.012043	-0.012683	-0.01265
0.421	-0.0020831	-0.0032282	-0.0044125	-0.0057355	-0.0071193	-0.008463	-0.0097187	-0.010723	-0.011224	-0.011036
0.4215	-0.0017753	-0.0027689	-0.0038004	-0.0049679	-0.006195	-0.0073802	-0.0084778	-0.0093298	-0.0096895	-0.0093463
0.422	-0.0014554	-0.0022907	-0.0031624	-0.0041664	-0.0052284	-0.0062471	-0.0071791	-0.0078729	-0.0080886	-0.007593
0.4225	-0.0011255	-0.0017968	-0.0025028	-0.0033365	-0.0042262	-0.0050713	-0.0058314	-0.0063624	-0.0064325	-0.0057878
0.423	-7.88E-04	-0.0012907	-0.0018261	-0.0024838	-0.0031951	-0.003861	-0.0044439	-0.0048084	-0.0047324	-0.0039432
0.4235	-4.45E-04	-7.76E-04	-0.0011369	-0.0016142	-0.0021423	-0.0026243	-0.003026	-0.0032216	-0.0030001	-0.0020717
0.424	-9.91E-05	-2.56E-04	-4.40E-04	-7.34E-04	-0.0010748	-0.0013697	-0.0015876	-0.0016128	-0.0012474	-1.86E-04
0.4245	2.48E-04	2.66E-04	2.60E-04	1.52E-04	4.90E-08	-1.06E-04	-1.38E-04	6.94E-06	5.14E-04	0.0017009
0.425	5.92E-04	7.86E-04	9.58E-04	0.0010367	0.0010749	0.0011589	0.0013119	0.0016267	0.0022717	0.0035763
0.4255	9.33E-04	0.0013012	0.0016496	0.0019142	0.0021424	0.0024156	0.0027532	0.0032353	0.004014	0.0054272
0.426	0.0012679	0.0018071	0.0023299	0.0027787	0.0031952	0.0036559	0.0041757	0.0048218	0.0057289	0.0072411
0.4265	0.0015938	0.0023006	0.0029944	0.0036242	0.0042263	0.0048712	0.0055697	0.0063755	0.0074047	0.0090056
0.427	0.0019088	0.0027785	0.0036384	0.004445	0.0052285	0.0060533	0.0069257	0.0078856	0.00903	0.010709
0.4275	0.0022108	0.0032373	0.0042576	0.0052355	0.0061951	0.0071941	0.0082345	0.009342	0.010594	0.012339
0.428	0.0024977	0.0036742	0.0048477	0.0059902	0.0071194	0.0082858	0.0094871	0.010735	0.012085	0.013884
0.4285	0.0027676	0.0040859	0.0054048	0.0067041	0.0079951	0.009321	0.010675	0.012054	0.013494	0.015336
0.429	0.0030186	0.0044698	0.005925	0.0073722	0.0088163	0.010293	0.01179	0.013291	0.014811	0.016682
0.4295	0.0032489	0.0048231	0.0064048	0.0079901	0.0095773	0.011194	0.012825	0.014438	0.016027	0.017915
0.43	0.0034572	0.0051436	0.0068408	0.0085534	0.010273	0.012019	0.013772	0.015485	0.017133	0.019025
0.4305	0.0036418	0.0054289	0.0072302	0.0090583	0.010899	0.012762	0.014625	0.016428	0.018123	0.020006
0.431	0.0038016	0.0056773	0.0075703	0.0095015	0.01145	0.013418	0.015378	0.017258	0.018989	0.02085
0.4315	0.0039354	0.0058869	0.0078587	0.0098798	0.011923	0.013982	0.016026	0.01797	0.019725	0.021552
0.432	0.0040424	0.0060563	0.0080935	0.010191	0.012315	0.014451	0.016565	0.01856	0.020327	0.022106
0.4325	0.0041218	0.0061844	0.008273	0.010432	0.012622	0.014821	0.016992	0.019023	0.02079	0.02251
0.433	0.0041731	0.0062703	0.0083962	0.010602	0.012844	0.015091	0.017302	0.019357	0.021111	0.022761
0.4335	0.0041959	0.0063134	0.008462	0.0107	0.012978	0.015257	0.017494	0.019558	0.021288	0.022856
0.434	0.0041901	0.0063135	0.0084701	0.010725	0.013023	0.015319	0.017566	0.019626	0.02132	0.022795
0.4345	0.0041557	0.0062704	0.0084204	0.010677	0.01298	0.015277	0.017519	0.01956	0.021207	0.022579
0.435	0.004093	0.0061846	0.0083133	0.010556	0.012848	0.01513	0.017353	0.019361	0.020949	0.022208
0.4355	0.0040023	0.0060566	0.0081494	0.010362	0.012628	0.01488	0.017067	0.019029	0.020548	0.021686
0.436	0.0038843	0.0058873	0.00793	0.010099	0.012323	0.014529	0.016666	0.018568	0.020006	0.021016
0.4365	0.0037398	0.0056778	0.0076564	0.0097658	0.011933	0.014079	0.016151	0.01798	0.019329	0.020203
0.437	0.0035698	0.0054296	0.0073306	0.0093664	0.011461	0.013532	0.015525	0.017269	0.018519	0.019252
0.4375	0.0033755	0.0051443	0.0069548	0.0089031	0.010912	0.012893	0.014794	0.01644	0.017583	0.018169
0.438	0.0031581	0.0048239	0.0065315	0.008379	0.010288	0.012167	0.013962	0.0155	0.016527	0.016963
0.4385	0.0029191	0.0044706	0.0060637	0.0077978	0.0095938	0.011357	0.013034	0.014453	0.015358	0.015641
0.439	0.0026603	0.0040868	0.0055545	0.0071634	0.0088342	0.010469	0.012018	0.013308	0.014085	0.014212
0.4395	0.0023833	0.0036752	0.0050074	0.0064801	0.0080144	0.0095107	0.010919	0.012072	0.012715	0.012686
0.44	0.00209	0.0032384	0.0044261	0.0057526	0.0071398	0.008487	0.0097462	0.010754	0.011258	0.011074
0.4405	0.0017825	0.0027796	0.0038147	0.0049858	0.0062166	0.0074055	0.0085068	0.0093623	0.0097253	0.0093856
0.441	0.0014628	0.0023018	0.0031772	0.004185	0.0052509	0.0062734	0.0072093	0.0079068	0.0081257	0.0076336
0.4415	0.0011331	0.0018082	0.002518	0.0033557	0.0042494	0.0050986	0.0058626	0.0063973	0.0064708	0.0058295
0.442	7.96E-04	0.0013024	0.0018417	0.0025035	0.0032189	0.0038889	0.0044759	0.0048442	0.0047716	0.0039856
0.4425	4.53E-04	7.88E-04	0.0011527	0.0016342	0.0021665	0.0026528	0.0030586	0.0032581	0.0030399	0.0021145
0.443	1.07E-04	2.68E-04	4.56E-04	7.54E-04	0.0010992	0.0013985	0.0016205	0.0016497	0.0012875	2.29E-04
0.4435	-2.40E-04	-2.54E-04	-2.44E-04	-1.32E-04	2.45E-05	1.35E-04	1.71E-04	3.00E-05	-4.74E-04	-0.001658
0.444	-5.85E-04	-7.75E-04	-9.42E-04	-0.0010166	-0.0010504	-0.0011301	-0.0012789	-0.0015898	-0.0022317	-0.0035337
0.4445	-9.26E-04	-0.0012895	-0.0016339	-0.0018944	-0.0021181	-0.0023871	-0.0027205	-0.0031988	-0.0039745	-0.0053854
0.445	-0.0012604	-0.0017956	-0.0023146	-0.0027592	-0.0031714	-0.0036279	-0.0041436	-0.004786	-0.0056902	-0.0072003
0.4455	-0.0015865	-0.0022895	-0.0029795	-0.0036052	-0.0042031	-0.0048439	-0.0055383	-0.0063405	-0.007367	-0.008966
0.446	-0.0019018	-0.0027678	-0.003624	-0.0044266	-0.005206	-0.0060268	-0.0068953	-0.0078518	-0.0089935	-0.010671
0.4465	-0.0022041	-0.0032271	-0.0042438	-0.0052178	-0.0061735	-0.0071686	-0.0082053	-0.0093094	-0.010559	-0.012302
0.447	-0.0024914	-0.0036645	-0.0048346	-0.0059735	-0.0070988	-0.0082615	-0.0094592	-0.010704	-0.012052	-0.01385
0.4475	-0.0027616	-0.0040768	-0.0053925	-0.0066883	-0.0079757	-0.0092981	-0.010649	-0.012025	-0.013463	-0.015304
0.448	-0.0030131	-0.0044613	-0.0059136	-0.0073575	-0.0087982	-0.010271	-0.011765	-0.013264	-0.014782	-0.016653
0.4485	-0.0032439	-0.0048154	-0.0063943	-0.0079766	-0.0095606	-0.011174	-0.012802	-0.014412	-0.016	-0.017888
0.449	-0.0034527	-0.0051367	-0.0068314	-0.0085412	-0.010258	-0.012001	-0.013751	-0.015463	-0.017109	-0.019001
0.4495	-0.0036379	-0.0054228	-0.0072219	-0.0090475	-0.010885	-0.012746	-0.014606	-0.016408	-0.018102	-0.019985
0.45	-0.0037982	-0.005672	-0.0075631	-0.0094921	-0.011438	-0.013404	-0.015362	-0.01724	-0.01897	-0.020832
0.4505	-0.0039327	-0.0058825	-0.0078527	-0.0098719	-0.011913	-0.01397	-0.016013	-0.017956	-0.01971	-0.021537
0.451	-0.0040403	-0.0060529	-0.0080887	-0.010184	-0.012307	-0.014442	-0.016554	-0.018548	-0.020315	-0.022095
0.4515	-0.0041203	-0.0061819	-0.0082696	-0.010427	-0.012616	-0.014814	-0.016983	-0.019014	-0.020781	-0.022503
0.452	-0.0041723	-0.0062688	-0.008394	-0.010599	-0.01284	-0.015086	-0.017296	-0.019351	-0.021105	-0.022757
0.4525	-0.0041957	-0.0063129	-0.0084612	-0.010699	-0.012976	-0.015254	-0.017491	-0.019555	-0.021286	-0.022855
0.453	-0.0041906	-0.0063139	-0.0084706	-0.010725	-0.013023	-0.015319	-0.017566	-0.019626	-0.021321	-0.022798
0.4535	-0.0041568	-0.0062719	-0.0084222	-0.010679	-0.012982	-0.015279	-0.017522	-0.019563	-0.021211	-0.022585
0.454	-0.0040947	-0.0061871	-0.0083164	-0.010559	-0.012852	-0.015135	-0.017358	-0.019367	-0.020956	-0.022218
0.4545	-0.0040047	-0.00606	-0.0081538	-0.010368	-0.012634	-0.014887	-0.017075	-0.019038	-0.020558	-0.0217
0.455	-0.0038873	-0.0058916	-0.0079356	-0.010105	-0.01233	-0.014538	-0.016676	-0.01858	-0.02002	-0.021033
0.4555	-0.0037434	-0.005683	-0.0076633	-0.0097742	-0.011943	-0.01409	-0.016164	-0.017995	-0.019345	-0.020223
0.456	-0.003574	-0.0054357	-0.0073386	-0.0093762	-0.011473	-0.013546	-0.015541	-0.017287	-0.018539	-0.019275
0.4565	-0.0033802	-0.0051512	-0.0069639	-0.0089144	-0.010925	-0.012909	-0.014812	-0.016461	-0.017606	-0.018196
0.457	-0.0031633	-0.0048316	-0.0065417	-0.0083917	-0.010303	-0.012184	-0.013982	-0.015522	-0.016552	-0.016992

B.2. Leading Edge

Time (s)	ppb12 (m)	ppb13 (m)	ppb14 (m)	ppb15 (m)	ppb16 (m)	ppb17 (m)	ppb18 (m)	ppb19 (m)	ppb20 (m)	ppb21 (m)
0.412	-5.70E-05	-2.02E-04	-8.61E-04	-0.0021885	-0.003778	-0.0053632	-0.0069604	-0.0085601	-0.01006	-0.011371
0.4125	-5.12E-05	-1.77E-04	-8.00E-04	-0.0020616	-0.0035735	-0.0050814	-0.0066032	-0.0081328	-0.0095715	-0.010849
0.413	-4.51E-05	-1.51E-04	-7.34E-04	-0.0019207	-0.0033446	-0.0047649	-0.0062009	-0.00765	-0.009018	-0.010253
0.4135	-3.86E-05	-1.23E-04	-6.63E-04	-0.0017667	-0.0030929	-0.0044158	-0.0057563	-0.0071149	-0.0084031	-0.0095866
0.414	-3.19E-05	-9.48E-05	-5.87E-04	-0.0016006	-0.0028201	-0.0040367	-0.0052725	-0.0065314	-0.0077308	-0.0088551
0.4145	-2.50E-05	-6.58E-05	-5.07E-04	-0.0014236	-0.002528	-0.00363	-0.0047527	-0.0059032	-0.0070057	-0.008063
0.415	-1.79E-05	-3.64E-05	-4.24E-04	-0.0012369	-0.0022187	-0.0031986	-0.0042004	-0.0052348	-0.0062329	-0.007216
0.4155	-1.07E-05	-6.78E-06	-3.38E-04	-0.0010417	-0.0018942	-0.0027453	-0.0036195	-0.0045307	-0.0054175	-0.0063197
0.416	-3.37E-06	2.29E-05	-2.50E-04	-8.39E-04	-0.0015568	-0.0022733	-0.0030139	-0.0037957	-0.0045652	-0.0053804
0.4165	3.95E-06	5.25E-05	-1.60E-04	-6.31E-04	-0.0012088	-0.0017857	-0.0023877	-0.0030347	-0.0036817	-0.0044043
0.417	1.12E-05	8.17E-05	-6.90E-05	-4.19E-04	-8.53E-04	-0.001286	-0.0017452	-0.0022531	-0.0027731	-0.0033981
0.4175	1.85E-05	1.10E-04	2.26E-05	-2.04E-04	-4.91E-04	-7.78E-04	-0.0010909	-0.0014561	-0.0018456	-0.0023688
0.418	2.55E-05	1.38E-04	1.14E-04	1.25E-05	-1.25E-04	-2.64E-04	-4.29E-04	-6.49E-04	-9.05E-04	-0.0013233
0.4185	3.25E-05	1.65E-04	2.05E-04	2.29E-04	2.41E-04	2.52E-04	2.36E-04	1.62E-04	4.08E-05	-2.69E-04
0.419	3.92E-05	1.91E-04	2.94E-04	4.44E-04	6.06E-04	7.66E-04	8.99E-04	9.72E-04	9.87E-04	7.88E-04
0.4195	4.56E-05	2.15E-04	3.81E-04	6.56E-04	9.66E-04	0.0012743	0.0015558	0.0017761	0.0019261	0.0018385
0.42	5.17E-05	2.38E-04	4.66E-04	8.63E-04	0.0013202	0.0017742	0.0022022	0.0025676	0.0028522	0.0028769
0.4205	5.75E-05	2.60E-04	5.47E-04	0.0010647	0.001665	0.0022621	0.0028336	0.0033416	0.0037589	0.0038957
0.421	6.28E-05	2.80E-04	6.25E-04	0.0012589	0.0019986	0.0027345	0.0034456	0.0040928	0.0046399	0.004888
0.4215	6.78E-05	2.97E-04	6.98E-04	0.0014446	0.0023185	0.0031882	0.0040341	0.0048161	0.0054893	0.0058468
0.422	7.23E-05	3.13E-04	7.67E-04	0.0016204	0.0026225	0.0036202	0.0045951	0.0055065	0.0063012	0.0067658
0.4225	7.62E-05	3.27E-04	8.30E-04	0.0017851	0.0029087	0.0040275	0.0051248	0.0061593	0.0070702	0.0076386
0.423	7.97E-05	3.38E-04	8.88E-04	0.0019377	0.003175	0.0044073	0.0056194	0.0067701	0.0077908	0.0084593
0.4235	8.26E-05	3.47E-04	9.40E-04	0.0020771	0.0034197	0.0047571	0.0060758	0.0073348	0.0084584	0.0092223
0.424	8.50E-05	3.54E-04	9.85E-04	0.0022022	0.0036411	0.0050744	0.0064906	0.0078494	0.0090682	0.0099224
0.4245	8.68E-05	3.58E-04	0.0010239	0.0023124	0.0038376	0.005357	0.0068612	0.0083104	0.0096162	0.010555
0.425	8.80E-05	3.60E-04	0.0010555	0.0024067	0.0040079	0.0056032	0.007185	0.0087147	0.010098	0.011115
0.4255	8.85E-05	3.59E-04	0.0010799	0.0024847	0.0041508	0.005811	0.0074598	0.0090596	0.010512	0.0116
0.426	8.85E-05	3.56E-04	0.0010969	0.0025457	0.0042655	0.0059793	0.0076837	0.0093426	0.010854	0.012005
0.4265	8.79E-05	3.50E-04	0.0011065	0.0025893	0.004351	0.0061067	0.0078551	0.0095619	0.011121	0.012328
0.427	8.67E-05	3.42E-04	0.0011085	0.0026153	0.0044069	0.0061925	0.0079729	0.009716	0.011313	0.012568
0.4275	8.49E-05	3.32E-04	0.0011029	0.0026234	0.0044327	0.006236	0.0080364	0.0098038	0.011428	0.012721
0.428	8.25E-05	3.20E-04	0.0010899	0.0026136	0.0044282	0.006237	0.008045	0.0098247	0.011464	0.012788
0.4285	7.95E-05	3.05E-04	0.0010693	0.002586	0.0043936	0.0061954	0.0079987	0.0097785	0.011423	0.012768
0.429	7.60E-05	2.88E-04	0.0010415	0.0025407	0.0043289	0.0061116	0.0078979	0.0096657	0.011303	0.01266
0.4295	7.20E-05	2.70E-04	0.0010066	0.0024782	0.0042347	0.0059861	0.0077432	0.0094869	0.011107	0.012466
0.43	6.75E-05	2.49E-04	9.65E-04	0.0023987	0.0041117	0.0058197	0.0075356	0.0092433	0.010834	0.012187
0.4305	6.25E-05	2.27E-04	9.16E-04	0.0023028	0.0039605	0.0056136	0.0072766	0.0089368	0.010488	0.011825
0.431	5.72E-05	2.03E-04	8.62E-04	0.0021912	0.0037824	0.0053692	0.006968	0.0085692	0.01007	0.011382
0.4315	5.14E-05	1.78E-04	8.01E-04	0.0020647	0.0035785	0.0050882	0.0066118	0.0081431	0.0095833	0.010862
0.432	4.52E-05	1.51E-04	7.35E-04	0.0019241	0.0033501	0.0047724	0.0062106	0.0076615	0.0090313	0.010267
0.4325	3.88E-05	1.24E-04	6.64E-04	0.0017703	0.0030989	0.0044241	0.0057669	0.0071277	0.0084177	0.0096026
0.433	3.21E-05	9.55E-05	5.89E-04	0.0016045	0.0028265	0.0040456	0.0052839	0.0065452	0.0077467	0.0088724
0.4335	2.52E-05	6.65E-05	5.09E-04	0.0014277	0.0025348	0.0036396	0.0047649	0.005918	0.0070228	0.0080817
0.434	1.81E-05	3.71E-05	4.26E-04	0.0012412	0.0022259	0.0032086	0.0042133	0.0052505	0.006251	0.0072359
0.4345	1.08E-05	7.45E-06	3.40E-04	0.0010462	0.0019018	0.0027558	0.003633	0.0045471	0.0054365	0.0063407
0.435	3.54E-06	-2.23E-05	2.52E-04	8.44E-04	0.0015646	0.0022842	0.0030279	0.0038127	0.004585	0.0054022
0.4355	-3.78E-06	-5.18E-05	1.62E-04	6.36E-04	0.0012169	0.001797	0.0024022	0.0030523	0.0037021	0.0044269
0.436	-1.11E-05	-8.10E-05	7.11E-05	4.24E-04	8.61E-04	0.0012975	0.00176	0.0022711	0.002794	0.0034213
0.4365	-1.83E-05	-1.10E-04	-2.05E-05	2.09E-04	4.99E-04	7.89E-04	0.0011059	0.0014744	0.0018669	0.0023925
0.437	-2.54E-05	-1.38E-04	-1.12E-04	-7.61E-06	1.33E-04	2.76E-04	4.44E-04	6.68E-04	9.27E-04	0.0013473
0.4375	-3.23E-05	-1.65E-04	-2.03E-04	-2.24E-04	-2.33E-04	-2.40E-04	-2.21E-04	-1.44E-04	-1.92E-05	2.93E-04
0.438	-3.90E-05	-1.90E-04	-2.92E-04	-4.39E-04	-5.98E-04	-7.54E-04	-8.84E-04	-9.54E-04	-9.65E-04	-7.63E-04
0.4385	-4.54E-05	-2.15E-04	-3.79E-04	-6.51E-04	-9.58E-04	-0.0012628	-0.001541	-0.0017579	-0.0019048	-0.0018147
0.439	-5.16E-05	-2.38E-04	-4.64E-04	-8.59E-04	-0.0013122	-0.001763	-0.0021876	-0.0025498	-0.0028313	-0.0028535
0.4395	-5.73E-05	-2.59E-04	-5.45E-04	-0.0010602	-0.0016573	-0.0022511	-0.0028194	-0.0033242	-0.0037385	-0.0038728
0.44	-6.27E-05	-2.79E-04	-6.23E-04	-0.0012546	-0.0019911	-0.0027239	-0.0034319	-0.004076	-0.0046202	-0.0048657
0.4405	-6.77E-05	-2.97E-04	-6.97E-04	-0.0014405	-0.0023113	-0.0031781	-0.004021	-0.0048	-0.0054704	-0.0058254
0.441	-7.22E-05	-3.13E-04	-7.65E-04	-0.0016165	-0.0026158	-0.0036106	-0.0045827	-0.0054912	-0.0062832	-0.0067454
0.4415	-7.62E-05	-3.26E-04	-8.29E-04	-0.0017815	-0.0029024	-0.0040185	-0.0051131	-0.0061449	-0.0070532	-0.0076193
0.442	-7.96E-05	-3.38E-04	-8.87E-04	-0.0019344	-0.0031692	-0.004399	-0.0056086	-0.0067567	-0.007775	-0.0084413
0.4425	-8.26E-05	-3.47E-04	-9.39E-04	-0.002074	-0.0034144	-0.0047495	-0.0060658	-0.0073225	-0.0084438	-0.0092056
0.443	-8.49E-05	-3.53E-04	-9.84E-04	-0.0021995	-0.0036363	-0.0050675	-0.0064817	-0.0078382	-0.009055	-0.0099072
0.4435	-8.67E-05	-3.58E-04	-0.0010231	-0.00231	-0.0038334	-0.005351	-0.0068533	-0.0083005	-0.0096044	-0.010541
0.444	-8.79E-05	-3.60E-04	-0.0010548	-0.0024048	-0.0040043	-0.005598	-0.0071782	-0.0087062	-0.010088	-0.011103
0.4445	-8.85E-05	-3.59E-04	-0.0010794	-0.0024831	-0.0041479	-0.0058068	-0.0074541	-0.0090524	-0.010503	-0.011589
0.445	-8.85E-05	-3.56E-04	-0.0010966	-0.0025445	-0.0042632	-0.0059759	-0.0076792	-0.0093369	-0.010847	-0.011997
0.4455	-8.79E-05	-3.51E-04	-0.0011064	-0.0025885	-0.0043494	-0.0061043	-0.0078518	-0.0095577	-0.011116	-0.012322
0.446	-8.67E-05	-3.43E-04	-0.0011085	-0.0026149	-0.004406	-0.006191	-0.0079709	-0.0097133	-0.01131	-0.012563
0.4465	-8.49E-05	-3.32E-04	-0.0011032	-0.0026234	-0.0044324	-0.0062355	-0.0080356	-0.0098026	-0.011426	-0.012719
0.447	-8.25E-05	-3.20E-04	-0.0010902	-0.002614	-0.0044287	-0.0062375	-0.0080455	-0.009825	-0.011464	-0.012788
0.4475	-7.96E-05	-3.05E-04	-0.0010699	-0.0025868	-0.0043947	-0.0061969	-0.0080004	-0.0097804	-0.011425	-0.012769
0.448	-7.61E-05	-2.89E-04	-0.0010422	-0.002542	-0.0043307	-0.006114	-0.0079008	-0.009669	-0.011307	-0.012664
0.4485	-7.21E-05	-2.70E-04	-0.0010075	-0.0024798	-0.0042372	-0.0059894	-0.0077473	-0.0094917	-0.011112	-0.012472
0.449	-6.76E-05	-2.49E-04	-9.66E-04	-0.0024007	-0.0041148	-0.0058239	-0.0075409	-0.0092496	-0.010841	-0.012195
0.4495	-6.27E-05	-2.27E-04	-9.18E-04	-0.0023052	-0.0039643	-0.0056187	-0.0072831	-0.0089445	-0.010497	-0.011834
0.45	-5.73E-05	-2.03E-04	-8.63E-04	-0.0021939	-0.0037868	-0.0053752	-0.0069756	-0.0085783	-0.01008	-0.011393
0.4505	-5.15E-05	-1.78E-04	-8.03E-04	-0.0020677	-0.0035834	-0.005095	-0.0066205	-0.0081535	-0.0095952	-0.010875
0.451	-4.54E-05	-1.52E-04	-7.37E-04	-0.0019274	-0.0033556	-0.00478	-0.0062202	-0.0076732	-0.0090447	-0.010282
0.4515	-3.89E-05	-1.24E-04	-6.66E-04	-0.001774	-0.0031048	-0.0044324	-0.0057775	-0.0071404	-0.0084324	-0.0096185
0.452	-3.22E-05	-9.61E-05	-5.91E-04	-0.0016084	-0.0028329	-0.0040546	-0.0052954	-0.006559	-0.0077626	-0.0088898
0.4525	-2.53E-05	-6.72E-05	-5.11E-04	-0.0014319	-0.0025417	-0.0036491	-0.0047771	-0.0059328	-0.0070399	-0.0081004
0.453	-1.82E-05	-3.78E-05	-4.28E-04	-0.0012456	-0.0022331	-0.0032187	-0.0042262	-0.0052661	-0.0062691	-0.0072558
0.4535	-1.10E-05	-8.13E-06	-3.42E-04	-0.0010508	-0.0019093	-0.0027664	-0.0036466	-0.0045636	-0.0054556	-0.0063616
0.454	-3.71E-06	2.16E-05	-2.54E-04	-8.49E-04	-0.0015725	-0.0022952	-0.003042	-0.0038298	-0.0046048	-0.0054241
0.4545	3.61E-06	5.11E-05	-1.64E-04	-6.41E-04	-0.0012249	-0.0018083	-0.0024167	-0.00307	-0.0037226	-0.0044495
0.455	1.09E-05	8.03E-05	-7.32E-05	-4.29E-04	-8.69E-04	-0.0013091	-0.0017748	-0.0022892	-0.002815	-0.0034446
0.4555	1.81E-05	1.09E-04	1.84E-05	-2.14E-04	-5.07E-04	-8.01E-04	-0.0011209	-0.0014927	-0.0018882	-0.0024162
0.456	2.52E-05	1.37E-04	1.10E-04	2.66E-06	-1.42E-04	-2.87E-04	-4.59E-04	-6.86E-04	-9.49E-04	-0.0013713
0.4565	3.21E-05	1.64E-04	2.00E-04	2.19E-04	2.24E-04	2.28E-04	2.05E-04	1.25E-04	-2.41E-06	-3.17E-04
0.457	3.89E-05	1.90E-04	2.90E-04	4.34E-04	5.89E-04	7.42E-04	8.69E-04	9.36E-04	9.44E-04	7.39E-04

Bibliography

[1] URL https://flapper-drones.com/wp/.

[2] The aerodynamics of hovering insect flight. ii. morphological parameters. *Philosophical Transactions of the Royal Society of London. B, Biological Sciences*, 305(1122):17–40, 1984. doi: 10.1098/rstb.1984.0050.

[3] Topology optimization overview, Jan 2017. URL http://topshape.bm-rd.com/topology-optimization-overview/.

[4] Arun Agrawal and Sunil K. Agrawal. Design of bio-inspired flexible wings for flapping-wing micro-sized air vehicle applications. *Advanced Robotics*, 23:979–1002, 2009. doi: 10.1163/156855309X443133.

[5] SA Ansari, R Żbikowski, and Kevin Knowles. Aerodynamic modelling of insect-like flapping flight for micro air vehicles. *Progress in Aerospace Sciences*, 42(2):129–172, 2006.

[6] A Azuma. The biokinetics of flying and swimming. *AIAA*, 2006.

[7] Ted Belytschko, Wing-Kam Liu, Jame Shau-Jen Ong, and Dennis Lam. Implementation and application of a 9-node lagrange shell element with spurious mode control. *Advances and Trends in Structures and Dynamics*, page 121–128, 1985. doi: 10.1016/b978-0-08-032789-1.50018-5.

[8] M. P. Bendsøe. Optimal shape design as a material distribution problem. *Structural Optimization*, 1(4):193–202, 1989. doi: 10.1007/bf01650949.

[9] Gordon Berman and Z. Wang. Energy-minimizing kinematics in hovering insect flight. *Journal of Fluid Mechanics*, 582:153–168, 2007.

[10] David Billingsley. Passively morphing ornithopter wings constructed using a novel compliant spine: design and testing. *AIAA*, 2009. doi: 10.1.1.721.8701.

[11] James M. Birch and Michael H. Dickinson. Spanwise flow and the attachment of the leading-edge vortex on insect wings. *Nature*, 412(6848):729–733, 2001. doi: 10.1038/35089071.

[12] Johan Blaauwendraad and Jeroen H Hoefakker. Structural shell analysis. *Springer, The Netherlands, p300. doi*, 10:978–94, 2014.

[13] K-U Bletzinger, Stefan Kimmich, and Ekkehard Ramm. Efficient modeling in shape optimal design. *Computing Systems in Engineering*, 2(5-6):483–495, 1991.

[14] Kai-Uwe Bletzinger, Matthias Firl, and Fernass Daoud. Approximation of derivatives in semi-analytical structural optimization. *Computers Structures*, 86(13-14):1404–1416, 2008. doi: 10.1016/j.compstruc.2007.04.014.

[15] H. De Boer, F. Van Keulen, and K. Vervenne. Refined second order semi-analytical design sensitivities. *International Journal for Numerical Methods in Engineering*, 55(9):1033–1051, 2002. doi: 10.1002/nme.533.

[16] C Bolsman, J.F.L. Goosen, and Fred Keulen. Design overview of a resonant wing actuation mechanism for application in flapping wing mavs. *International Journal of Micro Air Vehicles*, 1, 12 2009. doi: 10.1260/175682909790291500.

[17] M. L. Bucalem and K. J. Bathe. Finite element analysis of shell structures. *Archives of Computational Methods in Engineering*, 4(1):3–61, 1997. doi: 10.1007/bf02818930.

[18] Reginald Frederick Chapman and Reginald Frederick Chapman. *The insects: structure and function*. Cambridge university press, 1998.

[19] David Coleman, Moble Benedict, Vikram Hrishikeshavan, and Inderjit Chopra. Design, development and flight-testing of a robotic hummingbird. volume 1, 05 2015.

[20] David Colmenares, Randall Kania, Wang Zhang, and Metin Sitti. Bio-inspired flexible twisting wings increase lift and efficiency of a flapping wing micro air vehicle. *arXiv preprint arXiv:2001.11586*, 2020.

[21] SA Combes and T Daniel. Flexural stiffness in insect wings. i. scaling and the influence of wing venation. journal of experimental biology. *The Journal of experimental biology*, 206:2979–87, 10 2003. doi: 10.1242/jeb.00523.

[22] SA Combes and T Daniel. Flexural stiffness in insect wings. ii. spatial distribution and dynamic wing bending. *The Journal of experimental biology*, 206:2989–97, 10 2003. doi: 10.1242/jeb.00524.

[23] G. C. H. E. de Croon. *The DelFly: design, aerodynamics, and artificial intelligence of a flapping wing robot*. Springer, 2016.

[24] Oscar Curet, Sharon Swartz, and Kenneth Breuer. An aeroelastic instability provides a possible basis for the transition from gliding to flapping flight. *Journal of the Royal Society, Interface / the Royal Society*, 10:20120940, 12 2013. doi: 10.1098/rsif.2012.0940.

[25] M. H. Dickinson. Wing rotation and the aerodynamic basis of insect flight. *Science*, 284(5422): 1954–1960, 1999. doi: 10.1126/science.284.5422.1954.

[26] Michael Dickinson, Fritz-Olaf Lehmann, and Sanjay Sane. Wing rotation and the aerodynamic basis of insect flight. *Science (New York, N.Y.)*, 284:1954–60, 07 1999. doi: 10.1126/science.284.5422.1954.

[27] Gang Du and Mao Sun. Effects of unsteady deformation of flapping wing on its aerodynamic forces. *Applied Mathematics and Mechanics*, 29(6):731, 2008.

[28] M Elbanhawi, A Mohamed, R Clothier, JL Palmer, M Simic, and S Watkins. Enabling technologies for autonomous mav operations. *Progress in Aerospace Sciences*, 91:27–52, 2017.

[29] Charles P. Ellington, Coen Van Den Berg, Alexander P. Willmott, and Adrian L. R. Thomas. Leading-edge vortices in insect flight. *Nature*, 384(6610):626–630, 1996. doi: 10.1038/384626a0.

[30] Christophe Eloy. Optimal strouhal number for swimming animals. *Journal of Fluids and Structures*, 30:205–218, 2012. doi: 10.1016/j.jfluidstructs.2012.02.008.

[31] Matthias Firl. Optimal shape design of shell structures, 2010. URL https://mediatum.ub.tum.de/doc/981720/512948.pdf.

[32] Matthias Firl, Roland Wüchner, and Kai-Uwe Bletzinger. Regularization of shape optimization problems using fe-based parametrization. *Structural and Multidisciplinary Optimization*, 47(4): 507–521, 2012. doi: 10.1007/s00158-012-0843-z.

[33] Fleury, Claude, Pierre, and Beckers. Shape optimal design - an approach matching c.a.d. and optimization concepts, Jan 1985. URL https://orbi.uliege.be/handle/2268/92778.

[34] Steven Fry, Rosalyn Sayaman, and Michael Dickinson. The aerodynamics of hovering flight in drosophila. *The Journal of experimental biology*, 208:2303–18, 07 2005. doi: 10.1242/jeb.01612.

[35] Michael Goldfarb and John E Speich. A well-behaved revolute flexure joint for compliant mechanism design. 1999.

[36] MA Groen, BAP Bruggeman, BDW Remes, HM Ruijsink, BW van Oudheusden, and H Bijl. Improving flight performance of the flapping wing mav delfly ii. pages 1–17, 2009.

[37] R. Haftka and R. Grandhi. Structural shape optimization - a survey. *26th Structures, Structural Dynamics, and Materials Conference*, 1985. doi: 10.2514/6.1985-772.

[38] Thomas J.r. Hughes, Martin Cohen, and Medhat Haroun. Reduced and selective integration techniques in the finite element analysis of plates. *Nuclear Engineering and Design*, 46(1):203–222, 1978. doi: 10.1016/0029-5493(78)90184-x.

[39] M. Karásek and A. Preumont. Robotic hummingbird: design of a control mechanism for a hovering flapping wing micro air vehicle. 2014.

[40] M Keennon, K Klingebiel, and H Won. Development of the nano hummingbird: A tailless flapping wing micro air vehicle. *Physica B: Condensed Matter*, 2012. doi: 10.2514/6.2012-588.

[41] F. Van Keulen and H. De Boer. Rigorous improvement of semi-analytical design sensitivities by exact differentiation of rigid body motions. *International Journal for Numerical Methods in Engineering*, 42(1):71–91, 1998. doi: 10.1002/(sici)1097-0207(19980515)42:1<71::aid-nme350>3.0.co;2-c.

[42] Fred Van Keulen and Jan Booij. Refined consistent formulation of a curved triangular finite rotation shell elements. *International journal for numerical methods in engineering,*, 39:2803–2820, 1996.

[43] Fritz-Olaf Lehmann and K Götz. Activation phase ensures kinematic efficacy in flight-steering muscles of drosophila melanogaster. *Journal of comparative physiology. A, Sensory, neural, and behavioral physiology*, 179:311–22, 10 1996. doi: 10.1007/BF00194985.

[44] Fritz-Olaf Lehmann, Stanislav Gorb, Nazri Nasir, and Peter Schützner. Elastic deformation and energy loss of flapping fly wings. *The Journal of experimental biology*, 214:2949–61, 09 2011. doi: 10.1242/jeb.045351.

[45] Yongsheng Lian, Timothy Broering, Kyle Hord, and Russell Prater. The characterization of tandem and corrugated wings. *Progress in Aerospace Sciences*, 65, 01 2013. doi: 10.1016/j.paerosci.2013.08.001.

[46] Hao Liu. *An Introduction to Flapping Wing Aerodynamics*. 01 2007.

[47] Yang Liu and Masatoshi Shimoda. Two-step shape optimization methodology for designing free-form shells. *Inverse Problems in Science and Engineering*, 23(1):1–15, 2013. doi: 10.1080/17415977.2013.793322.

[48] Helmut Masching. *Parameter Free Optimization of Shape Adaptive Shell Structures*. PhD thesis, Technische Universität München, 2016.

[49] COMSOL Multiphysics. v. 5.4. comsol ab. *Structural Mechanics Users Guide, Stockholm*, 2018.

[50] Yanghai Nan, Matěj Karásek, Lalami mohamed esseghir, and A. Preumont. Experimental optimization of wing shape for a hummingbird-like flapping wing micro air vehicle. *Bioinspiration Biomimetics*, 12:1–16, 03 2017. doi: 10.1088/1748-3190/aa5c9e.

[51] A. Naranyan, H. Goosen, and F. Van Keulen. Design of a flapping wing for application in a mav. 2018.

[52] Ryusuke Noda, Toshiyuki Nakata, and Hao Liu. Effects of wing deformation on aerodynamic performance of a revolving insect wing. *Acta Mechanica Sinica*, 30(6):819–827, 2014.

[53] Ahmed Khairy Noor, Ted Belytschko, and J. C. Simo. *Analytical and computational models of shells: presented at the Winter Annual Meeting of the American Society of Mechanical Engineers, San Francisco, California, December 10-15, 1989*. American Society of Mechanical Engineers, 1989.

[54] H.J. Peters. The optimization of the flapping wings for a micro air vehicle, Jan 1970. URL http://resolver.tudelft.nl/uuid:f42d9d82-ed7f-450d-9c5b-7d34d3ae2725.

[55] Hoang Vu Phan and Hoon Park. Design and evaluation of a deformable wing configuration for economical hovering flight of an insect-like tailless flying robot. *Bioinspiration Biomimetics*, 13, 03 2018. doi: 10.1088/1748-3190/aab313.

[56] Ekkehard Ramm, Kai-Uwe Bletzinger, and Reiner Reitinger. Shape optimization of shell structures. *Revue Européenne des Éléments Finis*, 2(3):377–398, 1993. doi: 10.1080/12506559.1993.10511083.

[57] Meindert Ras. Design, fabrication and assembly of a flapping-wing with integrated compliant hinge: Application in a bio-inspired, resonant micro air vehicle, Jan 1970. URL http://resolver.tudelft.nl/uuid:2a355529-790a-426a-85bd-deb9e3732691.

[58] Derek Risseeuw. Fluid structure interaction modelling of flapping wings: Development and validation of a general open-source fluid structure interaction method with analysis of flexible flapping wing aerodynamics. 2019.

[59] Sanjay Sane and Michael Dickinson. The control of flight force by a flapping wing: Lift and drag production. *The Journal of experimental biology*, 204:2607–26, 09 2001.

[60] Sanjay P Sane and Michael H Dickinson. The aerodynamic effects of wing rotation and a revised quasi-steady model of flapping flight. *Journal of experimental biology*, 205(8):1087–1096, 2002.

[61] Arend L Schwab and Jaap P Meijaard. How to draw euler angles and utilize euler parameters. In *International Design Engineering Technical Conferences and Computers and Information in Engineering Conference*, volume 42568, pages 259–265. Citeseer, 2006.

[62] Masatoshi Shimoda. Free-form optimization method for designing automotive shell structures. *SAE International Journal of Passenger Cars - Electronic and Electrical Systems*, 4(1):42–54, Dec 2011. doi: 10.4271/2011-01-0064.

[63] Masatoshi Shimoda and Yang Liu. A non-parametric free-form optimization method for shell structures. *Structural and Multidisciplinary Optimization*, 50(3):409–423, 2014. doi: 10.1007/s00158-014-1059-1.

[64] W Shyy, H Aono, Satish Chimakurthi, P Trizila, C.-K Kang, Carlos Cesnik, and Hao Liu. Recent progress in flapping wing aerodynamics and aeroelasticity. *Progress in Aerospace Sciences - PROG AEROSP SCI*, 46, 03 2010. doi: 10.1016/j.paerosci.2010.01.001.

[65] Wei Shyy, Chang-kwon Kang, Pakpong Chirarattananon, Sridhar Ravi, and Hao Liu. Aerodynamics, sensing and control of insect-scale flapping-wing flight. *Proceedings of the Royal Society A: Mathematical, Physical and Engineering Science*, 472:20150712, 02 2016. doi: 10.1098/rspa.2015.0712.

[66] Eric C. Stewart, Mayuresh Patil, Robert A. Canfield, and Richard D. Snyder. Aeroelastic shape optimization of a flapping wing. *10th AIAA Multidisciplinary Design Optimization Conference*, 2014. doi: 10.2514/6.2014-0469.

[67] Amanda K Stowers and David Lentink. Folding in and out: passive morphing in flapping wings. *Bioinspiration Biomimetics*, 10, 12 2015. doi: 0.1088/1748-3190/10/2/025001.

[68] Haithem E Taha, Muhammad R Hajj, and Ali H Nayfeh. Flight dynamics and control of flapping-wing mavs: a review. *Nonlinear Dynamics*, 70(2):907–939, 2012.

[69] Hiroto Tanaka and Robert J Wood. Fabrication of corrugated artificial insect wings using laser micromachined molds. *Journal of Micromechanics and Microengineering*, 20(7):075008, 2010.

[70] M Tu and M Dickinson. Modulation of negative work output from a steering muscle of the blowfly calliphora vicina. *Journal of Experimental Biology*, 102, 1994. doi: 10.1016/S0921-4526(00)00753-5.

[71] Fred Van Keulen. On refined triangular plate and shell elements, Jan 1993. URL https://repository.tudelft.nl/islandora/object/uuid:5c549278-547e-4b17-abaf-409c0d496067.

[72] Q. Wang. Modeling, design and optimization of flapping wings for efficient hovering flighth, Jan 1970. URL https://repository.tudelft.nl/islandora/object/uuid:e6fc3865-531f-4ea9-aeff-e2ef923ae36f?collection=research.

[73] Q Wang, JFL Goosen, and F Van Keulen. Study of design parameters of flapping-wings. 2014.

[74] Q. Wang, H. Goosen, and F. Van Keulen. A predictive quasi-steady model of aerodynamic loads on flapping wings. *Journal of Fluids and Structures*, 800:688–719, 2016. doi: 10.1017/jfm.2016.413.

[75] Q. Wang, H. Goosen, and F. Van Keulen. An efficient fluid–structure interaction model for optimizing twistable flapping wings. *Journal of Fluids and Structures*, pages 82–99, 2017. doi: DOI:10.1016/j.jfluidstructs.2017.06.006.

[76] Q Wang, JFL Goosen, and F van Keulen. Optimal pitching axis location of flapping wings for efficient hovering flight. *Bioinspiration & biomimetics*, 12(5):056001, 2017.

[77] Qi Wang, JFL Goosen, and A Van Keulen. Optimal hovering kinematics with respect to various flapping-wing shapes. In *IMAV 2013: Proceedings of the International Micro Air Vehicle Conference and Flight Competition, Toulouse, France, 17-20 September 2013*, 2013.

[78] A A Wissa. Passively morphing ornithopter wings constructed using a novel compliant spine: design and testing. *Smart Materials and Structures*, 21, 2012. doi: 10.1088/0964-1726/21/9/094028.

[79] K. Yamazaki and G. N. Vanderplaats. Design sensitivity analysis with isoparametric shell elements. *Structural Optimization*, 5(3):152–158, 1993. doi: 10.1007/bf01743351.